NASA CR-54023
MB R 54 21

FEASIBILITY STUDY FOR DEVELOPMENT OF A HYPERVELOCITY GUN

by

D. E. Brast and D. R. Sawle

prepared for

NATIONAL AERONAUTICS AND SPACE ADMINISTRATION

CONTRACT NAS 3-1924

OTS PRICE
XEROX $
MICROFILM $

MB ASSOCIATES
San Ramon
(near San Francisco)
California

NOTICE

This report was prepared as an account of Government sponsored work. Neither the United States, nor the National Aeronautics and Space Administration (NASA), nor any person acting on behalf of NASA:

A) makes any warranty or representation, expressed or implied, with respect to the accuracy, completeness, or usefulness of the information contained in this report, or that the use of any information, apparatus, method, or process disclosed in this report may not infringe privately owned rights; or

B) assumes any liabilities with respect to the use of, or for damages resulting from the use of any information, apparatus, method or process disclosed in this report.

As used above, "person acting on behalf of NASA" includes any employee or contractor of NASA, or employee of such contractor, to the extent that such employee or contractor of NASA, or employee of such contractor prepares, disseminates, or provides access to, any information pursuant to his employment or contract with NASA, or his employment with such contractor.

Requests for copies of this report should be referred to

National Aeronautics and Space Administration
Office of Scientific and Technical Information
Attention: AFSS-A
Washington, D. C. 20546

189241

NASA CR-54028
MB-R-64/21

FINAL REPORT

FEASIBILITY STUDY FOR DEVELOPMENT OF A HYPERVELOCITY GUN

by

D. E. Brast and D. R. Sawle

prepared for

NATIONAL AERONAUTICS AND SPACE ADMINISTRATION

27 March 1964

CONTRACT NAS 3-1924

Technical Management
NASA Lewis Research Center
Cleveland, Ohio
Space Electric Power Office
E. A. Koutnik

MB ASSOCIATES
San Ramon
(near San Francisco)
California

TABLE OF CONTENTS

	List of Figures	ii
	List of Tables	iii
	SUMMARY	iv
I	INTRODUCTION	1
	A Description	1
	B History	4
II	RAIL GUN	6
	A Theory	6
	1 The jxB Force on the Arc	6
	2 Rail Sputtering Limitation on Velocity	10
	B Experimental Results	14
III	MHD GENERATOR	21
	A Generator Theory	21
	B Sabot Heating	24
	C Design Calculations	24
	D Experimental Results	29
IV	RECOMMENDATIONS	32
Appendix		
A	Generator Tests	34
B	Containment Tank	64
C	Condenser Bank and Instrumentation	70
D	Diagnostics	77
D-1	Piston Convergence and Velocity Measurements	77
-2	Magnetic Field Measurements for the Generator	77
-3	Ballistic Pendulum	79
-4	Photomultiplier Velocity Screens	79
-5	Crater Size	79
-6	Flux Loop Measurements for the Rail Gun	81
E	Theory of the After-Section	87

LIST OF FIGURES

Figure		Page
1	Schematic Drawing of Rail Gun Operation	2
2	Photograph and Schematic Drawing of Complete Rail Gun System	3
3	Construction of the Standard Rail Gun	5
4	The Arc Discharge between Parallel Rails	8
5	Velocity and Distance vs. Time for the Sputtering Limited Free Arc	12
6	Distance vs. Time for the Projectile and Free Arc--Theoretical and Experimental	13
7 & 8	Arc Position vs. Time	16
9 & 10	Arc Position vs. Time	17
11	Coaxial-Electrode Gun	19
12	Inductance Correction	22
13	Magnetic Field at Sabot vs. Remaining Piston Travel	26
14	Sabot and Projectile Acceleration vs. Velocity	27
15	Sabot Temperature at Current Skin Depth Median vs. Sabot Velocity	28
16	Schematic of Transducer Converging Loop	30

List of Figures (continued)

Appendix	Figure		Page
A	A-1	Interior of Experiment 4.5-1 Test Model	59
	A-2	Experiment 4.5-1 Test Model in Containment Tank	59
	A-3	Isochron Diagram of Piston	60
	A-4	Magnetic Compression Test Device	61
	A-5	Long Pulse Generator	63
B	B-1	Containment Tank (drawing)	65
	B-2	Containment Tank (photograph)	66
C	C-1	Condenser Bank	71
	C-2	Circuit Diagram of Detonator Panel	72
	C-3	Circuit Diagram of Condenser Bank Control Panel	73
	C-4	Circuit Diagram of Condenser Bank Power Supply	74
	C-5	Circuit Diagram of Condenser Bank	75
D	D-1	Location of Pin Probes	78
	D-2	Velocity Measurement Techniques	80
	D-3	Penetration vs. Projectile Velocity at the Target	82
	D-4	Flux Loop on the Standard Rail Gun	83
	D-5	Flux Loop Signals	84
	D-6	Flux Loop Circuit	85
	D-7	Description of Flux Loop Circuit	86

LIST OF TABLES

Table		
1	Summary of Rail Gun Experiments	15, 15-A
2	Summary of Generator Experiments	31, 31-A

FEASIBILITY STUDY FOR DEVELOPMENT OF A HYPERVELOCITY GUN

by D. E. Brast and D. R. Sawle

MB Associates

SUMMARY

20723 A

By means of a rail-type MHD accelerator, a 2.4 mg nylon ball was accelerated to 6.0 km/sec and an 8 mg nylon ball to 3.7 km/sec. Measurements of time vs. projectile position in the accelerator were made by means of magnetic flux loops. This data was explained by assuming mass input from the rails due to sputtering. Under this assumption, the data led to a value of 4.6 copper atoms sputtered per electron. A 142 microfarad, 28 kilojoule condenser bank was the electrical source in the experiments. A high explosive MHD generator was developed for possible future use with the accelerator.

Author

I INTRODUCTION

The subject of this report is a projectile accelerator system whose novel component consists of two copper rails, across which an arc is struck so that the resulting magnetic field accelerates the arc and the projectile in front of it down the rails. (See Figure 1)

The peculiar attractiveness of this device is its advantage over the light gas gun, namely that, whereas there is no inherent practical limitation on the speed of an arc plasma, the speed of a practical strong shock in a gas is less than, say, five times the speed of sound. Light gas guns have been able to accelerate projectiles to speeds of about 10 km/sec. On the other hand, arc plasmas have been driven to speeds of 100 km/sec. If the magnetic force on an arc can be transferred successfully to a projectile, one should be able to accelerate the projectile to 100 km/sec.

During this contract we have successfully built and tested the large ultra-low inductance energy source for such a system (a condenser bank and high-explosive generator), a diagnostic system for measuring the velocity of the projectile; and, using only the condenser bank as the energy source, have accelerated--by means of a rail gun--a 2.4 mg nylon ball to a velocity of 6.0 km/sec and an 8 mg nylon ball to 3.7 km/sec. This velocity was achieved with only an overall understanding of the mechanism of projectile acceleration based on the known behavior of arcs in rail-type plasma accelerators.

Following is, first, a discussion of the technical aspects of the problem consisting of a detailed description of the system; a brief history of the program; theoretical discussions; and summaries of results. Then, based upon the considerations of this technical discussion, our recommendations for future work are given.

A DESCRIPTION

Figure 2 shows a complete rail gun system consisting of an energy source, the rail gun, and devices for measuring the final velocity of the projectile. The energy source and velocity measuring devices, which are practically solved problems, are treated in detail in Appendices C and D. It remains to discuss the construction and operation of the rail gun.

Rail guns have the following common operation and structure:

1) A high voltage is applied across the ends of a pair of conducting rails.
2) An arc is struck between the rails either through a conductor which is vaporized by the initial current, or at a constriction which provides a place where the initial spark is sure to jump.

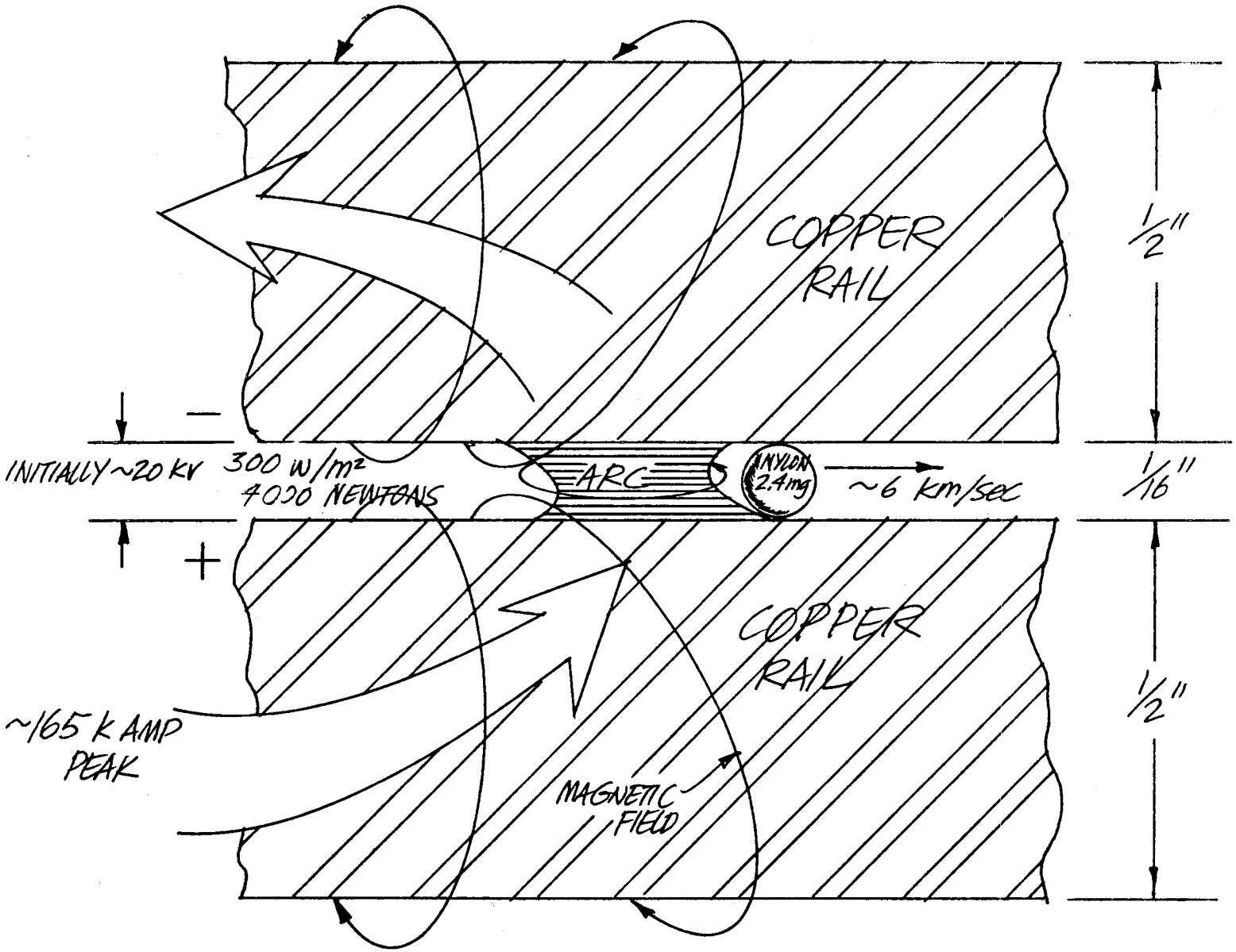

SCHEMATIC DRAWING OF RAIL GUN OPERATION

FIGURE 1

MBA 1237

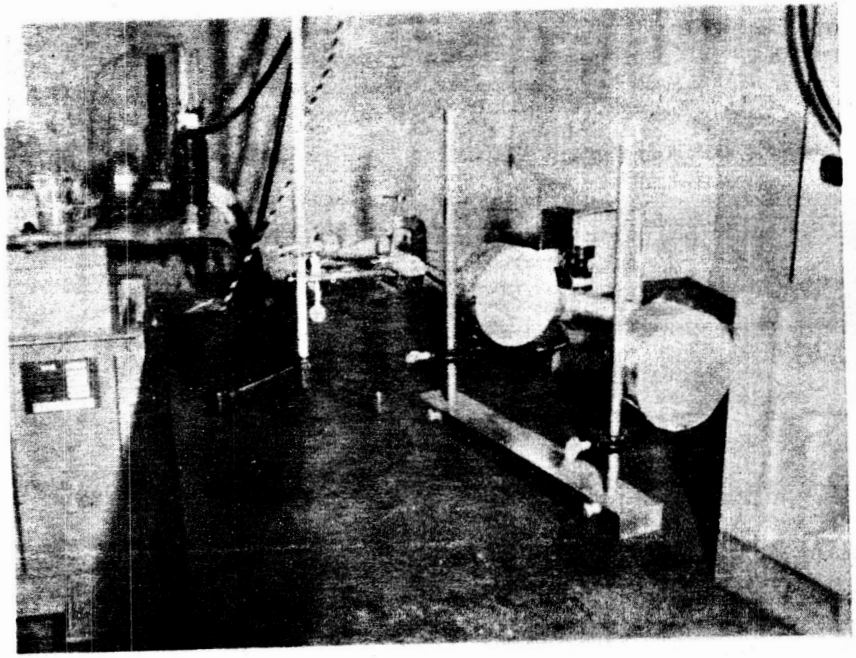

NOTE: The set-up in the photograph has a condenser bank but no explosive generator as the energy source.

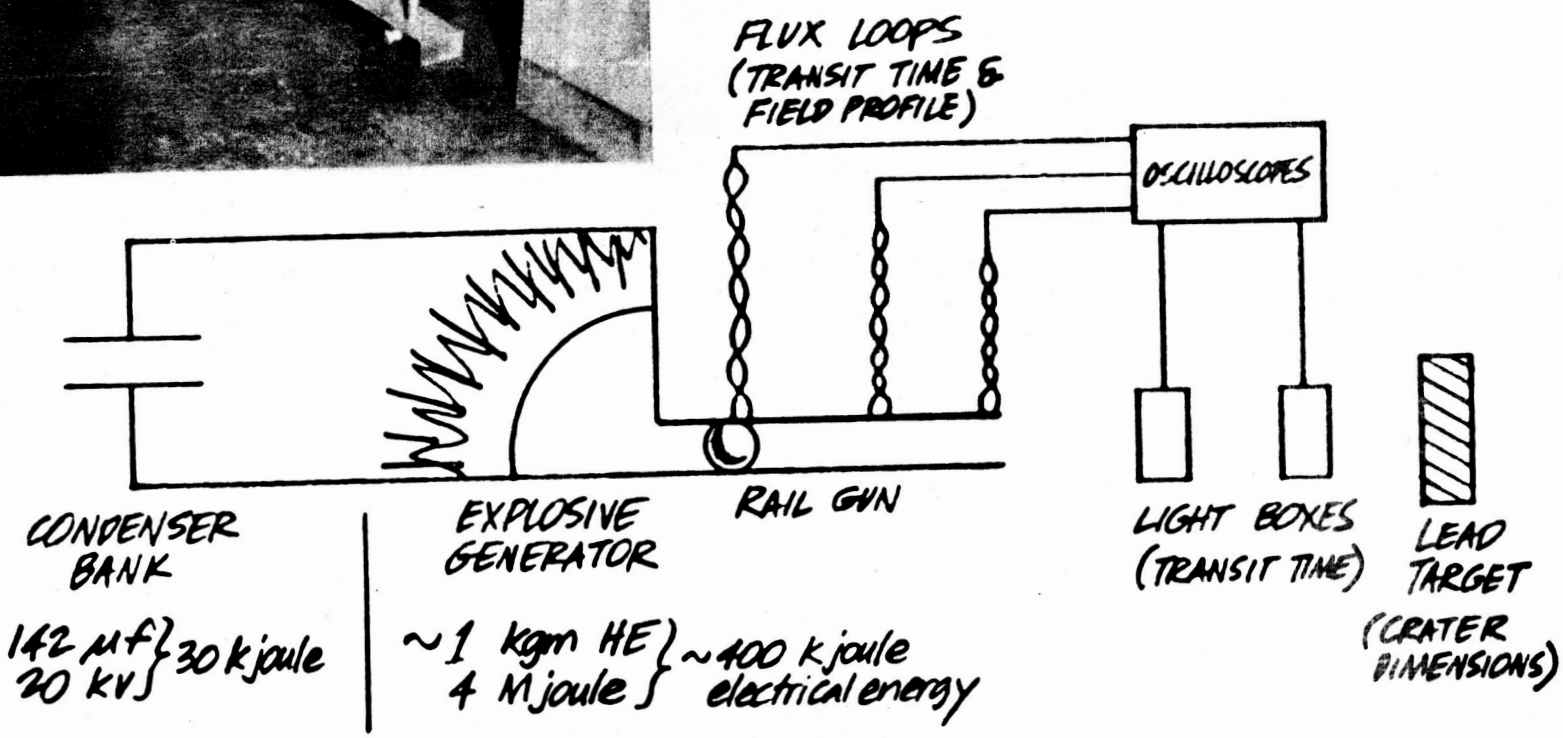

PHOTOGRAPH AND SCHEMATIC DRAWING OF A COMPLETE RAIL GUN SYSTEM

Figure 2

MCA 1239

3) Insulating material holds the rails and the arc-initiating conductor together; forms, together with the rails, a barrel for the projectile; and prevents the arc from occuring except in that barrel.

Figure 1 is a schematic representation of such a rail gun in operation. Figure 3 contains construction drawings of our most successful gun.

B HISTORY

In the early stages of the program we believed the problem could be solved by designing, building, and testing, as a whole, a complete system; and then, if necessary, improving it. However, the experimental results indicated that the problem could be solved only piecemeal.

Early in the present program the first test of a complete system was performed. Pin measurements (see Appendix D-1) showed that something was moving between the rails at about 10 km/sec. That something could have been the 100 mg tungsten carbide projectile or it could have been the arc. The target showed many small craters which could have been caused by pieces of the projectile, the pins, or the sabot. Besides the question of what caused the craters, and how fast it was going, there was also doubt about the magnetic field compression.

In early experiments on the generator only, we found that there was little field compression. This could have been due to poor piston motion (see Appendix D-1) or to flux leakage. To discover which, the problem was simplified by observing only the piston motion. These experiments did show poor piston convergence. The design was changed, field compression tests were made with the improved design, and the results were good.

Rail gun experiments were then begun. Continuation of these experiments has been the entire effort of the rest of the program. The results of this effort have been threefold:

1) The development of reliable diagnostic techniques including transit time measurements with flux loops and light boxes, and accurate crater depth-velocity correlation.

2) Design improvements including a strong easily fabricated gun with a smooth cylindrical bore (see Figure 3), a nylon--and, therefore, nonconducting--ball which will not vaporize or break up under the action of the arc, and an easy and reliable method for loading the ball and initiating the arc. (This has resulted in a velocity of 6 km/sec for a 2.4 mg ball.)

3) The uncovering of the basic questions concerning the mechanism of acceleration, the generation of data pertaining to these questions, and the evolution of a theoretical explanation of this data.

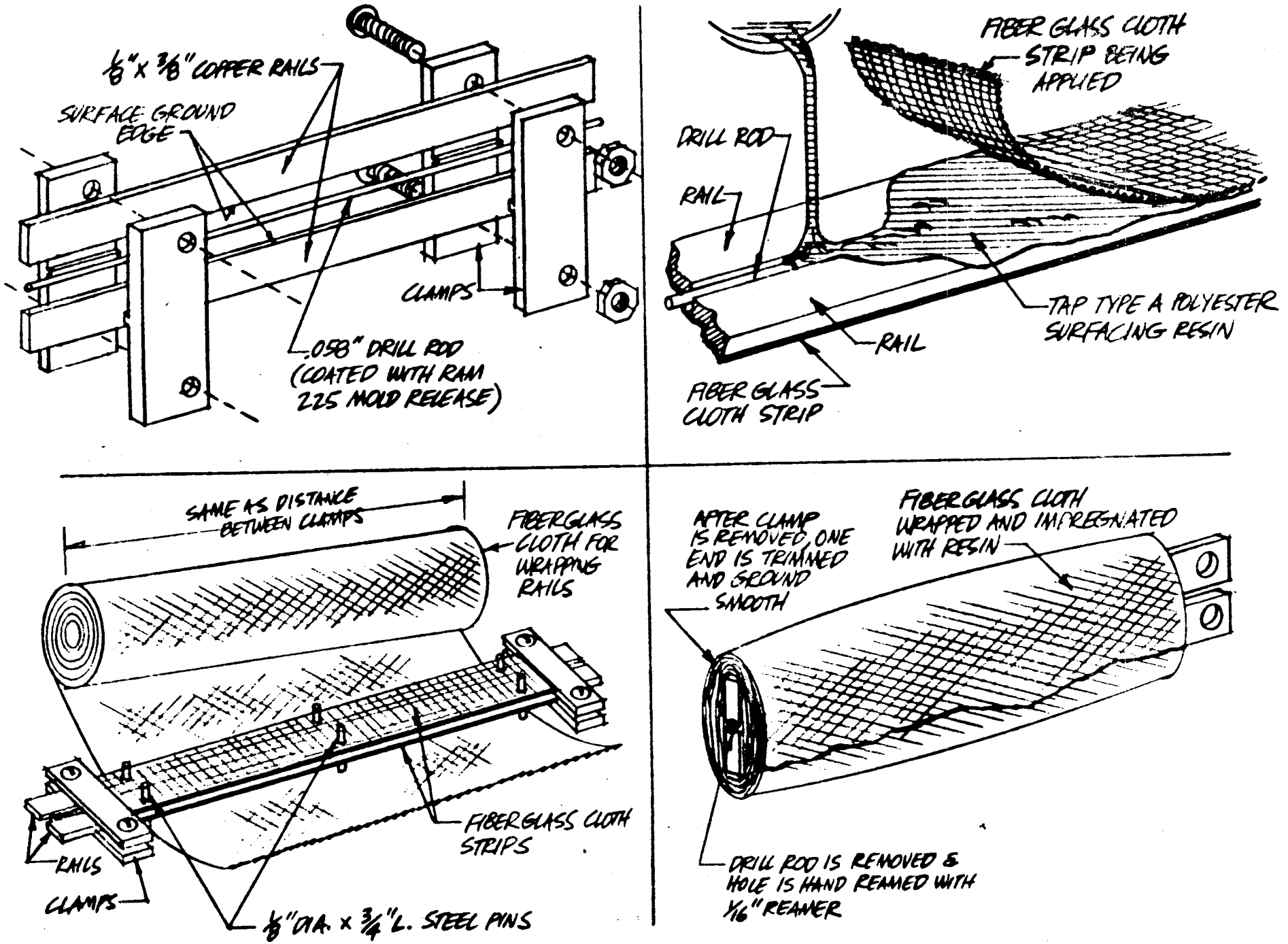

Construction of the Standard Rail Gun

Figure 3

MBA 1226

II RAIL GUN

A THEORY OF THE RAIL GUN

A good deal of theoretical and experimental work has been done on the problem of the magnetohydrodynamically driven shock in a rail gun. Philip J. Hart (Phys. of Fluids 5, 38 (1962)) has solved by machine the differential equations of motion of a plasma disc in a coaxial gun under the assumption of the "snowplow model" and also for constant mass. His experimental results agree well with his calculations.

The situation of a projectile in a small bore differs in two important aspects from that above:

1) The force is dependent on the current distribution because of certain asymmetry.

2) Mass input from the electrodes becomes considerable because of the close electrode spacing.

The general statement of the problem is: Given

1) the nature of the current source,
2) the shape and composition of the rails,
3) the shape and composition of the initial short circuit,
4) the composition of the insulator,
5) the initial distance from the short to the projectile, and
6) the mass of the projectile,

find the position of the projectile as a function of time. As a first step in the solution, we specify the following forces and masses:

1) jxB forces on the arc,
2) frictional forces between the barrel and arc plasma,
3) the mass of the ball, and
4) the mass of the arc.

Our theoretical work so far has been to use these quantities to find the motion of the center of mass of the projectile and arc taken as a whole without considering the internal dynamics of the composite system. This approach has provided a good explanation of the experimental results. The following are the details of this work.

1. The jxB Force on the Arc

The usual expression for the jxB force on an arc in a rail gun is $1/2L'I^2$, where I is the instantaneous current and L' is some inductance per unit

length. Since the inductance of a circuit depends in general upon the current distribution, it is not obvious offhand what the correct value of L' should be. In the case of rails with spacing large compared to cross section, the inductance per unit length is nearly independent of the current distribution, and, by considering conservation of energy and Faraday's Law, or by means of the Maxwell stress tensor, it can be shown that L' is just that inductance. If the rail spacing is small, L' will depend on the current distribution, and, therefore, in general upon time. Even in this case, however, we can get a useful estimate of L' by means of the stress tensor in the following way.

The jxB force on an arbitrary volume, V, is given by

$$F = \int j \times B \, dV$$
$$= \frac{1}{\mu_0} \oint_S \left(BB - \frac{1}{2} |B|^2 \mathbb{1} \right) \cdot dS \tag{1}$$

where S is the surface enclosing V, dS is outward, and $\mathbb{1}$ is the unit tensor. For S, (see Figure 4) we take the truncated spherical surface, $\mathcal{S}$, centered about the arc, and the disc, $\mathcal{P}$, perpendicular to the axis of symmetry. The integral over S is the jxB force on the portion of the rails enclosed by S and upon the arc.

We now let $\mathcal{S}$ go to infinity. On $\mathcal{S}$, B is proportional to $1/r^2$. Therefore, the integral on $\mathcal{S}$ is proportional to $1/r^2$ and goes to zero. As $\mathcal{P}$ moves back, B becomes more and more nearly parallel to $\mathcal{P}$, i.e., $B \cdot dS$ goes to zero. This implies that the total force on the rails and arc is given by

$$F_{total} = -\int_{\mathcal{P}} \frac{1}{2\mu_0} |B|^2 dS \tag{2}$$

where $\mathcal{P}$ is now the entire plane.

Of course, in reality we cannot let $\mathcal{P}$ move back indefinitely, because the rails have a finite length. But, for $\mathcal{P}$ back more than a few gap widths (g in Figure 4) from the arc, the magnetic field due to the arc is negligible compared to the field due to current in the rails. The latter field is approximately co-planar with $\mathcal{P}$, more so as $\mathcal{P}$ moves back from the arc. Therefore, for $\mathcal{P}$ at that distance, $BB \cdot dS \ll |B|^2 dS$, and Equation (2) is a very good approximation.

The z component in the forward direction of the force on the rails is

$$F_{rails} = \int_{\Delta\mathcal{P}} \frac{1}{2\mu_0} |B|^2 |dS| + \int_{\mathcal{R}} \frac{1}{\mu_0} B_z B \cdot dS \tag{3}$$

where $\Delta\mathcal{P}$ is the cross section of the rails, $\mathcal{R}$ is the surface of the rails, and dS is now outward from the rails.

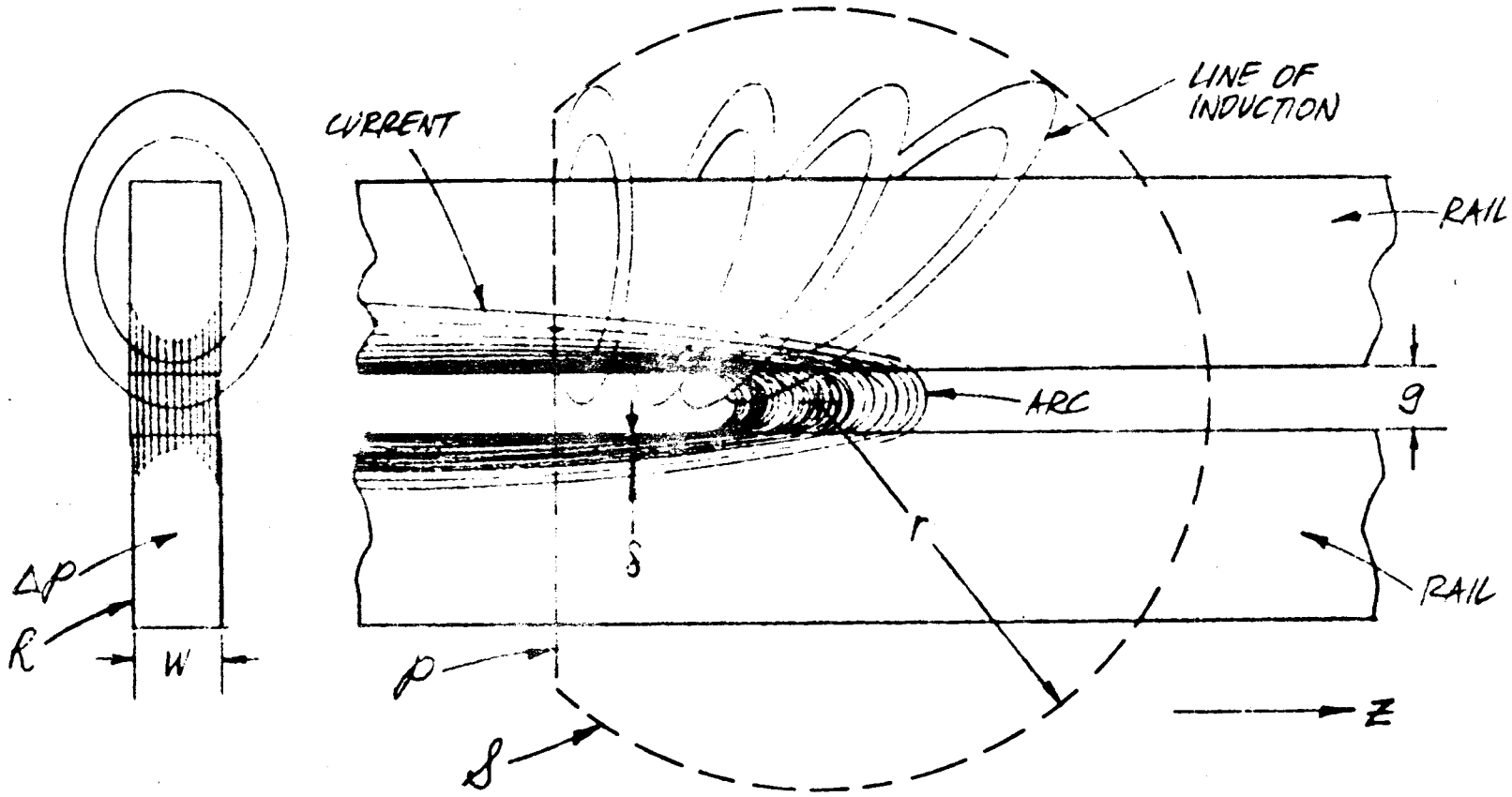

THE ARC DISCHARGE BETWEEN PARALLEL RAILS
Figure 4

MRA 1222

The forward component of the force on the arc, F_{arc}, is just F_{total} minus F_{rails}, or

$$F_{arc} = \int_{\mathcal{P}-\Delta\mathcal{P}} \frac{1}{2\mu_0} |B|^2 |dS| - \int_{\mathcal{R}} \frac{1}{\mu_0} B_z B \cdot dS \qquad (4)$$

The first integral is the external magnetic energy per unit length far behind the arc.

In the case of an azimuthally symmetrical discharge in a coaxial-cylinder rail gun, B is azimuthal, and B·dS is exactly zero over $\mathcal{P}$ and over the entire electrode surface. This implies that the second integral in Equation (4) is zero. The first integral is $\frac{\mu_0}{4\pi} I^2 \ln \frac{r_{outer}}{r_{inner}}$ that is, L' is just the geometrical external inductance per unit length. Because of the azimuthal symmetry, L' is independent of the radial distribution of the current in the electrodes.

Even in case the discharge is not azimuthally symmetrical or in the case of parallel rails, the first integral is still very nearly $\frac{1}{2} L'_{external} I^2$. This becomes evident if we take $\mathcal{P}$ several gap widths behind the initial position of the arc. In that region the problem has approximate translational symmetry in the z - direction for all time.

However, the second integral may no longer be negligible. Near the arc, lines of induction which cut the rails because of their finite conductivity have components both normal to the surface of the rails and along the z - direction. In order to estimate this integral we take a skin depth, δ, corresponding to the time for the arc to travel one gap width. Letting v be the velocity of the arc, σ the conductivity of the rails, and w their thickness, we have

$$g = vt$$

$$\delta^2 = t/\mu_0\sigma$$

$$|B|g \approx L'_e I$$

$$L'_e \approx \mu_0 g/w$$

$$\frac{1}{\mu_0}\int_{\mathcal{R}} BB\cdot dS \approx \frac{g\delta}{\mu_0}|B|^2$$

$$= \left(\tfrac{1}{2} L'_e I^2\right)\left(\sqrt{\frac{g}{w}}\,\frac{2}{\sqrt{v\mu_0\sigma w}}\right)$$

Therefore,

$$F_{arc} = \frac{1}{2} L_e' I^2 \left[1 - \mathcal{O}\left(\sqrt{\frac{g}{W}} \frac{2}{\sqrt{v \mu_0 \sigma W}}\right)\right]$$

where $\mathcal{O}$ stands for "something of the order of." Putting in the typical values

g = 1.5 mm

W = 3 mm

$v \approx$ 5 km/sec

σ = 5.8 x 10^7 mho/m for copper

we have

$$\sqrt{\frac{g}{W}} \frac{2}{\sqrt{v \mu_0 \sigma W}} \approx 0.04$$

This crude result indicates that to a fair approximation the force on the arc is given by

$$F_{arc} \cong \frac{1}{2} L_e' I^2$$

2 Rail Sputtering Limitation on the Projectile Velocity

Some of the experimental data indicates that the mass input to the arc from the rails may be limiting the projectile velocity. This sputtering effect can be taken into account in the equation for the projectile or the arc velocity.

The equation for the projectile (or the arc) velocity is as follows:

$$\frac{d}{dt}\left[M + \int m\, dt\right] v + \text{skin friction} = \frac{1}{2} L' I^2$$

where

v = the velocity of the arc-projectile system

M = the mass of the projectile

m = the rate of change of mass of the arc

I = the current

L' = external inductance per unit length of the rails, which can be measured experimentally.

The skin friction between the plasma and the wall is given by

$$c_f \rho \frac{v^2}{2} (\pi D l)$$

where l is the length of the arc. If it is assumed that the arc very rapidly achieves an equilibrium velocity (as has been shown experimentally), and if the skin friction term was the limiting factor, it would be necessary for the following inequality to hold:

$$c_f \rho \frac{v^2}{2} (\pi D l) \gtrsim \frac{dp}{dt}$$ where p is the momentum of the arc

This is approximately the condition

$$c_f \frac{l}{D} \gtrsim 1$$

Although it is difficult to accurately estimate the effective Reynolds number and the skin friction coefficient, preliminary calculations indicate that for the case under consideration, the skin friction term is negligible.

For $I = I_p \sin \omega t$, which was the experimental case, and neglecting the skin friction, the velocity becomes

$$v = \frac{1}{2} L' \frac{\int_0^t (I_p \sin \omega t)^2 dt}{M + \int_0^t m\, dt}$$

If it is assumed that m is proportional to the current, or $m = m' I$ then

$$v = \frac{L' I_p}{4 m'} \frac{\omega t - \frac{1}{2} \sin 2\omega t}{\frac{\omega M}{I_p m'} + 1 - \cos \omega t}$$

This equation and its integral (position vs. time) is shown in Figure 5 for the case of $M = 0$. Figure 6 shows the integral of the velocity equation plotted for the assumed value of 4.6 atoms sputtered per electron and for the actual experimental values of L' = 0.35 μh/meter, I_p = 150,000 amperes, and M = 2.4 mg. The value of 4.6 atoms sputtered per electron was calculated assuming the equation for the arc position vs. time (plotted in Figure 6) must follow the estimated center of mass of the arc found experimentally. (At much lower current densities there is data which indicates that for some cases there can be as much as one atom lost from the electrode per each eight electrons striking the electrode. (Cobine, James C. Gaseous Conductors. New York, Dover, 1958. p. 301))

It can be seen that the theoretical position vs. time curve is very close to the experimental data. The curve omitting the rail sputtering effect has been made to fit through at 30 μsec. This required L' to be 0.13 μh/meter, approximately one third of the measured value. Furthermore, it can be seen that its shape is not quite right.

MBA 1224

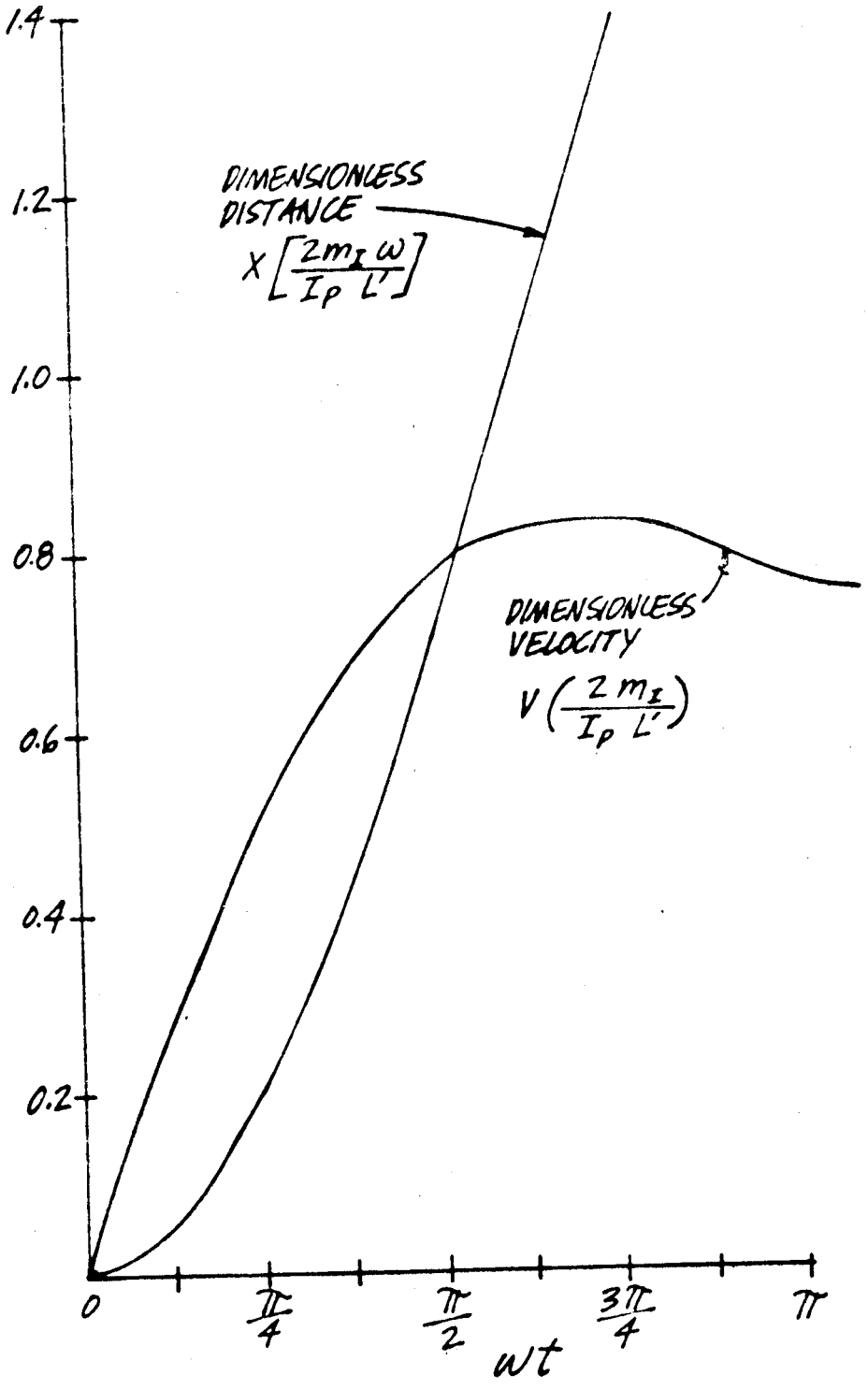

Velocity and Distance Versus Time
for the Sputtering Limited Free Arc

Figure 5

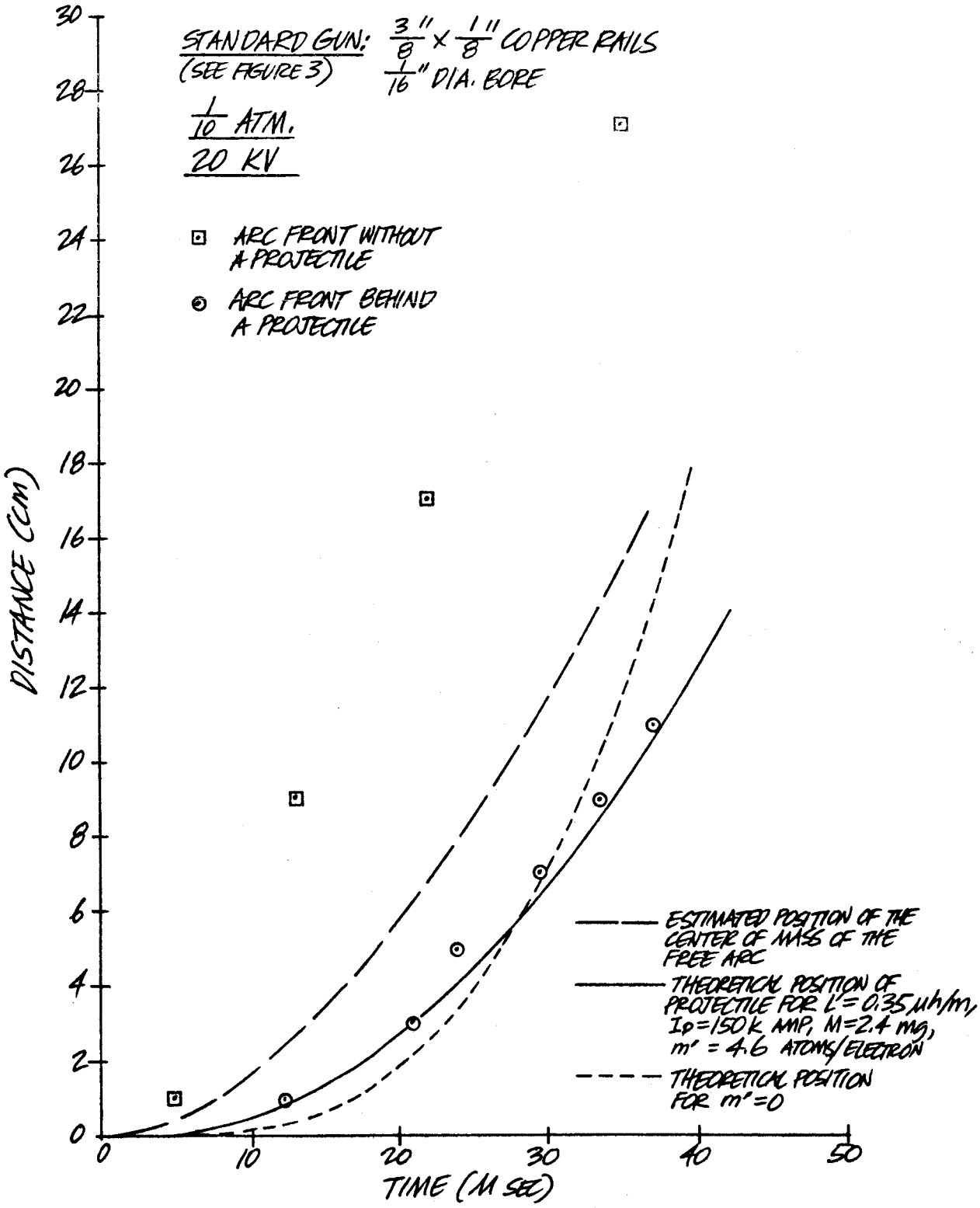

DISTANCE VS. TIME FOR THE PROJECTILE AND

FREE ARC - THEORETICAL AND EXPERIMENTAL

FIGURE 6

B EXPERIMENTAL RESULTS

Table I is a systematic description of experiments in which a projectile was accelerated. (One of the incidental products of these experiments is a number of penetration vs. velocity data. See Appendix D-5.) Figures 7, 8, 9, and 10 represent the results of many flux loop measurements of arc position vs. time. (See Appendix D-6 for the method of measurement.) This section is a discussion of these experiments as well as others not suitable for presentation as tables or graphs.

In the course of these experiments, we determined the effect of several operating conditions and construction features upon the velocity of the projectile. These were:

1) the relative fit between the projectile and the barrel,
2) the height and rise time of the current pulse,
3) the inductance per unit length of the gun,
4) the rate of mass input to the arc,
5) the mass of the projectile,
6) the mechanical construction of the gun,
7) the position of the initial short with respect to the projectile,
8) the ambient pressure,
9) an after-section (see Appendix E).

The following is a summary of these experiments:

1) Projectile-Barrel Fit

A series of experiments was made with a 0.093" nylon ball in barrels of 0.120", 0.116", 0.096" and 0.093" diameter. The projectile velocity increased as the fit improved. The best explanation of this is that unless the fit is good, the arc slips past the ball and transfers momentum by means of drag (see Appendix E).

2) Current

Data for the arc with no ball definitely show that the arc velocity goes up with current (see Figure 9). Because of mechanical failure of the gun, data for currents above 165 kamp have been inconclusive in experiments with projectiles.

3) Inductance per Unit Length

Experiments with various rail cross sections showed that the velocity is a strongly increasing function of rail inductance per unit length in accordance with the theory of Section II-A-1. In the direction of high-inductance

SUMMARY OF RAIL GUN EXPERIMENTS

Shot No.	Rise Time μ sec	Ball Dia. Inches	Bore Dia. Inches	Bore Length cm.	Ambient Pressure	P/D %	Target Velocity km/sec	Muzzle Velocity km/sec	
10.18-1	28-1/2	3/32	.096	8	1 atm	66	2.0	2.7	
21-2	32					41	1.2	1.6	2 mm
22-2	30					74	2.4	3.2	5 mm
23-2	30					55	1.8	2.4	10 mm } between foil and ball
24-1	31					--	.96	1.3	2 mm
24-2	29				18 μHg	52	(1.4)	(1.5)	5 mm
24-3	30				1 atm	121	0.37	0.37	steel ball
25-1	29					63	2.0	2.7	
25-2	29	3/32x.128 cyl				--	1.3	1.7	nylon cylinder 13.3 mg mass
26-1	31	3/32	3/32	4		74	2.2	2.9	
28-1	32			2		57	(1.7)	(2.2)	
29-1	30			1		52	1.4	1.9	
29-2	32			7		85	3.0	4.0	
30-1	32					--	--	1.0	insulator sandwiched between rails
31-1	--					80	2.6	3.5	
11. 1-1	--					88	3.3	4.4	
1-2	30					74	2.7	3.6	
2-1	--	1/16	1/16	6		74	2.9	4.7	
4-1	--	3/32	3/32	7		86	2.8	3.7	
4-2	26	1/16	1/16	6		146	(6.7)	(7.0)	
5-1	26	3/32	3/32	7		97	(3.7)	(3.8)	
5-2	--	1/16	1/16	6	12 μ Hg	107	4.7	5.3	
7-1	--	3/32	3/32+?	7	1 atm	59	(1.8)	(1.8)	molded barrel, flat rails
8-1	--	3/32	3/32+?	7	1 atm	85	(3.0)	(3.0)	molded barrel, beveled rails
8-2	21-1/2	1/16	1/16	6	1/10 atm	114	(4.5)	(4.8)	
11-1	--	3/32	3/32	6	1/10 atm	96	3.1	3.3	
12-1	20	1/16	1/16	9	1 atm	--	--	--	
13-1	23-1/2	1/16	1/16	7	1/10 atm	128	3.9	4.2	
15-1	25	1/16	1/16	7	1/10 atm	66	(2.0)	(2.1)	glass filament wound
18-1	--	1/16	1/16	7	1/10 atm	50	(1.4)	(1.5)	

TABLE 1

Summary of Rail Gun Experiments (continued)

Shot No.	Rise Time μsec	Ball Dia. Inches	Bore Dia. Inches	Bore Length cm.	Ambient Pressure	P/D %	Target Velocity km/sec	Muzzle Velocity km/sec	
11.20-1	--	1/16	1/16	12.5	1/10 atm	158	5.4	5.8	
21-1	--	↑	1/8	9.5	33 μHg	40	(1.0)	(1.1)	ball in 4.75" after section
22-1	--	↓	1/16	13.5	1/10 atm	157	5.6	$\boxed{6.0}$	
25-1	--	.040x.042x.050	.042x.042	13.5	1/20 atm	68	2.2	2.4	crater was rather square
12.13-1	29	1/16	1/16	13.8	1/10 atm	147	5.0	5.4	
13-2	29	1/16	↑	16	↑	63	(1.9)	(2.1)	beveled rails
26-1	30	1/16		16		122	3.6	3.8	
1. 1-4	26	.063		13.5		76	(2.5)	(2.6)	thin rails
8-1	26	1/16		13	↓	146	5.5	5.8	
16-1	30	1/16		11	1 atm	140	(4.9)	5.05	
28-1	28	1/16		9	1/10 atm	58	(1.7)	(1.7)	beveled rails
30-1	29	.065	↓	11.8	1/10 atm	71	(1.9)	(1.9)	coaxial electrodes
2. 6-1	--	3/32	3/32	15	1/10 atm	61	1.7	1.8	

Velocity calculated from transit time ± 2%
Velocity calculated from crater depth ( ) ± 10%
The bank potential was always 20 kv, and except where noted otherwise: (1) The projectile was a nylon ball. (2) The foil was directly behind the ball. (3) The gun was of the standard construction. (See Figure 3)

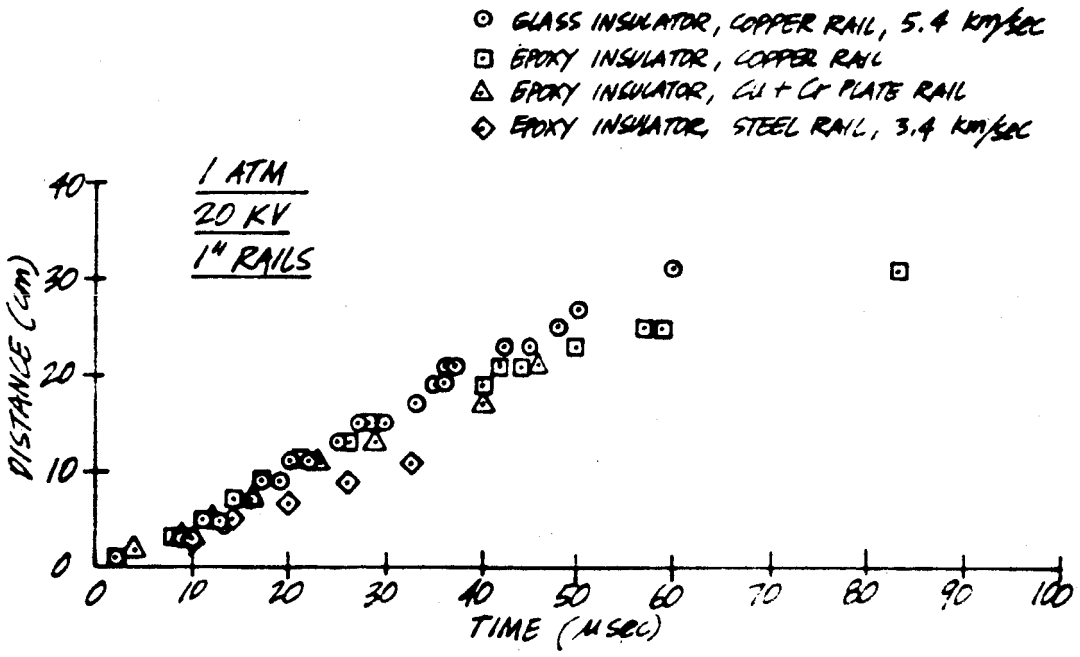

Figure 7

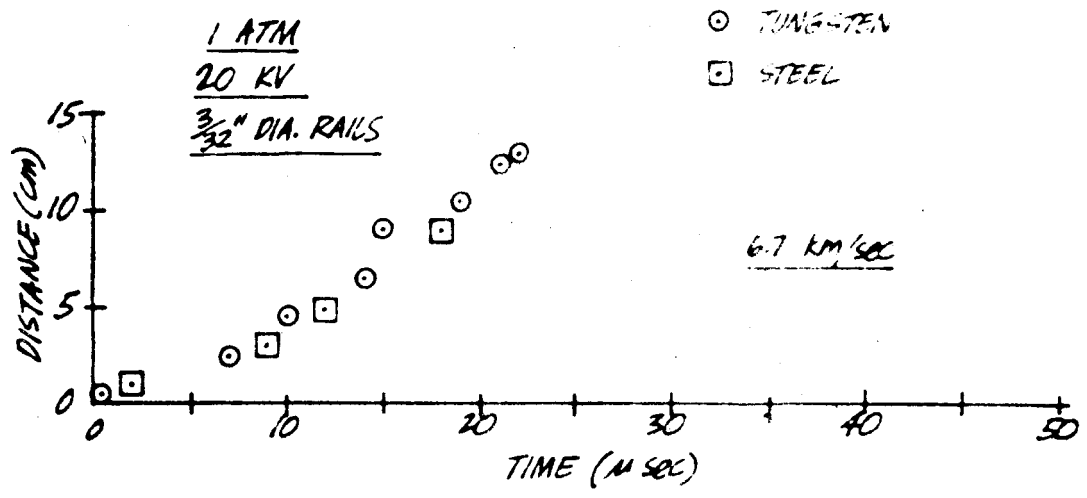

ARC POSITION VS. TIME
(As determined from flux loop measurements)

Figure 8

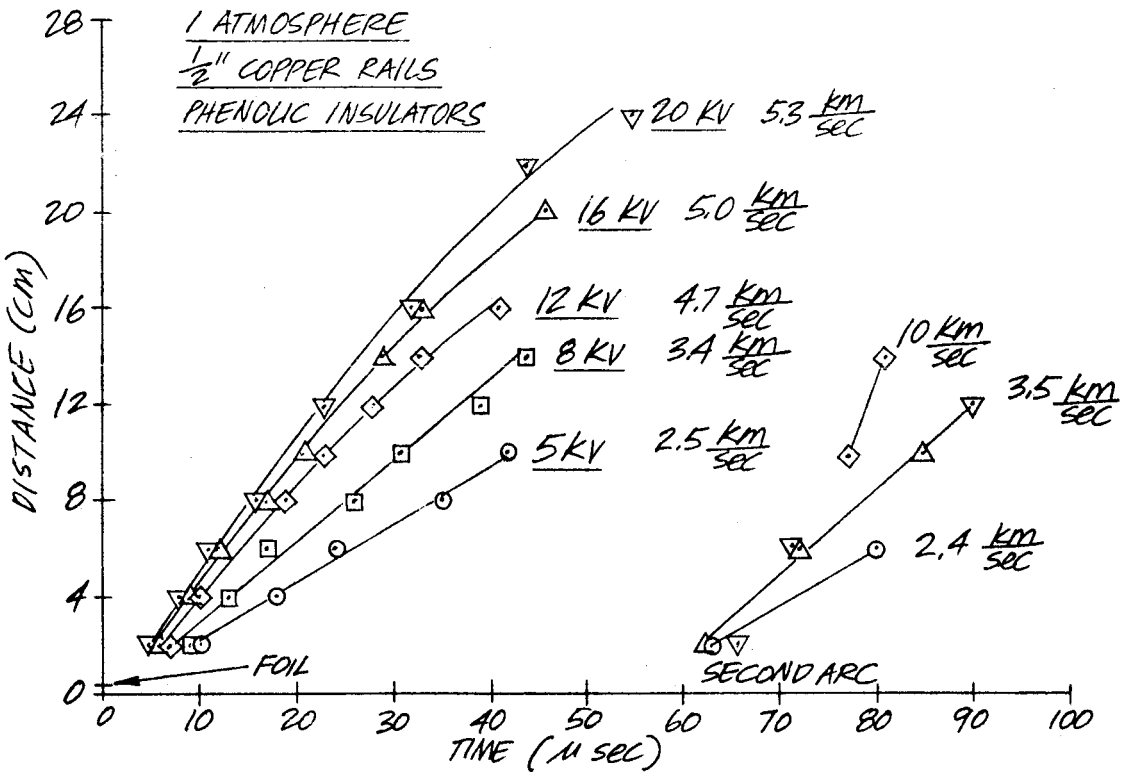

FIGURE 9

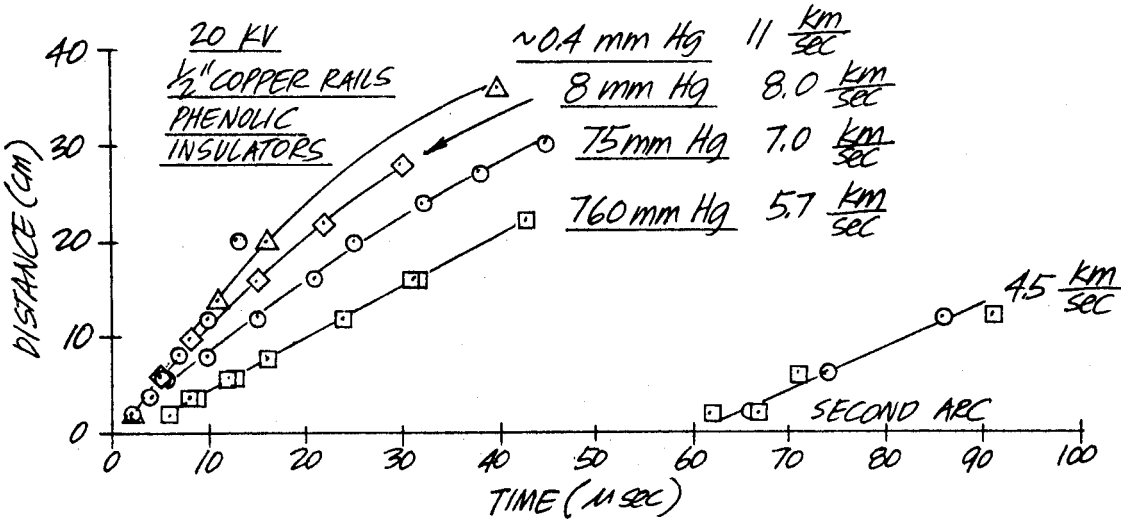

FIGURE 10

ARC POSITION vs TIME
(As Determined by Flux Loop Measurements)

knife edges, however, the difficulty of fabricating the barrel proved to be a limitation. The present shape (see Figure 3) is a compromise between high inductance on the one hand and mechanical strength and close tolerances on the other.

4. Mass Input to the Arc

Weight measurements of the rails before and after a shot showed weight losses of from 5 to 10 milligrams per half cycle of the electrical circuit for both copper and steel rails. This is of the right order of magnitude to account for the velocity limitation discussed in Section II-A-2. Arc position vs. time measurements for rails of copper, chrome plated copper, steel, and tungsten, and insulators of epoxy, phenolic, and glass (see Figures 7 and 8) showed that copper rails are somewhat better than steel and tungsten and that there is no decisive difference between the insulator materials.

5. Mass of the Projectile

Experiments comparing steel spheres and nylon cylinders with nylon spheres of the same diameter showed that the velocity is a strongly decreasing function of mass as is predicted by the theory of Section II-A-2. This is qualitatively obvious on the basis of Newton's Second Law.

5. Mechanical Construction

Since distortion is propagated with the speed of sound, which is roughly 1 or 2 km/sec in the materials of the gun, one expects that the projectile will be outrunning damage everywhere except at the back of the gun where the projectile is traveling slowly. With a sinusoidal current, the jxB forces, which are proportional to $\sin^2 \omega t$, are small when the projectile is starting out. Because of this, we have been able to avoid failures due to distortion of the barrel without elaborate precautions. However, mechanical failure of the electrical connections has occurred occasionally. This will probably become a more serious problem at higher currents.

In addition to parallel rails, we have also tried a coaxial design (see Figure 11) for mechanical reasons. This gun has the advantages over the parallel rail gun we have been using in that it is inherently stronger than the equivalent parallel rail gun. The strength of the gun can be seen as follows:

The arc flows along a radial spoke across the barrel from one electrode to the other. In the region of the arc, the current is heavily concentrated on the side of each electrode near the arc. But, some distance away from the arc--say a few electrode diameters--the current is nearly uniformly distributed over each electrode. Therefore the magnetic field behind this region

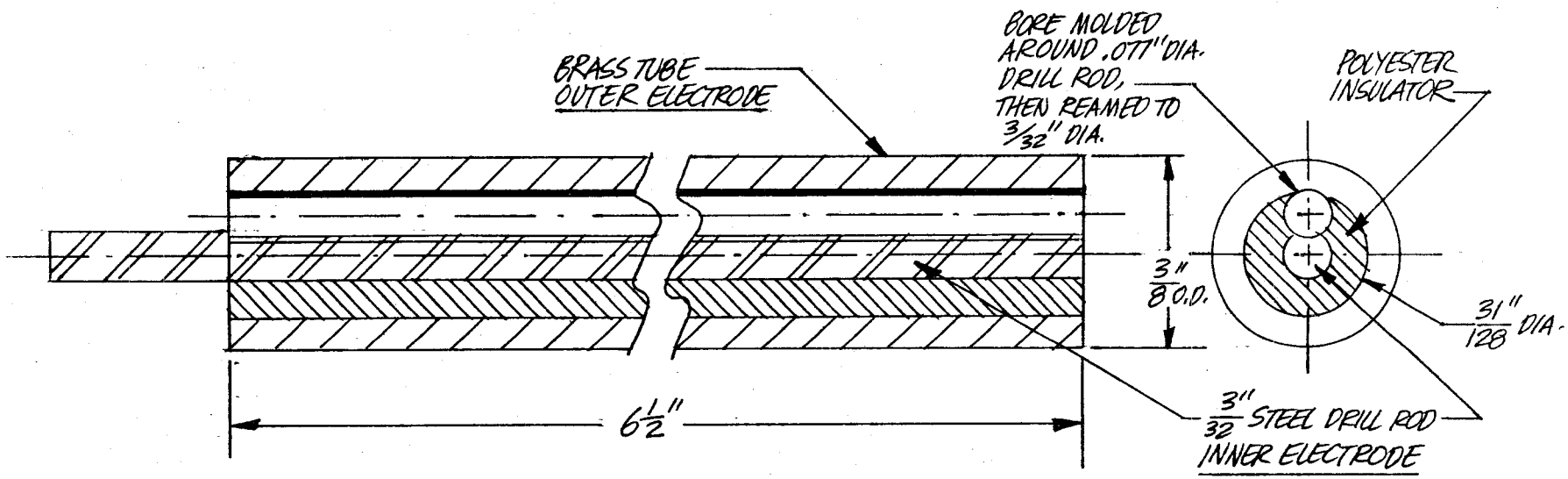

COAXIAL - ELECTRODE GUN

Figure 11

MBA 1099

will be purely azimuthal and the force on each electrode will be a pure uniform pressure. This means that, for one thing, there will be no stress on the insulator except near the arc. For parallel rails, the force tending to separate the rails must be contained by the insulative wrapping.

The condition of both types of guns after a shot confirms this reasoning. The electrodes and insulator of the coaxial gun are hardly damaged at all; the electrodes of a parallel rail gun are twisted, its insulator is pushed away from the rails, and the portion of the insulator that formed the barrel has been completely blown out of the gun. However, the coaxial gun was abandoned because of difficulty in forming the barrel and because of its low inductance compared to the gun of Figure 3 (about one half as much) with resulting lower velocities.

7. Position of the Initial Short

A series of experiments were performed with a 0.093" ball in a 0.096" barrel and spacings of 0, 2, 5, and 10 mm between ball and shorting foil. The velocity showed a reproducible minimum at 2 mm spacing.

8. The Ambient Pressure

Experiments with the free arc at various pressures showed an inverse dependence of the shock front velocity upon, roughly, the logarithm of the ambient pressure. (See Figure 10) One is tempted to explain this in terms of the familiar "snowplow effect." However, the snowplow limited velocity for these guns even at 1 atmosphere is of the order of 1000 km/sec. A likely explanation is that the center of mass of the arc is moving under the limitation of mass input from the rails as described in Section II-A-2, and that the front of the arc, which carries only a fraction of the current, is limited by the snowplow effect. In experiments with a projectile, in which the front of the arc must be behind the projectile and, therefore, near the center of mass of the arc-projectile system, the arc velocity was independent of the ambient pressure.

9. After-Section Guns

Before it was discovered that the arc could be retained behind the projectile by means of a close fit between projectile and barrel, several experiments were performed with after-sections. (See Appendix E) It was found that a projectile could be accelerated by such a device, but that the velocity achieved was lower than that from direct acceleration in the same gun with a close fit.

III MHD GENERATOR

A GENERATOR THEORY

The circuit equation for a closed, flux-containing loop with moving boundaries has been given by Fowler (Bulletin Am. Phys. Soc., 1957). In an elementary form, the idealized circuit has been formulated by Anderson and Whitcomb (SCTM 150-58-51). The sum of the loop voltages must be zero or

$$\frac{\partial \phi}{\partial t} + IR = 0$$

where

ϕ = flux $\left(\int B \cdot dA\right)$

R = resistance

I = current

Now, since $\phi = LI$, the equation can be written $\frac{\partial \phi}{\partial t} + \frac{R\phi}{L} = 0$ (1)

The solution of Equation (1) is $\phi = \phi_0 e^{-\int \frac{R}{L} dt}$

or

$$LI = L_0 I_0 e^{-\int \frac{R}{L} dt} \tag{2}$$

From Equation (2), the current can be calculated for any loop motion once the inductance and resistance are known. The inductance of the loop can be determined from its shape by the usual inductance formulae. The resistance value to be used in Equation (2) should be estimated for each time interval from the heating equation. If a current density j is passed through a conductor, the ohmic losses raise the temperature of the conductor and cause corresponding increases in the resistance. In equation form the heating is given by

$$\eta j^2 dt = \rho c \, dT \tag{3}$$

where

η = resistivity

j = current density

ρ = density

c = specific heat

T = temperature

Using the approximation that $\frac{\eta}{T} = \frac{\eta_0}{T_0}$ (good for most metals up to the melting point) the terms in Equation (3) can be rearranged to give

$$\frac{dT}{T} = \frac{\eta_0}{\rho c T_0} j^2 dt \tag{4}$$

which has the solution

$$\ln \frac{T}{T_0} = K \int j^2 dt$$

where $K = \frac{\eta_0}{\rho c T_0}$ (K is nearly constant for Cu up to the melting point.)

Equation (4) and its solution have been used in an iterative process to determine the temperature change in the loop.

Once the sabot begins to move, a correction must be applied to the inductance profile which includes the inductance added by the sabot motion as shown in Figure 12. For a uniform width sabot and loop, the inductance correction

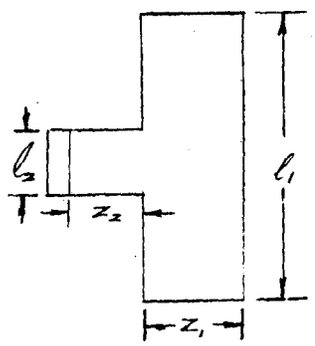

Figure 12

Inductance Correction

amounts to $l_1 z_1 + l_2 z_2$ compared with $l_1 z_1$. The correct value of the inductance can be determined from the sabot displacement and substituted into Equations (1) or (2) to determine the current profile in time.

Deceleration of the pusher plate can be calculated by using the relation

$$\ddot{z}_1 = -\frac{F}{m} = -\frac{F/A}{m/A}$$

where

$\ddot{z}_1$ = acceleration of the plate

F = force

m = mass

A = area

Since the plate starts at velocity, v, the new velocity after deceleration is easily calculated by an iterative process.

In all cases the calculations were stopped when the accelerations became greater than 10^8 g, or when the temperature of the system exceeded the melting point of the metal. Higher melting point metals might be used to reach higher temperatures by using a bimetallic strip arrangement. Steel would be an excellent metal for this type of arrangement. From a theoretical point of view, the bimetallic system greatly complicates the calculations, and has been omitted.

Vacuum pipe has been incorporated into the design to prevent projectile burnup at high velocity. Some thought has been given to sabot separation and, while the problem is exceedingly difficult, a few calculations have been made which indicate a novel feature of the magnetic gun system. If the sabot continues to carry a current at the time of maximum velocity, then it can be decelerated by a magnetic field and hence separated from the projectile.

The force per unit length produced by the interaction of the sabot current and a static field applied by Alnico (or similar permanent magnets) can be calculated from the expression j×B where j is current density and B is the permanent magnet field. Since $F = I dl B$, the deceleration force on the sabot is estimated to be as large as 10 g during passage of the sabot through the static field.

In practice it may prove possible to eliminate most of the sabot by deceleration and a velocity selection system based on timed closure of the launch tube.

Every attempt has been made to reach the desired velocities using a relatively simple system. The original calculations have been refined and carefully redone to include all known effects such as heating, motion, etc. The most serious effect uncovered is the heating of the sabot system to melting temperatures for most of the calculations which reached high velocity. Addition of more high explosive can partially reduce this effect since the sabot system can then be increased to accomodate the required heating. Bimetallic sabot systems have not been completely evaluated but appear to be capable of reducing the effect still further.

B SABOT HEATING

The rate of heat transfer from the sabot to the projectile is given by the equation of thermal conduction

$$Q = KA\nabla T$$

K = thermal conductivity

A = contact area

∇T = temperature gradient

Since the currents fall off exponentially in the sabot material (the skin depth is about 0.08 cms for the current at 300° C), the sabot temperature varies by a large factor from one surface to the other. The maximum gradient possible is about $\frac{1200°C}{0.1\ cm}$ or 12,000°/cm. Under this gradient of temperature, and at a thermal conductivity K_o = 0.91/cal/cm/sec/°C, the maximum rate of heat transfer across the sabot is about 6.5×10^3 cal/sec or less than 2.7×10^{-2} joules/μ sec at the melting point of copper. This rate of heat flow will raise the projectile temperature about 1°C/μ sec. For this reason, the projectile does not heat rapidly by contact with the sabot. Since the time is very short, the total heat transferred to the projectile is almost negligible. Again the bimetallic strip could all but eliminate even the small amount of heat transferred since materials with smaller K could be utilized.

C DESIGN CALCULATIONS

Various combinations of parameters have been tried in an iterative calculation procedure. The general effect of changing parameters is discussed below.

1. Increasing S_o, the initial loop width permits more complete energy transfer and reduces the peak acceleration, but increases the temperature.

2. Increasing the current density in the sabot, J**, increases the magnetic field strength, thus increasing efficiency and velocity, but causes the temperature to increase sharply.

3. Increasing the initial piston velocity, V_o, helps hold down the temperature and increases ultimate velocity, but more high explosive is required and overall system efficiency is reduced (due to greater difficulty of effectively tamping the explosive).

4. Reducing the initial temperature, T_o, not only reduces the ultimate temperature, but drastically reduces the rate of temperature rise. It also improves overall system efficiency by reducing the L/R current decay.

1. Rectangular Loop

The following parameters are for a system which accelerates a 0.1 projectile to 90,000 feet per second, using 600 grams of high explosive.

1) S_o = 12 cm; length = 20 cm; thickness = 1.9 cm. Inductance is 0.425 μh.

2) $J^{**} = 1.5\ J^*$ (J^* = true current density in the loop)

3) $T_o = 77^oK$

4) Sabot mass m = 1.14 gm; sabot dimensions 1.27 x 0.635 cm x 0.159 cm. The pressure required to shear the sabot from the main loop is 4.1×10^9 dynes/cm^2. Projectile mass for all calculations is 0.1 gm.

5) V_o = 3.75 m/sec

6) $I_o = 3.90 \times 10^5$ amperes, and $H_o = 2.5 \times 10^5$ gauss at the sabot.

The results of this calculation are represented by Figures 13, 14, and 15.

Figure 13 shows that the magnetic field strength behind the sabot reaches 1 megagauss. This is a pressure of 4.14×10^{10} dynes/cm^2 (6×10^5 psi). Without sabot motion the rate of rise would be much greater and about 4 megagauss would be attained. The rate of acceleration increase is shown in Figure 14. The peak acceleration is 27.5 megagauss. The reduction of the rate of rise that occurs around 15,000 ft/sec velocity is due to the effect of sabot motion on the overall inductance of the MHD circuit.

The temperature rise in the backside of the sabot is shown in Figure 15. This curve is actually the average temperature in the skin depth layer in which 63% of the current is flowing.(1) Since δ = 0.08 cm, the median of the temperature profile occurs at about 0.03 cm (since the temperature on the graph at 90,000 ft/sec is 75% of the melting point of copper. Therefore, at this velocity the sabot will be liquid to a depth of 0.015 to 0.020 cm, which is about 10% of its thickness.

(1) The skin depth, δ, is the distance of current penetration into a conductor at which the current density is $1/\ell$ times that at the surface.

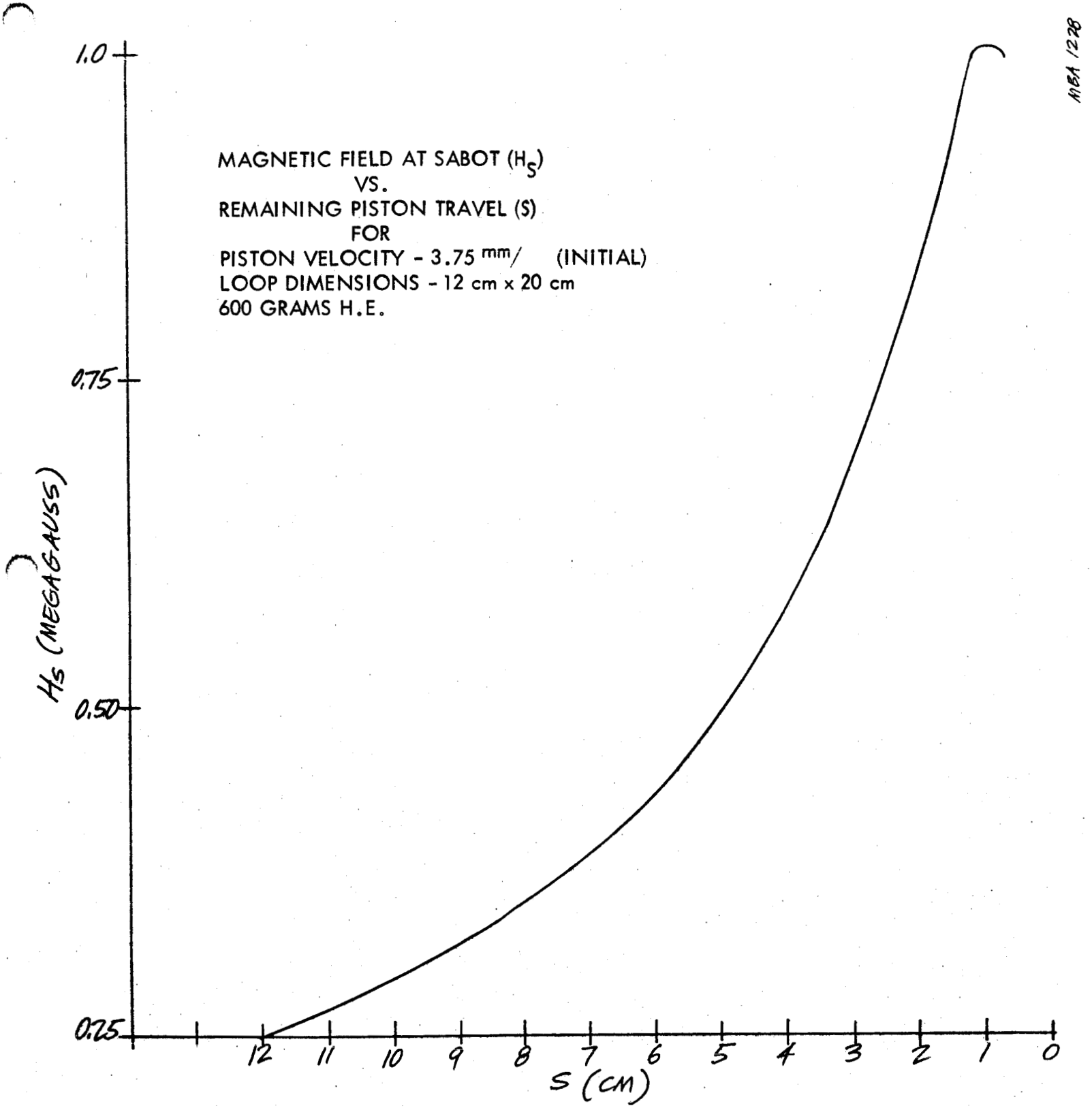
MAGNETIC FIELD AT SABOT (H_S)
VS.
REMAINING PISTON TRAVEL (S)
FOR
PISTON VELOCITY - 3.75 mm/ (INITIAL)
LOOP DIMENSIONS - 12 cm x 20 cm
600 GRAMS H.E.
1.0
0.75
0.50
0.25
H_S (MEGAGAUSS)
12
11
10
9
8
7
6
5
4
3
2
1
0
S (CM)

FIGURE 13

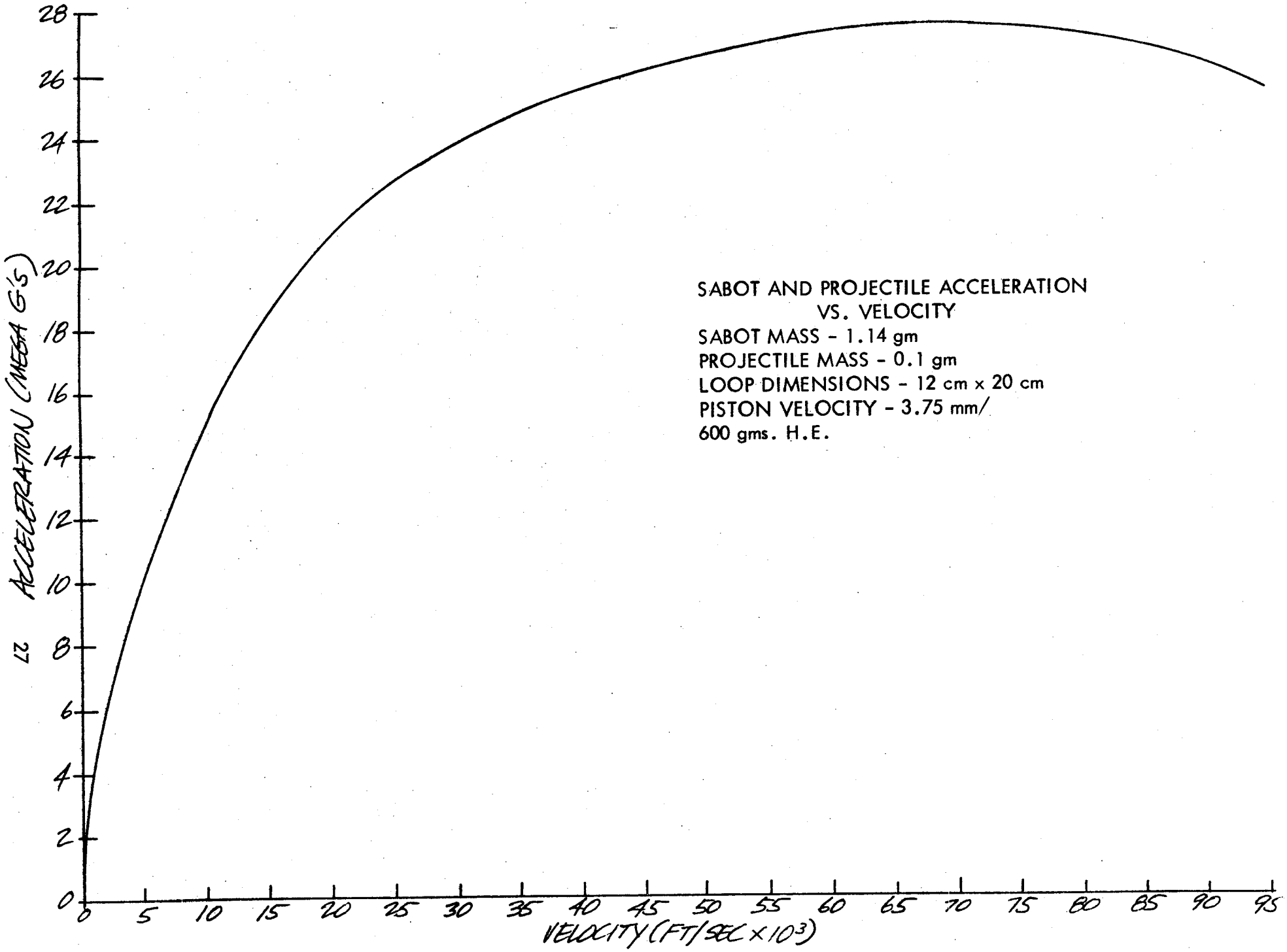

FIGURE 14

MBA 1229

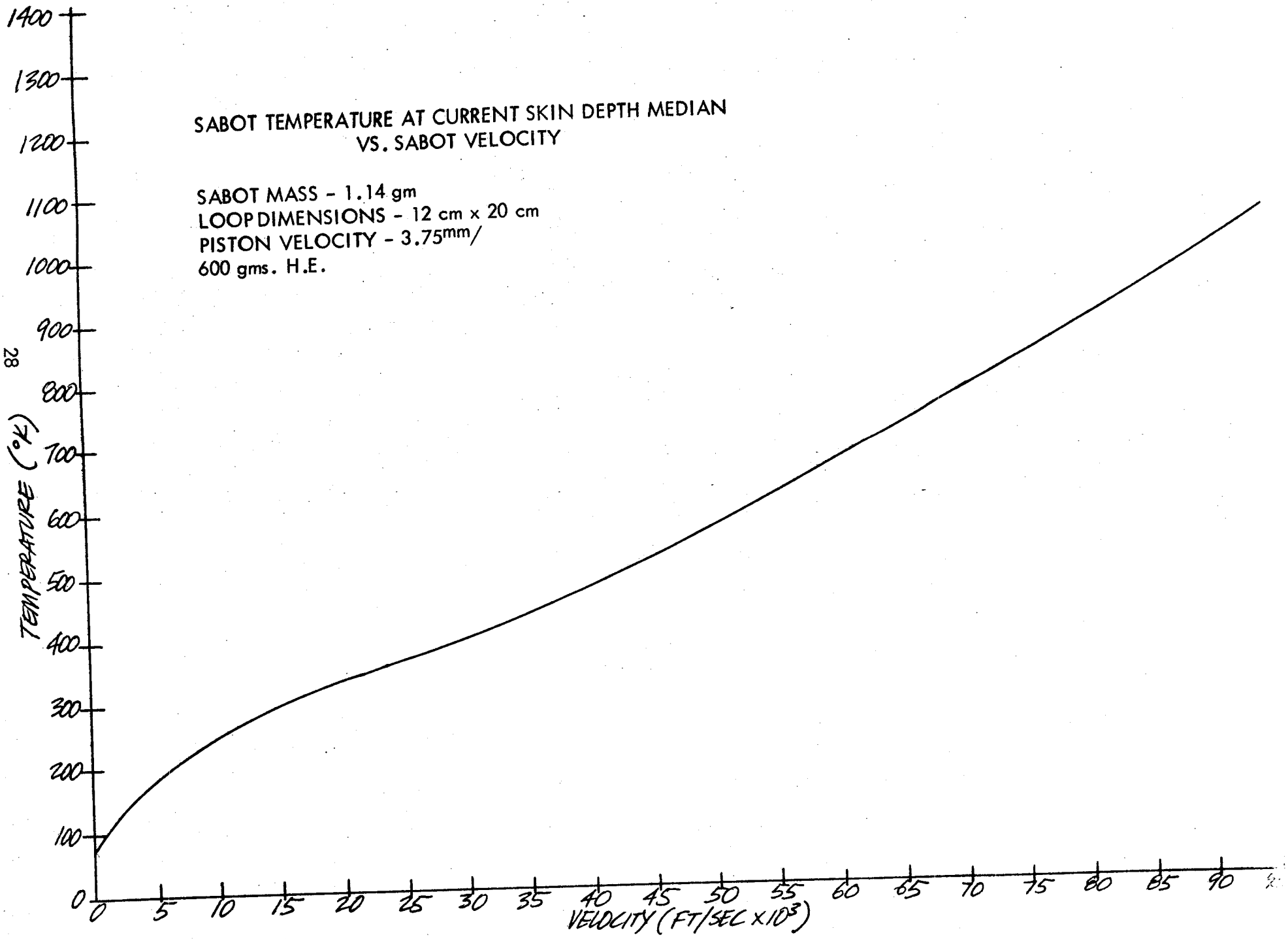

FIGURE 15

MBA 1230

2. Converging Loop

For a loop radius of curvature of 12 centimeters, a piston thickness of two millimeters and an H. E. thickness of 4.5 to 5.6 centimeters (360 - 470 grams), the desired piston velocity (3 millimeters per microsecond) can be obtained. This design improves the coupling due to convergence, reduces plate losses due to decreased path length, and provides higher piston velocity at critical times due to thickening of the piston in convergence. A loop inductance can be made to fit the parameters between the values of 0.12 to 0.18 microhenry. The frequency and skin depth can be calculated; ideal skin depth at late time is about 1.5 millimeters. In this geometry, $B_{(sabot)}$ is greater than $B_{(pusher)}$, resulting in higher percentage of coupling and greater velocity multiplication potential and helping to overcome losses. The ratio of B_s to B_p can be made as large as 8.1. The converging loop is shown schematically in Figure 16.

The current needed to produce the driving field is 400,000 to 500,000 amps if the loop is driven directly. External coils permit initially high flux at zero loop current resulting in lowered heating of the system. Also, the higher inductance of the external coils increases the magnetic field rise time, thus reducing the chance for error in timing the firing of the explosive. Another advantage of this sytem is that shrapnel from the piston should be diverted from the path of travel of the sabot and projectile.

There is a possibility that the higher temperature characteristic of the converging loop could be used to advantage. If the sabot can be vaporized completely, which is likely to happen, then the problem of separating the sabot from the projectile will be solved. During this time period, the projectile temperature should not increase significantly due to the short time available for heat transfer to take place.

D EXPERIMENTAL RESULTS

Table 2 is a summary of the results of the generator tests. A more complete discussion of each experiment is shown as Appendix A. These experiments were planned basically as tests of the complete system. Considerable difficulty in explaining the results was encountered during the early tests due to insufficient diagnostics. It was believed that the relatively poor results were a fault of the generator (basically a current multiplier). Later, it became apparent that the primary problem was in the launch tube. Experiment 4.5-1 showed good convergence for the purpose of generation. Experiment 4.6-1 gave a field compression of 10 with a peak field of 0.3 Mg. Although this was not as high as desired, it was sufficient for the purpose of achieving a reasonable energy multiplication. At this point, generation experiments were terminated and the primary emphasis was placed on the design of a satisfactory launch tube.

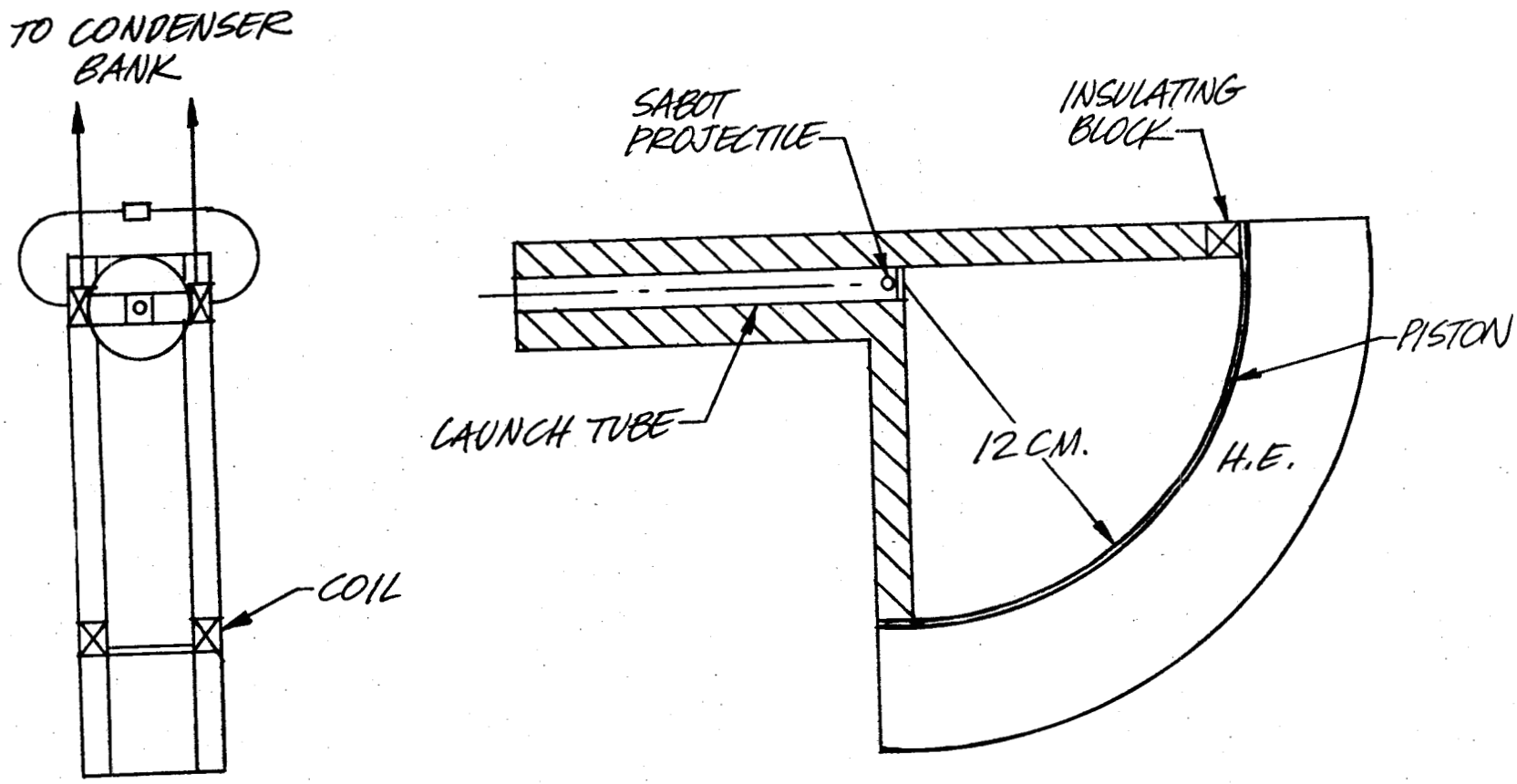

SCHEMATIC OF TRANSDUCER

CONVERGING LOOP

FIGURE 16

MBA 1240

Experiment No.	Purp
4.2-1	Piston Velocity, Convergence, Field Compressio
4.2-2	"
4.2-3	"
4.3-1	"
4.3-2	"
4.3-3	"
4.3-4	"
4.3-5	"
4.3-6	"
4.3-7	"

SUMMARY OF GENERATOR EXPERIMENTS

ose	Device	Energy Into Device	Explosive	Projectile Size	Sabot Size	Remarks
n	Converging Loop, No Launch Tube	15.4 kj	450 gm	None		Measured 1.75 Mg
Sabot Velocity	Converging Loop And Launch Tube	27.5 kj	450 gm	-		Launch tube pins shorted at velocity of 31,500 ft/sec target pitted.
"	-	27.5 kj	450 gm	-		Piston velocity 3.8 mm/msec No Launch tube pin measure ment due to ground loops.
"	12 cm radius converging loop	Ext coils 27.5 kj	450 gm	None		Piston convergence appearec good. Sabot sheared late.
"	Rectangular loop system, slug sabot	350,000 amps peak current	300 gm	43 mg steel sphere	1/8x1/8x 1/4 cm	No measured velocity.
"	"	Ext coils 27.5 kj	425 gm	59 mg steel sphere	1/8x1/8x 1/4 cm	Timing error
"	"	5 kj input	200 gm	0.5x1.25x0.040 2 gm, 1/2 round		1/2" deep crater
"	"	Ext coils 27.5 kj	425 gm	0.187" dia. 54 mg 0.197 long sphere		Crater volume 6 times projectile volume
"	"	Ext coils 14 kj	200 gm	0.5x1.25x0.040 2 gm 1/2 round		
"	"(12 cmx20cm)	Ext coils 27.5 kj	525 gm	54 mg steel sphere	1/4x1/4x 1/4 cm	No field multiplication

Experiment No.	Purpose
4.4-1	Piston Velocity, Convergence, Field Compression
4.4-2	"
4.4-3	Hydrodynamic Test
4.4-4	Magnetic Field Co
4.4-5	Field Compression
4.5-1	Hydrodynamic Tes
4.6-1	Magnetic Field C
4.6-2	Long Pulse Length

Summary of Generator Experiments (Continued)

e	Device					
Sabot Velocity	Converging loop system 12 cm radius, 20 cm launch tube	12 kj	450 gm	3/64 steel sphere	1.5mm dia. 1.5mm long	Condenser bank triggered late
"	Converging loop, 12 cm radius	13 kj	450 gm	None		No field multiplication
	Converging loop, 12 cm radius	None	450 gm	None		Piston velocity 4 mm/msec, good convergence
mpression	Converging loop, 12 cm radius	13 kj	450 gm	None		No field compression (appeared to be poor piston contact)
Sabot Velocity	Converging loop, 12 cm radius	Ext coils 25 kj	450 gm	3/64 steel sphere	1.5mm dia. 1.5mm long	No field compression (probably due to arcing)
	Converging loop, 8.5 cm radius	None	156 gm	None		Good convergence
mpression	Converging loop, 8.5 cm radius	30 kj input	160 gm	None		Field compression of 10 was measured, peak field 0.3 Mg
Generator	45° loop, 11.6 cm radius	None measured	600 gm	1/8" nylon sphere		Electrical breakdown occurred in generator, no field measured.

TABLE 2

IV RECOMMENDATIONS

The partially verified theoretical considerations of Section II-A indicate that, for a given projectile, higher velocities can be obtained by:

1) decreasing rail sputtering
2) increasing the external inductance per unit length of the rails
3) increasing the current

Experiments with several kinds of rail materials have been unsuccessful in accomplishing the first. (See Section II-B) One expects that greater effort in this direction would yield only marginal improvement.

Also, several attempts have been made to increase the inductance of the rails by making the electrode portion tend towards a knife edge or a thin wire. With these small cross sections, it has proved difficult to make a good barrel. Furthermore, mechanical strength and current capacity impose a lower limit on the cross section of the rails for a given barrel diameter. As an estimate of the inductance at such a limit, consider the following design:

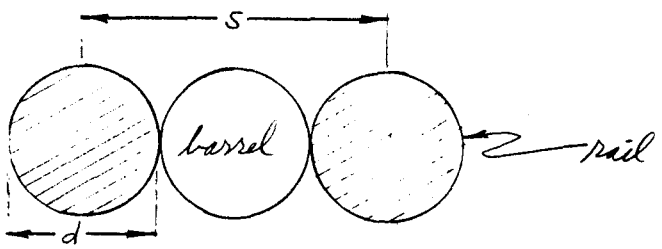

where $s = 2d$. The external inductance per unit length of such a rail pair is

$$L' = \frac{\mu_0}{\pi} \cosh^{-1} \frac{s}{d}$$

which in this case is 0.43 μh/m. This compares with about 0.35 μh/m for the design of Figure 3. The 23% increase in velocity to 7.4 km/sec due to the increase in inductance ($v\ (\omega t = \frac{\pi}{2}) \propto L'$) would be far short of the final goal of 30 km/sec.

On the other hand, increasing the current should give improvement up to the point of mechanical failure. Since, at present, we have 28 kjoules of electrical energy poorly coupled to the rail gun, the natural way to gain this increase in current is to use a setpdown pulse transformer between the condenser bank and the gun. A pulse transformer of the proper inductance and mechanical strength can be built fairly easily with a coupling efficiency of 80%.

A reasonable method of operation using such a transformer would be to make the coupling ratio the geometric mean between the gun inductance and the source inductance. Almost all of the bank energy would then be dumped in one pulse. The projectile would be accelerated during the first half of the pulse in order to achieve the maximum velocity. About half the bank energy would go into resistive heating.

Of the remaining half, about a quarter would go into the projectile, and three quarters into acceleration of plasma and neutral gas. This amounts to, say, 4,000 joules into the projectile, enough to accelerate an 8 mg mass to 30 km/sec.

In accordance with these considerations, we recommend the following:

1. Increase the current by means of a pulse transformer, at the same time increasing the mechanical strength of the gun as necessary.

2. Replace the condenser bank source with the high explosive MHD generator in case a compact source is desired.

APPENDIX A

GENERATOR TESTS

This appendix gives a discussion of each of the experiments conducted with the explosive generator system. Instrumentation was basically the same in all the tests and is discussed in detail in Appendix C.

The experiments are numbered, for example, as 4.2-1 where the 4 stands for NASA hypervelocity project at MBA, the number to the right of the decimal point is the quarter during which the experiment was performed, and the hyphenated digit is the experiment number during the quarter.

A. 1. Experiment 4.2-1

Purpose

a) Measure piston velocity and convergence.

b) Measure compression of magnetic field.

Device

Converging type magnetohydrodynamic transducer loop without sabot, projectile, and launch tube.

Instrumentation

a) Piston velocity - six pin switches placed as shown below.

b) Magnetic field - one turn of #34 wire in convergence corner of loop. Area perpendicular to B field $5 \times 10^{-6} m^2$.

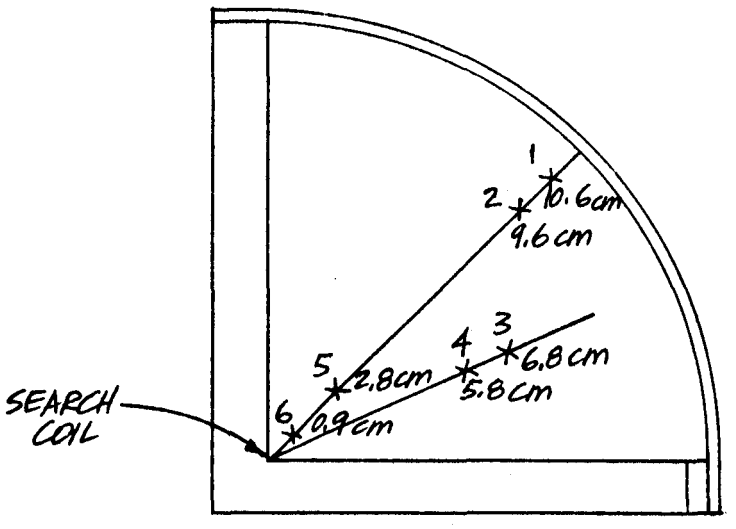

Input Conditions

Approximately half the available condenser bank energy.

a) Magnetic field energy - 15.42 kilojoules

Results

a) Piston velocity - The signals from pins 1, 3, and 5 are valid whereas pins 2, 4, and 6 did not function properly.

b) Piston convergence - Post shot recovery of loop parts indicates proper convergence along the axis.

c) Magnetic Field - The maximum field measured was 1.75 megagauss at 80.5 μsec, at which time the pickup coil was struck by the piston.

d) Comments - The increase in velocity of the piston was expected and due to the velocity increment added to the front face during convergence.

Because of the space occupied by the search coil, the peak magnetic field was probably much higher than the maximum measured. This would occur within an additional 0.5 μsec, which agrees with the calculations. The oscillatory signal after the magnetic field signal is typical of the action when the search coil is struck, putting it in direct contact with the loop currents during final breakup of the device.

2. Experiment 4.2-2

Purpose

a) Test complete gun system.

b) Measure projectile velocity and acceleration.

Device

Converging type magnetohydrodynamic transducer loop with 0.050 inch thick sabot and 103.5 milligram tungsten carbide projectile.

Instrumentation

a) Transducer loop closure--two pin switches placed as shown below.

b) Sabot and projectile velocity and acceleration--four pin switches and three magnetic field pickup loops placed as shown below.

c) Magnetic fields--two search coils, one 0.200 inches diameter; the other 0.100 inches in diameter. Area of the coils perpendicular to the B field is 2.025×10^{-5} meters^2 and 5.06×10^{-6} meters^2 respectively. The large coil is for measuring the low level B field, and $\frac{dB}{dt}$.

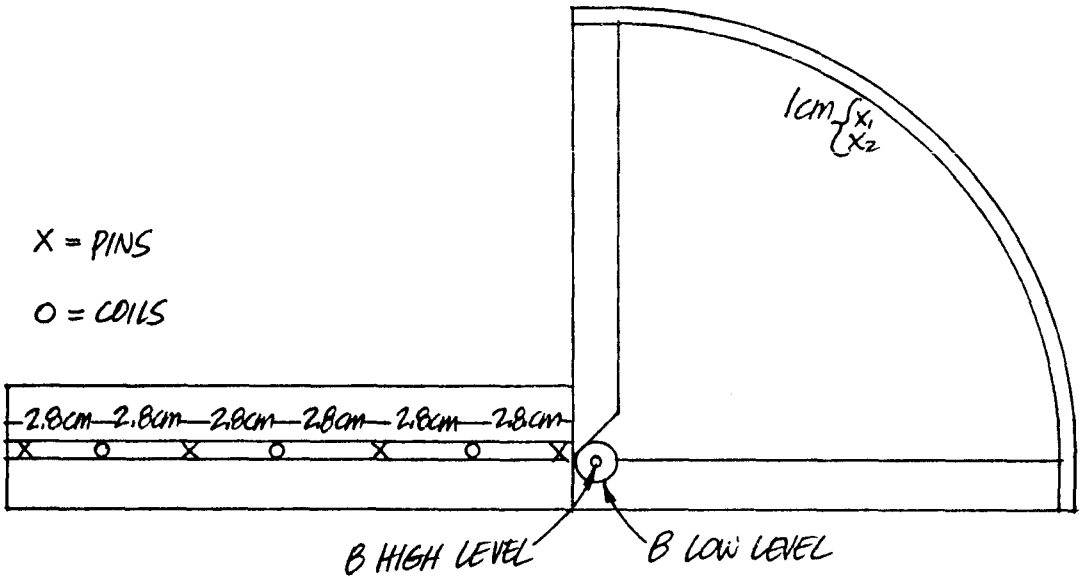

Input Conditions

a) Magnetic field energy - 27.5 kilojoules

b) Barrel air pressure less than 1 micron Hg

c) Target - 356-T6 aluminum

Results

Electronic data acquisition on this experiment was poor due to a ground loop in the condenser bank causing spurious signals in the oscilloscopes. No magnetic field information was obtained however, the pin signals did come through very well on the rasterscope.

a) Pin measurements on the launch tube show the sabot and projectile velocity increasing smoothly to a maximum of 31,500 ft/sec. The peak acceleration occurred at the maximum velocity, and was 130 megag.

b) No single large particle impact was observed on the target, however, the target was struck by many small particles, and possibly some vapor, in a well-defined circular zone about half the target diameter. The chemical analysis of the target shows the presence of tungsten.

c) A pin signal was received which indicated that the sabot sheared early, possibly from the charging magnetic field from the condenser bank. A post-shot experiment, however, disproves this possibility, and the signal must be considered in error.

d) Pin measurements in the loop itself indicate a lower piston velocity than in experiment 4.2-1. This is in doubt, as pins often give erroneous signals. However, the pin signals from the velocity measurement on the launch tube also are delayed in time. This is not inconsistent with a low piston velocity.

e) Comments - Two design innovations were tried on this experiment. In one of them the explosive was built into a separate compartment which was slipped into place after the loop was mounted in the tank, and all pre-shot checkouts accomplished. This was to simplify handling; however, it could have caused a loss of tamping effectiveness, resulting in a lower piston velocity. A second experiment which was tried was to make an HE shorting switch which would automatically crowbar the condenser bank out of the circuit after the field had been trapped. It is believed that this switch was not particularly effective, and in general it is probably not necessary. Post-shot recovery fragments showed proper piston convergences.

3. Experiment 4.2-3

Purpose

a) Repeat experiment 4.2-2, using less brittle projectile.

b) Utilize more pin-type instrumentation to try to improve data acquisition.

Device

Converging type magnetohydrodynamic transducer loop with 0.050 inch thick sabot and 59.3 milligram Inconel-X projectile.

Instrumentation

a) Piston velocity - 6 pin switches placed as shown in the diagram below.

b) Sabot and projectile velocity accelerations - 6 pin switches placed as shown in the diagram.

c) Magnetic field - 2 search coils potted into the lead epoxy sides just behind the sabot, both coils with an effective area of 1.05 x 10^{-5} meters^2. Since the coils are outside of the plane of the transducer loop, they are calibrated to the field in the transducer loop plane. The signal from the B high level field must be multiplied by 1.25 to obtain the true field, and the signal from the B low level coil must be multiplied by 1.67 to obtain the true field.

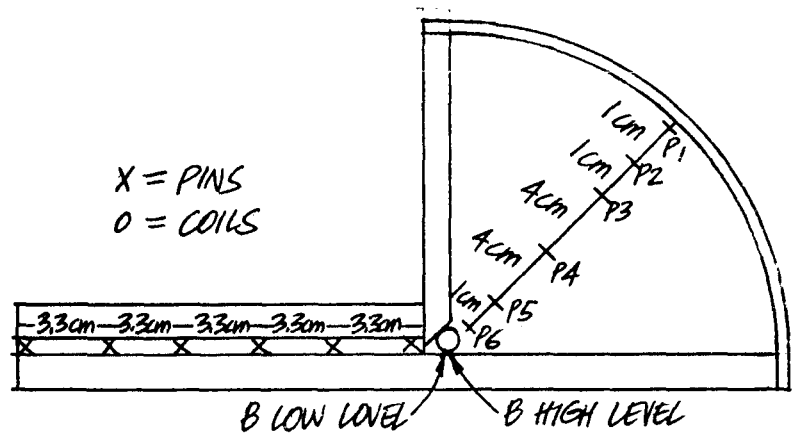

Input Conditions

a) Magnetic field energy - 27.5 kilojoules

b) Barrel air pressure - approximately 1 mm Hg

c) Target - 356-T6 aluminum

Results

Before firing this experiment, ground loop interference signals from the condenser bank were carefully eliminated. During the shot, however, an insulator in a condenser bank control circuit broke down, causing an arc which connected the condenser bank ground circuit into the instrument ground; therefore practically all of the data was lost. A clean, low level magnetic field signal was obtained, however.

a) The B low level field trace indicated that the magnetic field reached megagauss values. Loop closure was approximately 12 μsec late, resulting in a lower trapped magnetic field. Considerable arcing and poor contacts of the piston to the side of the loop apparently occurred during the first fifteen microseconds of piston run. However, the piston recovered contact and compressed the magnetic field.

b) No single large impact was observed on the target, and fewer small particles struck the target than in experiment 4.2-2. Chemical analysis of the target, however, does show the presence nickel, so that at least part of the projectile struck the target. A chemical analysis of the launching rails was also made, and much nickel was found plated on the inside of these. It appears therefore that the projectile was partially vaporized during the acceleration. This may be due to contact with the arc running behind the sabot, or to pulverization of the projectile because of acceleration with the fine particles being deposited on the rails.

c) Recovery fragments indicate proper convergence.

d) Comments - The late closure of the loop had been previously suspected. Post-shot experiments indicated that the detonator functioning time is considerably longer than that stated by the manufacturer. This time, which is approximately 10 μsec, will be accounted for in future experiments. The magnetic field trace does show that the piston velocity must have been corrected--that is, approximately 3.8 mm/μsec. This corresponds to experiment 4.2-1. No separate explosive compartment was used on this shot as was in experiment 4.2-2, and there was no explosive crowbarring switch across the charging coils from the condenser bank.

On this shot an attempt was made to evacuate the launch tube rail region besides the barrel. Difficulties with sealing the vacuum around the sabot and projectile resulted in the higher air pressure. If the projectile came out with high velocity, it could have been vaporized by air friction. This may partially account for the apparent small amount of projectile material which struck the target.

4. Experiment 4.3-1

Purpose

a) Determine time of sabot shearing.

b) Determine uniformity of piston convergence.

c) Check detonator, line wave generator and explosive function times.

Description of Test Model

The device was a 12 cm radius converging transducer loop without launch tube.

a) Sabot - 0.129" x 0.139" x 0.053" thick, shear type, area of shear 0.0882cm^2.

b) Projectile - 0.094" diameter chrome alloy steel sphere, weight 54 mg.

c) Explosive - 450 gm Composition C.

d) Input energy from external charging coils - 27,500 joules input.

Instrumentation

a) Sabot shearing time - two pin switches placed as shown in diagram below.

b) Magnetic field strength and rate of change - one turn pick-up loop in convergence corner.

c) Piston convergence - eight pin switches placed as shown in the diagram.

d) Explosive train function times - two pin switches placed as shown.

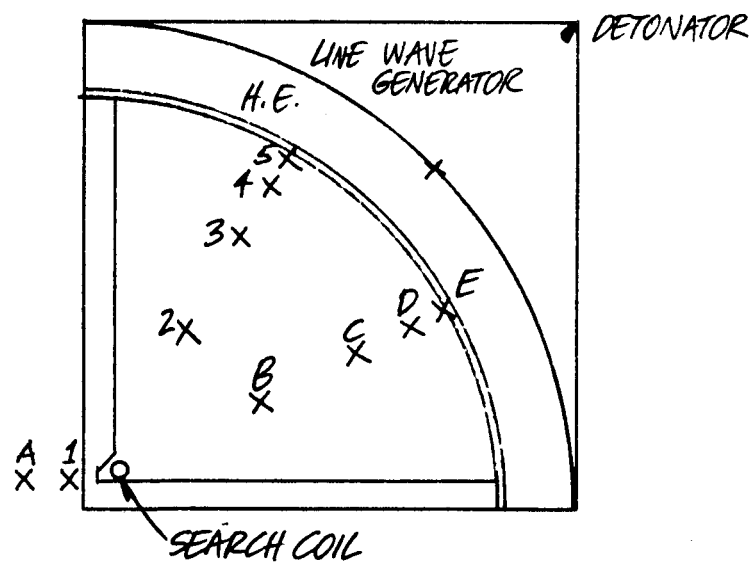

Results

The explosive train functioned very nearly as scheduled. The detonator delay was measured to be 10 microseconds. This compares with previous measurements but is much greater than that given by the manufacturer. The line wave generator's functioning time was measured to be 42.3 microseconds which agrees well with the predicted time of 41.4 microseconds. The detonation time of the explosive was measured to be 8 microseconds, the predicted time was 8.3 microseconds.

The measurements which were obtained indicate that the sabot sheared very late in time, at approximately 90% of the piston run. This indicates that the dynamic shear strength of copper under the conditions imposed, is much greater than had been expected. There is a possibility, ofcourse, that the piston hit the sabot, but it is believed that it was sheared by magnetic field pressure. This late shearing time resolves a time discrepancy in the data on experiment 4.2-2.

The pin signals indicate that the uniformity of piston convergence was excellent. The signals from corresponding pins in the two strings of pin switches occurred virtually simultaneously.

5. Experiment 4.3-2

Purpose

a) Test rectangular loop system.

b) Try slug type sabot.

Description of Test Model

The device used in this experiment was a 12 cm x 20 cm rectangular transducer loop, with a 17 cm long launch tube. This loop was designed to impart a much lower acceleration force to the projectile. Also, the sabot was made as a separate piece, press-fitted between the launch rails, so that no delay in acceleration run would occur.

a) Sabot - 0.125" x 0.125" x 0.250" long copper slug.

b) Projectile - 0.0[illegible]" diameter chrome alloy steel sphere, weight 54 mg.

c) Explosive - 300 gm Composition C-3.

d) Input energy from condenser bank was applied to the loop. The peak initial current in the loop was 350,000 amperes.

Instrumentation

a) Magnetic field strength and rate of change - one turn pick-up loop at junction of launch tube and compression loop.

b) Piston velocity - six pin switches placed as shown in the diagram below.

c) Projectile and sabot velocity - six pin switches placed as shown.

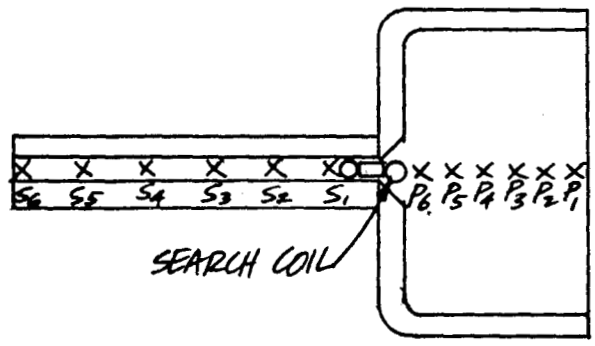

Results

The sabot was heated very drastically, probably by the very large initial charging current. It proceeded a few centimeters down the launch tube before apparently vaporizing. By this time the projectile had acquired a velocity of several thousand feet per second. Without the sabot to continue the acceleration down the launch tube, the projectile gained no further velocity and without guidance from the sabot, it began to bounce between the inside walls of the launch tube. This is quite evident from recovery of parts after the shot. Because of the slow velocity of the projectile, the piston completed its run and impacted on the end of the launch tube connected to the loop. The shock from this running down the launch tube closed the rails on the projectile and it was trapped just before leaving the end of the tube. Marks and indentations on the inside of the launching rails show this very clearly and prove that the projectile was intact when it was trapped near the end of the tube.

It was observed from the recovery fragments from the shot that the piston did not make as good a contact as desired with the inside of the transducer loop.

6. Experiment 4.3-3

Purpose

a) To test modified rectangular loop system.

b) Obtain particle impact on aluminum target.

Description of Test Model

The device used in this experiment was a 12 cm x 20 cm rectangular transducer loop with each side converging at 10° for better piston contact, and external energy input coils to avoid sabot pre-heating. A shorter, 11 cm, launch tube was used.

a) Sabot - 0.125" x 0.125" x 0.125" long copper slug.

b) Projectile - 0.094" diameter chrome alloy steel sphere, weight 54 mg.

c) Explosive - 425 gm Composition C-3.

d) Input energy from external charging coils, 27,500 joules.

Instrumentation

a) Magnetic field strength and rate of change - one turn pick-up loop at junction of launch tube and compression loop.

b) Piston velocity - six pin switches placed as shown in the diagram.

c) Sabot acceleration time - one turn pick-up loop at the end of launch tube.

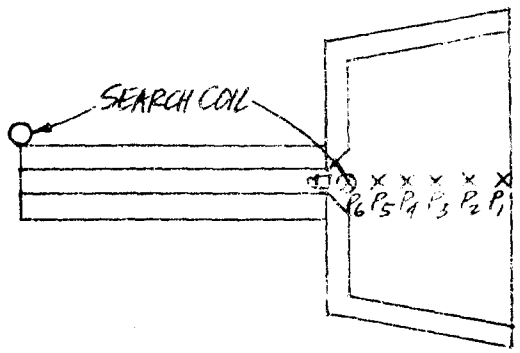

Results

Due to an error in timing, the crowbarring action of the loop occurred when the magnetic field was near a minimum instead of a maximum, thus there was essentially no magnetic field compression. No significant material was observed on the target. The piston velocity information was obscured by a light leak in the recording camera, which fogged the film.

7. Experiment 4.3-4

Purpose

a) Test simple rectangular loop system.

b) Obtain particle impact on target.

Description of Test Model

This simple device was a 10 cm x 10 cm rectangular loop with converging sides for piston contact. The loop was bent out of 1/8" strap which was backed up by wood. As shown in the diagram below, a projectile was soldered to a long thin section of the loop which forms the sabot. The 6 cm long launch tube rails were separated from the main loop and beveled on the inside. The magnetic field pressure pushed out the thin sabot section impacting it onto the beveled inside surface of the launch tube and the projectile continued on between the rails so that the device operated somewhat as a punch press.

a) Sabot - 0.5" x 1.25" x 0.040" thick.

b) Projectile - 2 gram steel half round.

c) Explosive - 200 grams Composition C-3.

d) Input energy directly applied to loop - 5,000 joules input.

Instrumentation

Magnetic field strength and rate of change - four coils picced as shown in the diagram.

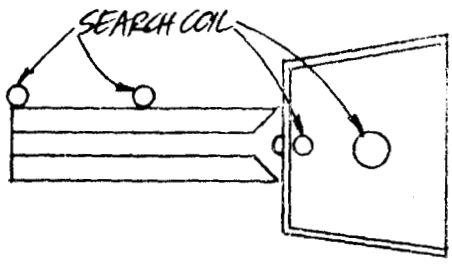

Results

The primary purpose of this shot was to obtain a particle impact on the target. Significant cratering was observed. The largest crater was 1/2" deep and 1/4" wide at the rim. Presence of iron on the aluminum target was proved with a Thiocyanate test.

8. Experiment 4.3-5

Prupose

a) Test regular modified rectangular loop with 6 cm long launch tube and round slug type sabot.

b) Obtain particle impact on aluminum target.

Description of Test Model

The device was a 12 cm x 20 cm rectangular loop with slightly converging sides. A short launch tube was used to insure that the projectile would exit the tube and would not be subjected to very large acceleration forces.

a) Sabot - 0.187" diameter x 0.197" long copper slug.

b) Projectile - 0.094" diameter chrome alloy steel sphere, weight 54 mg.

c) Explosive - 425 grams Composition C-3.

d) Input energy from external charging coils, 27,500 joules input.

Instrumentation

Magnetic field strength and rate of change - three coils placed as shown in the diagram.

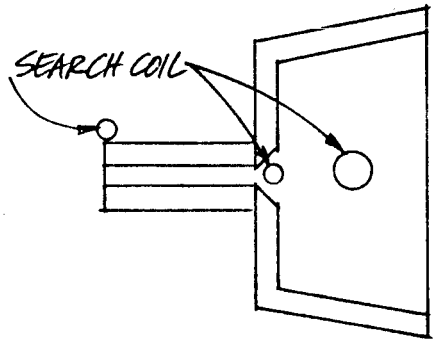

Results

A single particle impact was obtained on the target in this shot. The crater size was approximately six times the volume of the projectile. No velocity data was taken but it is believed that the velocity was fairly low. This is because the crater is not particularly large and also because the magnetic field multiplication was rather poor.

The round type sabot which run in circular section grooves in the launching rails worked very well. The grooves obviously give the sabot much better guidance than the square cross-section used previously.

9. Experiment 4.3-6

Purpose

a) Test simple strap loop system with external energy input coils.

b) Obtain particle impact on aluminum target.

Description of Test Model

Same as in Experiment 4.3-4, except that external energy input coils were used instead of direct drive. The input energy was also much higher.

a) Sabot - 0.5" x 1.25" x 0.040" thick.

b) Projectile - 2 gram steel half round.

c) Explosive - 200 grams Composition C-3.

d) Input energy from external charging coils - 14,000 joules input.

Instrumentation

Magnetic field strength and rate of change - four coils placed as shown in the diagram.

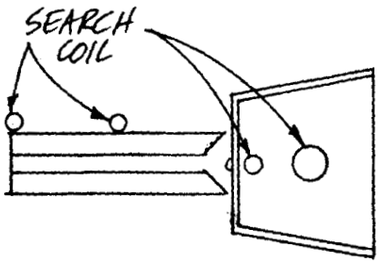

Results

Cratering of the target was obtained on this shot but was less than in Experiment 4.3-4. The magnetic field data indicated poor field multiplication thus the velocity of the projectile was probably not as great as in Experiment 4.3-4. It should be noted that very massive projectiles were used in this shot and in Experiment 4.3-4 at the expense of velocity in order to keep down the acceleration.

10. Experiment 4.3-7

Purpose

a) To test regular modified rectangular loop with 14 cm long edge set launching rails.

b) Obtain particle impact.

Description of Test Model

This device was a 12 cm x 20 cm rectangular transducer loop with slightly converging sides for piston contact. The 15.2 cm long launch tube was a square section with 1/4 inch wide rails. The purpose of this was to test a launch tube which was much simpler to fabricate.

a) Sabot - 0.25" x 0.25" x 0.25" copper slug.

b) Projectile - 0.094" diameter chrome alloy steel sphere, weight 54 mg.

c) Explosive - 525 grams Composition C-3.

d) Input energy from external charging coils - 27,500 joules input.

Instrumentation

a) Piston velocity - six pin switches placed as shown in the diagram below.

b) Magnetic field strength and rate of change - three one turn pick-up loops placed as shown in the diagram.

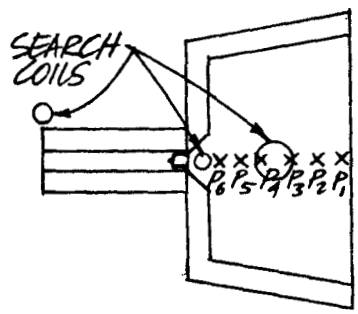

Results

There was no magnetic field multiplication on this shot. Only a very small amount of material, roughly in the shape of the sabot cross section, was observed on the target.

11. Experiment 4.4-1

Purpose

Test converging loop system with small sabot and projectile and long launch tube.

Description of Test Model

The device was a 12 cm radius converging transducer loop with 20 cm long launch tube.

a) Sabot - 1.5 mm diameter x 1.5 mm long, slug-type.

b) Projectile - 3/64" diameter chrome alloy, steel sphere, set 1/64" into sabot.

c) Loop size and tamping - 1/2" thick lucite, lead strip backing on H. E. compartment.

d) Explosive - 450 grams Composition C-3.

e) Input - directly applied to loop
Peak current 2.9×10^5 amperes
Rise time - 15 microseconds
Magnetic field energy - 12 kilojoules (approx.)

Instrumentation

a) Magnetic field strength - 1 turn pick-up loop in sabot corner of transducer.

b) Projectile acceleration - magnetic pick-up coils placed as shown in the diagram below.

c) Projectile velocity - 3 foil switches placed as shown.

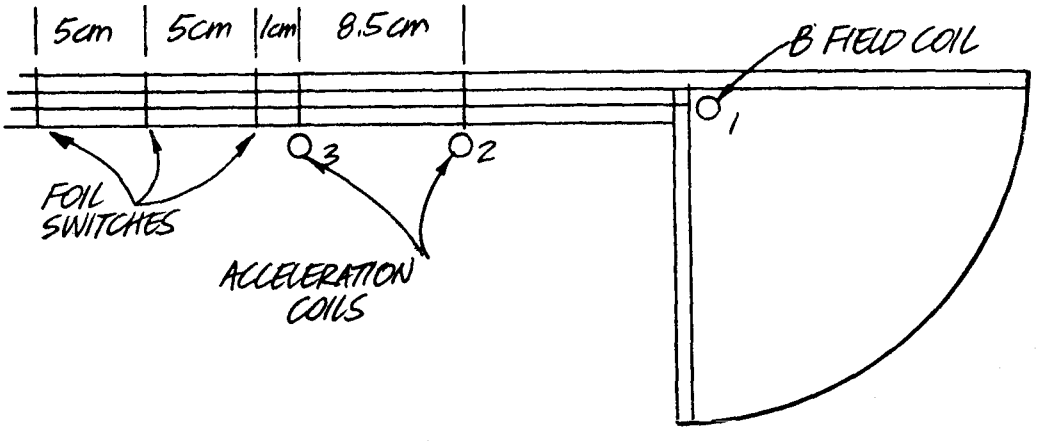

Results

a) The condenser bank triggered late, thus the magnetic field strength in the loop was low when crowbar occurred. The maximum magnetic field measured was 50 kilogauss. The launching rails show metal flow at the sabot end and there is evidence of an arc running the full length of the rails. This would be due to the condenser discharge. There is implication that the direct drive condenser discharge could have severely damaged the small sabot. This would contribute to loss of magnetic field multiplication.

b) No signals observed from pick-up coils on launch tube.

12. Experiment 4.4-2

Purpose

a) Magnetic field compression for comparison with Experiment 4.2-1.

b) Repeat of first attempt at this experiment which was damaged due to premature condenser bank discharge.

Description of Test Model

The device was a 12 cm radius converging transducer loop without sabot or launch tube.

a) Tamping and side pieces - 1/2" thick lucite, lead strip backing on H.E. compartment.

b) Explosive - 450 grams Composition C-3.

c) Input - directly applied to loop
Peak current - 3.1×10^5 amperes
Rise time - 14 microseconds
Magnetic field energy - 13 kilojoules (approx.)

Instrumentation

a) Magnetic field and rate of change - two one turn pick-up coils placed as shown in the diagram.

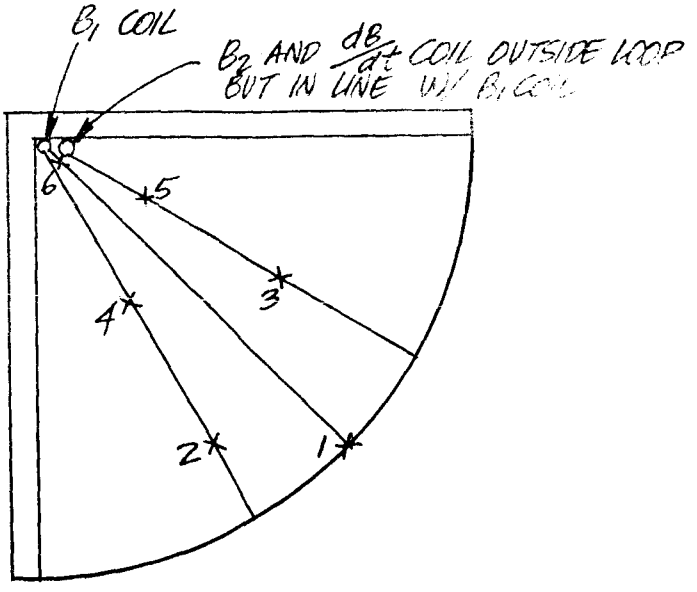

Results

a) All functions occurred properly; however, the magnetic field was not trapped.

b) Pin switch data was extremely erratic and hashy. These results seemed to confirm the belief that trapping the magnetic field has been a major problem in the past.

c) Recovery fragments indicate poor piston contact during early part of compression.

13. Experiment 4.4-3

Purpose

a) Hydrodynamic experiment to check operation of the explosive system and piston compression.

b) Device to be identical to that in 4.4-2.

Description of Test Model

The device was a 12 cm radius converging transducer loop without launch tube or sabot.

a) Side pieces and tamping - 1/2" thick lucite, lead strip backing on H.E. compartment.

b) Explosive - 450 grams Composition C-3.

c) No electrical input.

Instrumentation

All instrumentation of this experiment was by means of pin switches. Twenty pins were placed as shown in the diagram. Measured quantities were:

a) Detonator function time

b) Line wave generator and explosive function time

c) Piston velocity and convergence uniformity

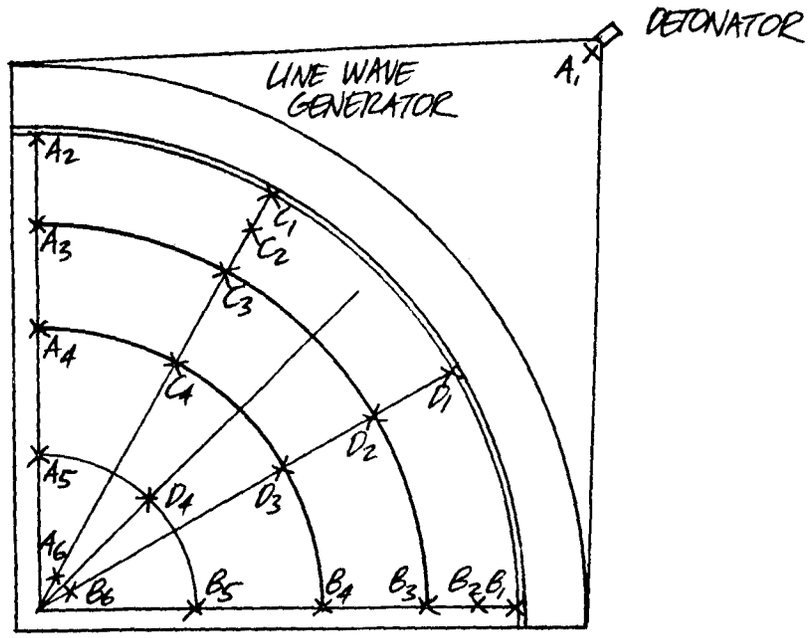

Results

a) Detonator function time was measured to be 8 microseconds, which was about as expected.

b) Line lighter and explosive total function time was measured to be 49.5 microseconds at the edges and 47.5 in the center. This indicates some non-uniformity of the detonation front in the line wave generator. The times were slightly less than expected.

c) The pin data indicates that the uniformity of piston convergence was very good with one end of the piston slightly leading the other. The data indicates an average piston velocity of approximately 4 millimeters per microsecond. This is in good agreement with previous measurements.

14. Experiment 4.4-4

Purpose

a) Magnetic field compression.

b) Device to be the same as in 4.4-2, except for modification to aid magnetic field trapping.

Description of Test Model

The device was a 12 cm radius converging transducer loop without sabot or launch tube.

a) Side pieces and tamping - 1/2" thick lucite, each side piece laterally converged at a 1.5° angle towards the sabot corner of the loop to prevent gas blow-by.

b) Explosive - 450 grams Composition C-3.

c) Input - directly applied to transducer loop
Peak current - 3.1×10^5 amperes
Rise time - 14 microseconds
Magnetic field energy - 13 kilojoules (approx.)

Instrumentation

a) Magnetic field strength and rate of change - two one turn pick-up coils placed as shown in the diagram below.

b) Piston motion - 6 pin switches placed as shown

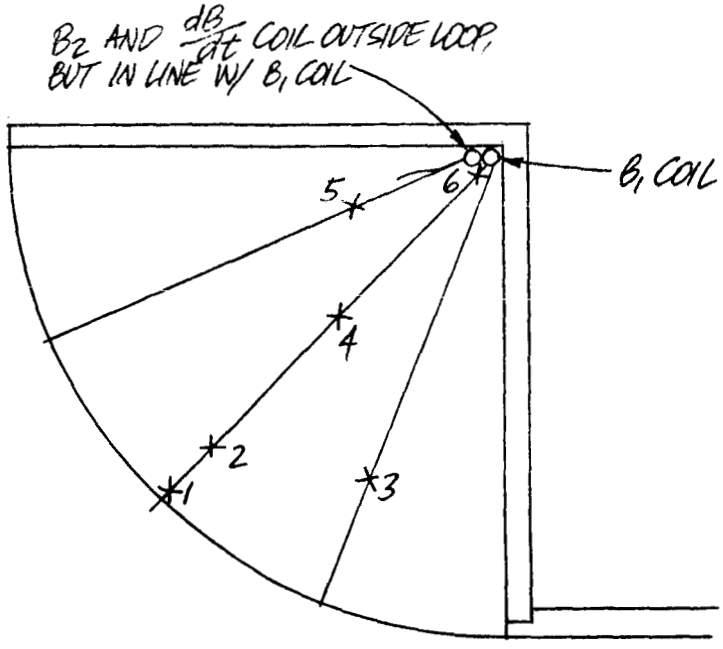

Results

a) As in Experiment 4.4-2 there was no magnetic field trapping.

b) The pin switch data indicates proper time of piston motion.

c) The recovery fragments indicate very poor piston contact at the beginning of the piston run. The contact pattern was nearly identical to that in Experiment 4.4-2.

15. Experiment 4.4-5

Purpose

a) Test converging transducer loop with small sabot and projectile.

b) Use external energy input coils.

c) Monitor condenser bank voltage before and during compression to determine if energy is pumped back to the bank via the external coils during piston compression.

Description of Test Model

The device was a 12 cm radius converging transducer loop with 20 cm long launch tube.

a) Sabot - 1.5 mm diameter by 1.5 mm long, copper slug.

b) Projectile - 3/64" diameter, chrome alloy, steel sphere set 1/64" into sabot.

c) Side pieces and tamping - 1/2" thick lucite, lead strip backing on H.E. compartment.

d) Explosive - 450 grams Composition C-3.

e) Input - external coils made from 4 strands of solid #12 insulated electrical wire, 3.5 turns per coil.
Coil inductance - 4 micro Henry's (total)
Rise time - 39 microseconds
Peak current - 1.12×10^5 amperes
Magnetic field energy - 25 kilojoules

Instrumentation

a) Magnetic field and rate of change - one pick-up coil placed as shown in the diagram below.

b) Projectile exit time - one pick-up loop placed at end of launch tube as shown.

c) Condenser bank voltage as a function of time - voltage divider and oscilloscope directly across condenser bank.

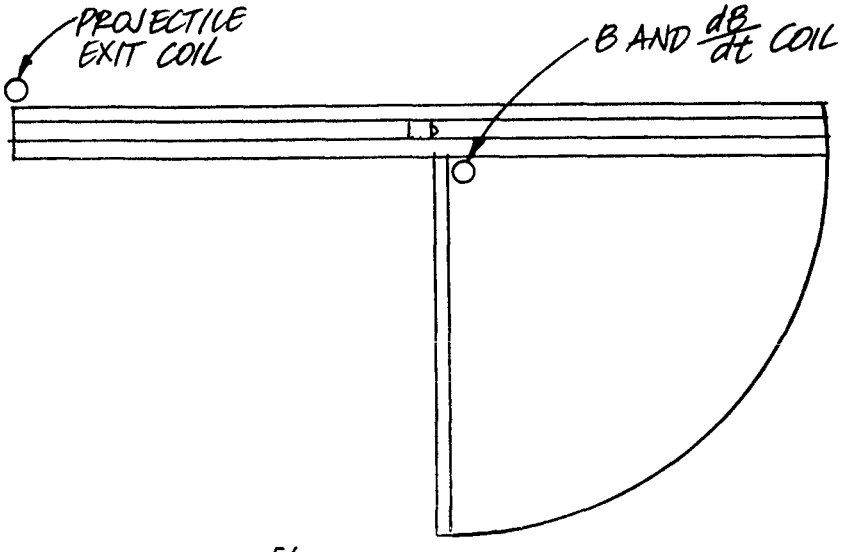

Results

a) Magnetic field - the oscilloscope traces indicate that there was no initial magnetic field present, although it appears that the condenser bank functioned properly.

b) No signal was observed from the sabot exit pick-up coil.

c) The condenser bank voltage trace indicates normal operation during the rise to peak current, and fall-off of the voltage in a normal fashion after the time the loop was supposed to crowbar. The trace shows many spurious pulses, however, which could possibly be attributed to arcing and possible shorting of coil turns or of the input leads to the coil. At 84 microseconds, which is very close to the time when one would expect complete loop closure, there is a strong pulse of hash and a sudden rising of the voltage.

It is difficult to explain the hump in the voltage on the basis of magnetic field, since no magnetic field was seen by the pick-up coils (although a considerable amount of hash was detected by these coils). One possibility is that the hash during the early part of the voltage trace is due to shorting of coil leads and turns and that the hump in voltage was caused by the explosive driving the coils apart. If the main input leads of the coil had been shorter or the coil was otherwise eliminated from the condenser bank circuit, the rise time of the hump should have been around 10 microseconds, which is about half that indicated.

17. Experiment 4.5-1

Purpose

Investigate hydrodynamic convergence of the piston. Test for instabilities.

Description of Test Model

Piston radius - 8.5 cm	H. E. radius - 13.5 cm
Piston thickness - 1.12 mm	H. E. type - Composition C-3
Loop depth - 1.41 cm	H. E. weight - 156 grams
Side plate thickness - 2 cm	Lead backing - 1/4" thick

Instrumentation

Explosive detonation front linearity - 6 pin switches spaced 0.5 cm from the piston, in the explosive. Piston convergence - 36 pin switches is arranged as in Figure A-1. Three cut-off pins in pin dome.

Figure A-1 shows the interior of the test model. The pin dome and pins can be clearly seen. The nest of signal wires and the methane gas tubes are at the top center of thephotograph. The high explosive is at the bottom half. Details of the piston joint are visible to the left. Figure A-2 shows the device installed in the containment tank and ready for the experiment. The triple line wave generator arrangement can be seen in the photograph.

Results

Figure A-3 is an isochron diagram of the piston in this experiment. It shows the piston shape and location at various time intervals as interpreted from the pin data. Although the convergence was good, the ends lagged somewhat at the slide planes. This caused an acceleration of the sections of the piston about 10° - 15° from each slide plane.

18. Experiment 4.6-1

Magnetic Compression Test

A 2 scale down magnetic compression device was designed as shown in Figure A-4. The test gave a magnetic field of 300 kilogauss, with a compression ratio of approximately 10. Although this was less than expected, it is more than sufficient for coupling to current model launch tubes. With this design the current amplification is approximately equivalent to the compression ratio.

One of the major difficulties is that the device gives a relatively short pulse. The total length of the piston travel is 3.3 inches. The typical piston velocities are 3 mm/microsecond. Thus, the pulse length at most can be 27 microseconds. In addition, the pulse shape is given by

$$I = I_o (L_i/L_2) \exp(-R/L_t)$$

I_o = initial current
L_1 = initial inductance
L_2 = inductance at time t
R = circuit resistance

The shape of the curve is exponential so that the greatest current amplification occurs in the last few microseconds.

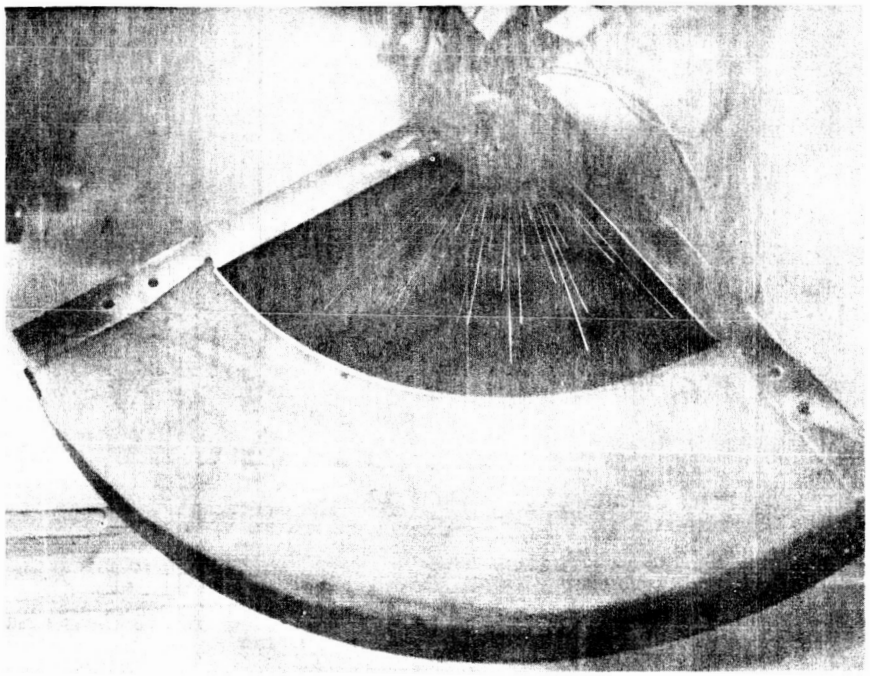

Figure A-1 Interior of Experiment 4.5-1 Test Model

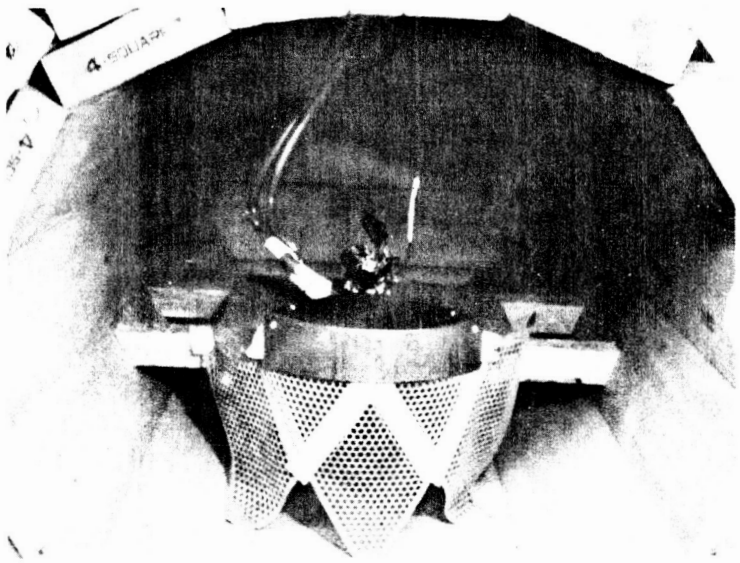

Figure A-2 Experiment 4.5-1 Test Model in Containment Tank

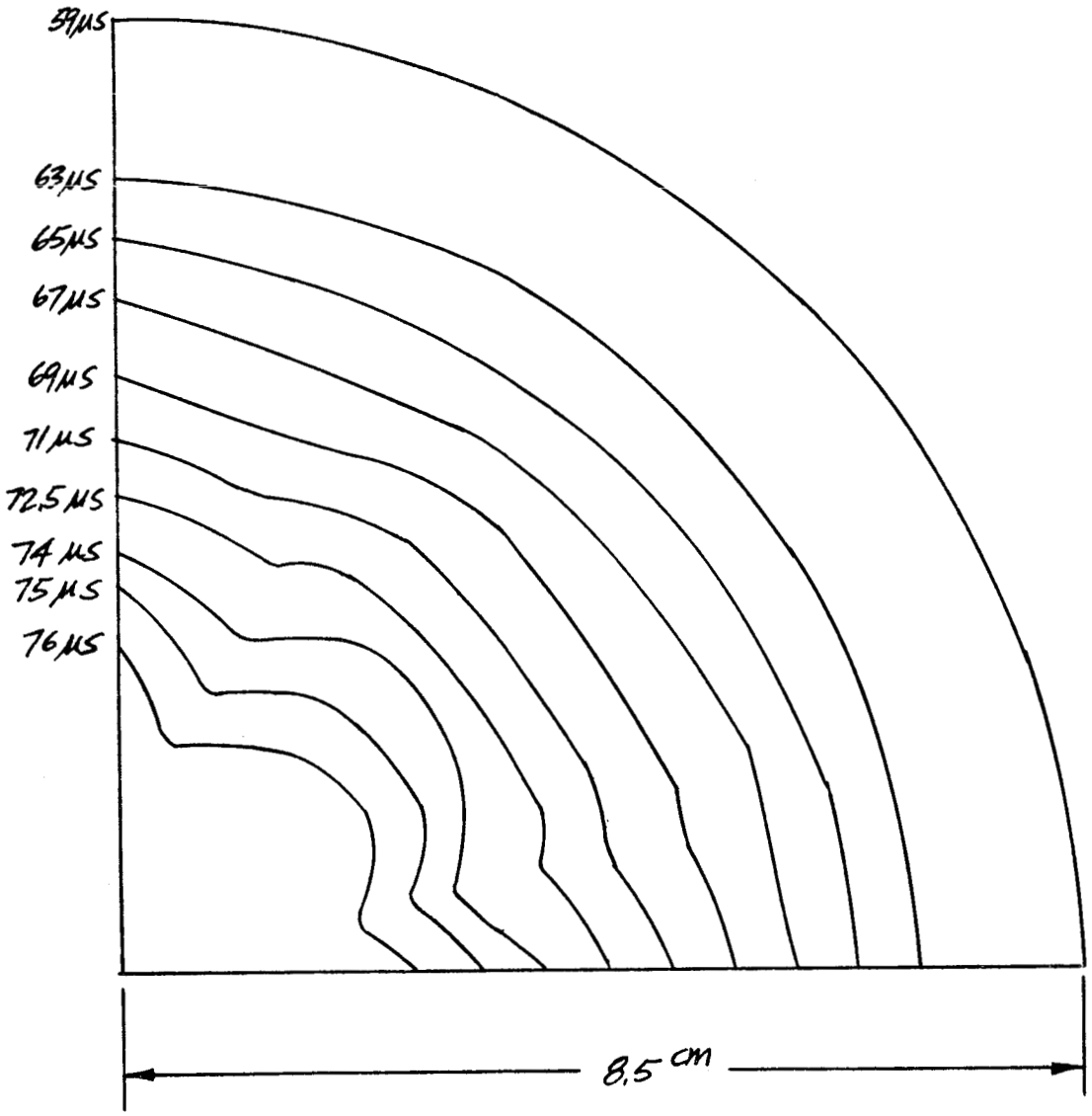

ISOCHRON DIAGRAM OF PISTON

FIGURE A-3

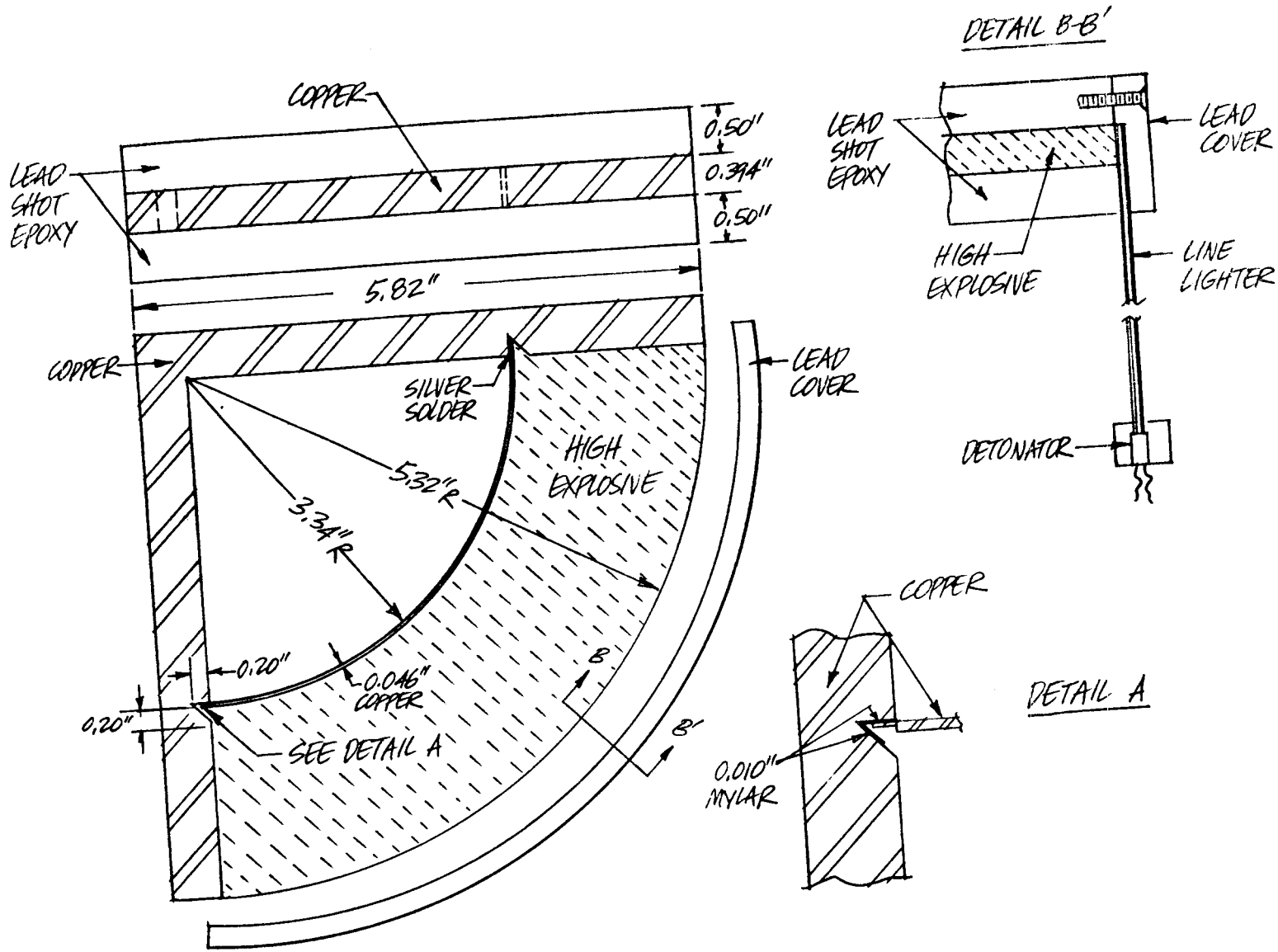

MAGNETIC COMPRESSION

TEST DEVICE

FIGURE A-4

MBA 5005

19. Experiment 4.6-2

Longer Pulse Length Generator

A second generator was designed to achieve a longer pulse length (see Figure A-5). This was done by extending the distance which the piston travels to 11.6 inches. Assuming the piston travels 3 mm/microsecond, the pulse length should be about 100 microseconds. The ratio of initial to the expected final inductance is not as large as in the previous guns. Thus a lower current amplification would be expected. However, for the type of launch tubes being studied at present it should be more than sufficient.

The long pulse length generator was tested but no magnetic field was measured in the gun. Apparently an arc between the piston and the notched copper bar (detail A, Figure A-5) occurred during the initial magnetic field buildup.

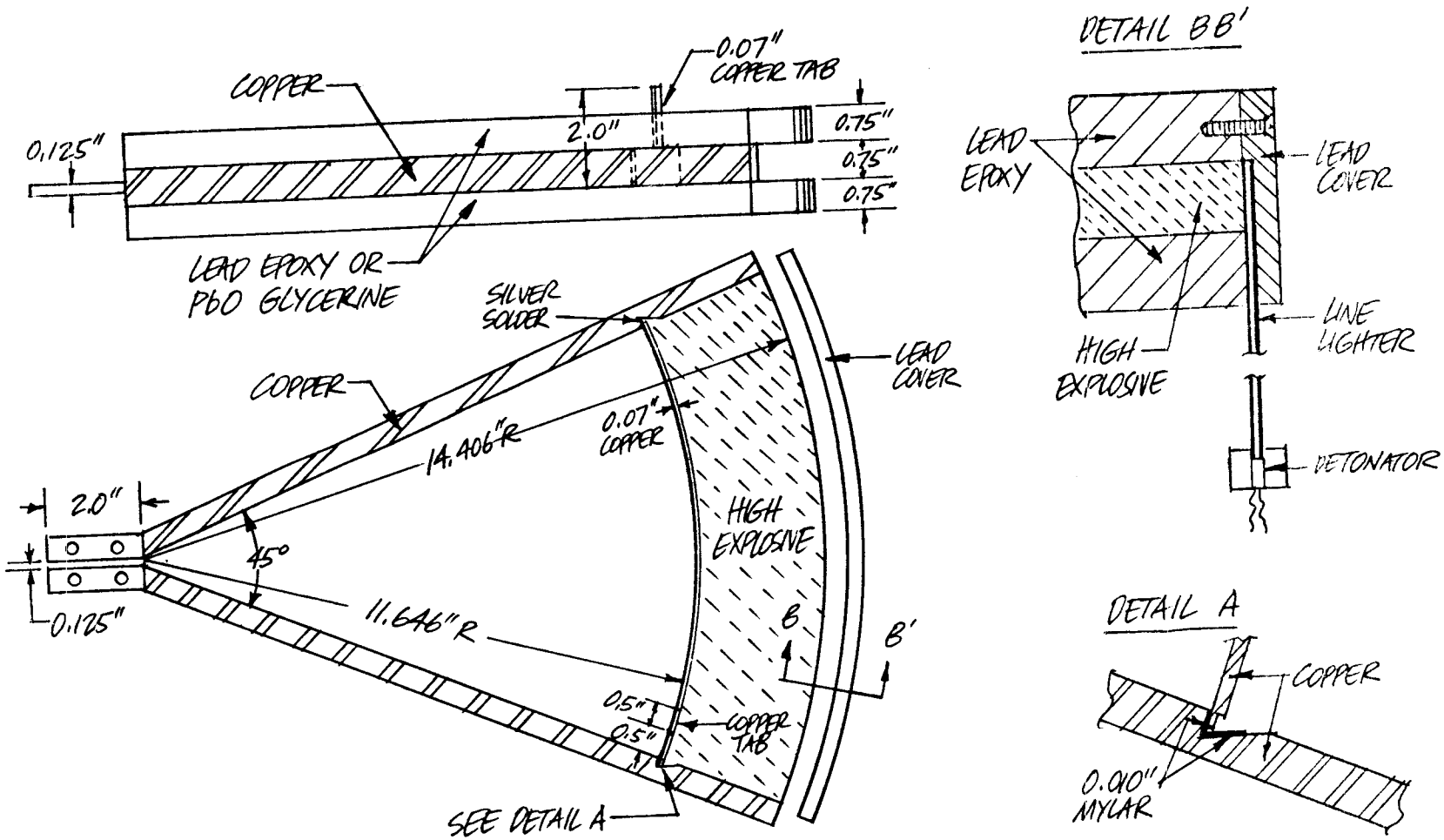

LONG PULSE GENERATOR

FIGURE A-5

MBA 5006

APPENDIX B

CONTAINMENT TANK

Experimental operations on the hypervelocity gun are greatly facilitated by the ability to fire the high explosive right in the laboratory. To permit this, a containment tank was built similar to those currently in use for HE blast containment.

1. Design Discussion

The design is based on criteria established at the Lawrence Radiation Laboratory, Livermore, California, for containment spheres. This criteria states that for 20,000 psi tensile stress on a 1/4" thick steel tank wall from the detonation of PBX explosive, the minimum inside radius of the sphere should be $R = \sqrt{W} / 0.767$, where R = the radius in feet, W = the number of pounds of explosives. Thus for 1.32 pounds (600 grams) of explosive, R = 1.5 feet.

To reduce cost, a cylindrical, instead of spherical, tank was designed. Figures B-1 and B-2 show side and end views. It is 3 feet in diameter; the volume was increased by making the length 5 feet. The purpose of this is to reduce the pressure on the flat end door. Since the sources of the design criteria are empirical, it was deemed advisable to make the tank wall 3/4 inch thick instead of 1/4 inch thick. The domed end is 1 inch thick spun steel, and the door 2 inches thick.

To facilitate portability, the tank is mounted on skids. Attached to one skid is a centrifugal blower for purging the noxious gases which result from the detonations. The gate valve is opened and the blower turned on immediately after a shot, and the fumes forced out through a long pipe. Various ports are provided for transmission line entry and instrumentation, while the 1 foot diameter port on the end door is for access.

Inside the tank, the transducer loop is installed horizontally, and the launch tube is coupled to a heavy barrel through which the projectile egresses.

Provision has been made for evacuation of the barrel. The loop assembly is surrounded by 1 foot thick styrofoam blocks to reduce shrapnel damage to the inside of the tank. Also, the tank has a 1/4 inch thick steel liner which can be replaced when the damage becomes excessive.

2. Fabrication

All major seams of the tank were radiographed. These were the welds of the main cover flange, the longitudinal tank seam, the circumferential seam of the dished head, transducer loop port and gun barrel port seams. The results showed several imperfect weld areas. These were opened and rewelded, and the repaired areas were again radiographed. The circumferential seam of the dished heads showed a slag deposit and what appeared as cracks due to

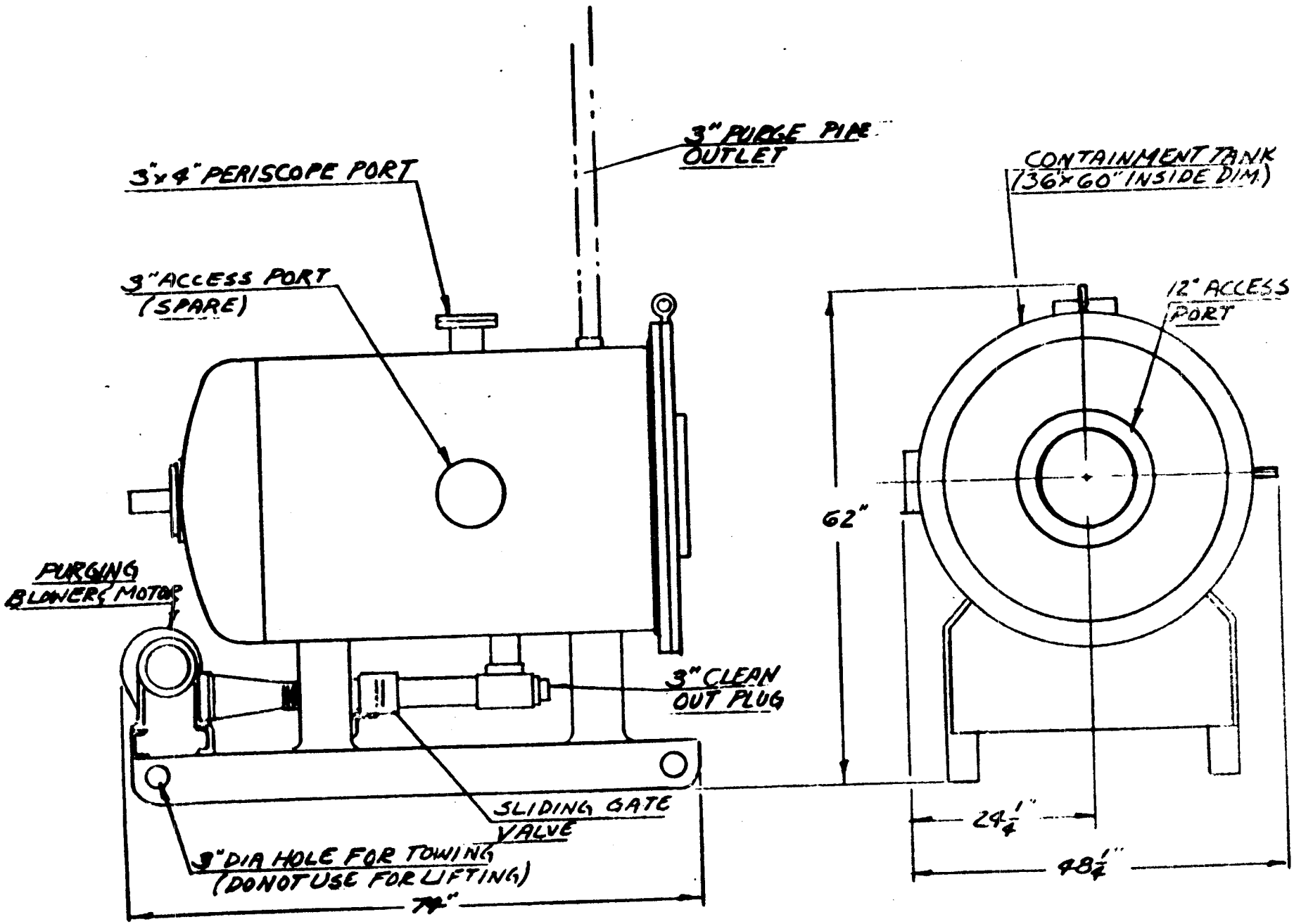

CONTAINMENT TANK

FIGURE B-1

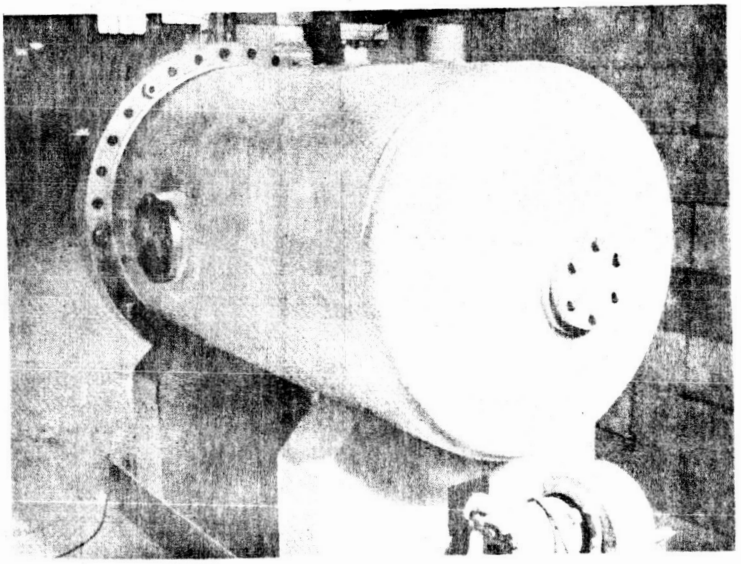

Containment Tank

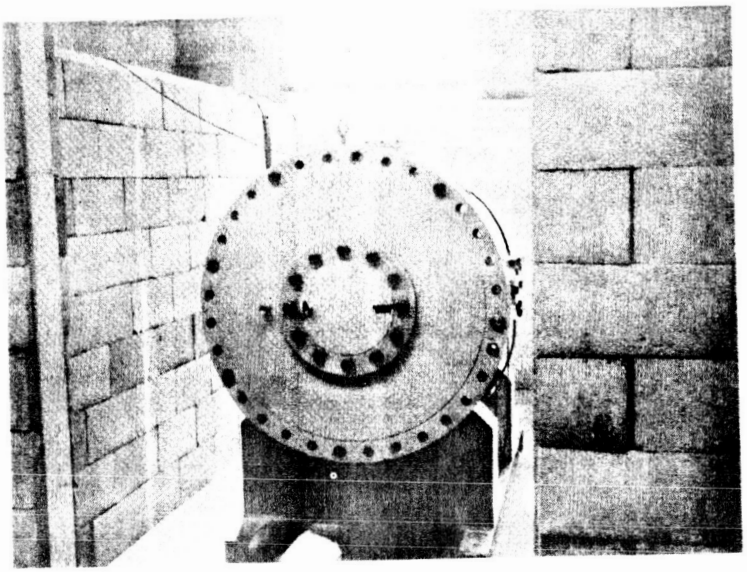

Figure B-2

improper penetration of welds. On close examination of the tank and the radiograph films, it was concluded that these cracks could very well have been due to the weld line on the inside of the tank where a three inch straight flange of the dished head was tapered to 3/4 inch to match the 3/4 inch shell. Instructions were issued to chip out the slag deposit and reweld and to grind smooth the circumferential weld on the inside of the dished head. The areas were radiographed and found to be 100% sound. The tank was then sent out for stress relieving and sand blasting. After this it was sent to a special machine shop for machining of the surfaces of the main flange and door.

3. Testing

It was originally intended to pressure test the tank with explosives at the plant building behind a concrete barrier wall. As a precautionary measure, it was decided to first field test the tank for integrity. All ports were closed off with blind flanges, and the only outlet was the 3 inch purge pipe extending 20 feet above the tank. The tank was checked over carefully as to proper torquing of head and port bolts. Loading of the composition "C" explosive was done through the transducer loop port for these experiments. The detonators used were X-98 arc firing type. Previous dimensional checks were recorded for comparison with later measurements. The tank footing was marked to check for movement. Six explosive charges of increasing weight were fired in the following order:

Shot No.	H. E. Weight
1	28 grams
2	75 grams
3	150 grams
4	300 grams
5	450 grams
6	600 grams

4. Test Results

No tank movement was observed or measured on any of the shots. The noise level, in general, was fairly low and, in fact, the rush of gases up the purge line at the time of the explosion was louder than the noise from the explosion itself. For comparison, after the shots in the tank a 225 gram charge was detonated on the open ground the same distance away from the personnel as the tank had been. The noise from this open explosion can be only described as orders of magnitude louder than the shots fired in the tank that were of two to three times the amount of explosive. We, therefore, anticipate no problems with the noise level using the tank in a building.

After each shot the tank head was checked for permanent deformation with a special measuring bar. Also bolt loosening was checked by reapplying the torque wrench. Grade one mild steel bolts were used throughout the tank for this test with a minimum tensile strength of 55,000 psi. The bolts were torqued to the following values.

Bolt	Torque Value
1"	320 foot pounds
3/4" 10 NC	160 foot pounds
5/8" 11 NC	100 foot pounds
1/2" 13 NC	46 foot pounds

Data on head deformation, tank movement, and bolt loosening follows.

Head Deformation

Shot No.	Deformation
1 - 6	0 inches

Tank Movement

Shot No.	Movement
1 - 6	0 inches

Main Head Bolts (1" - 8 NC)

Shot No.	Torque Reading After Firing
1	0
2	300
3	320
4	320
5	200 (top)
	250 (bottom)
6	100 (top)
	125 (bottom)

Gun Barrel Port (3/4" - 10 NC)

Shot No.	Torque Reading After Firing
1	160
2	160
3	160
4	140
5	120
6	60 (top)
	100 (bottom)

The bolts on the camera port and the three inch port to the tank were not affected. The 2 inch thick flat end door, which was our major concern, held up very well. Some bolt elongation was expected and was observed. After this, however, grade five steel heat treated bolts were used. The testing was carried out in a safe and orderly fashion. Color movies were made of the tests.

5. Condition of Hypervelocity Tank After Testing

The tank was again radiographed. Two areas about 3/4" to 1" long at the top port of the main bolting flange were found which could possibly be cracked in the weld area. The first set of films taken right after manufacture were checked, and it was evident on close examination that these slight imperfections were present before the test firing. These findings were confirmed by the radiographing company. These areas were radiographed again after the next two firings, and no difficulty was found. The cracks are more visible on the second radiograph because of a different film exposure density.

Measurements of the inside diameter of the tank were made before and after testing. The measurements were taken in three places on the vertical center line and three places on the horizontal centerline. The first set of measurements was taken 11 inches in from the tank flange. The second at 30 inches and the third set at 48 inches. These are tabulated as follows:

Vertical Measurements	Before Firing	After Firing
Distance 11"	34.340 inches	34.444 inches
Distance 30"	34.452 inches	34.454 inches
Distance 48"	34.447 inches	34.449 inches

Horizontal Measurements	Before Firing	After Firing
Distance 11"	34.433 inches	34.433 inches
Distance 30"	34.435 inches	34.437 inches
Distance 48"	34.443 inches	34.445 inches

The only appreciable amount of increase was in the vertical measurement at 11 inches, an increase of 0.104 inches. This point on the tank was dished in slightly due to repairs after relocation of the purge outlet during fabrication. The explosions would have a tendency to round off this portion, therefore, the increase is understandable.

APPENDIX C

CONDENSER BANK AND INSTRUMENTATION

1. Condenser Bank

Figure C-1 shows the general appearance of the condenser bank which provides the current for the initial magnetic field in the transducer loop. The bank consists of two carts holding 5 condensers each. The total capacitance is 142 microfarads, at 20 kilovolts maximum, which is an energy storage of 30 kilojoules. A parallel plate transmission line connects the condensers in parallel, while ten RG-8/u coaxial cables in parallel transmit the power from the bank to the load. Switching is by triggered spark gap.

2. Timing and Firing System

Also shown in Figure C-1 is the electronics rack. At the top is an Abtronics Model 100 pulse and time delay generator which initiates and times the sequence of events. One delay channel is used for establishing the proper time relationship between firing of the detonator and switching of the condenser bank, while the other three channels are available for timing instrumentation devices. The second chassis contains the power supply and control system for firing the detonator. It can furnish 25 joules at 5 kilovolts. Figure C-2 is the detonator panel circuit diagram. The third panel is the condenser bank control system. Its circuit is shown in Figure C-3. The charging power supply for the condenser bank is located behind a blank panel at the bottom of the rack cabinet. Its circuit is shown in Figure C-4. The charging time for the condenser bank will be about 30 seconds. The circuit of the bank is shown in Figure C-5.

All the electronics are interconnected so as to operate as a system. This is particularly important for safety. Various automatic interlocks and high voltage crowbars are provided. A main circuit breaker, located below the condenser bank control panel, feeds power to the entire system and a key switch prevents unauthorized operation. Another key switch prevents operation of the detonator system. The key for this switch was carried by the ordnance man when assembling and arming the high explosive charge.

In the early experiments the timing and firing system consisted only of a four channel time delay generator which also had a zero time pulse output. This time delay generator was to be actuated by a button on its front panel which would be the firing key. It controlled only the timing relationship of the condenser bank to the detonator panel and also triggered instrumentation devices. There are, however, a number of other functions which must be performed during a firing. These can be done by manually operated switches but require that the operator be rather close to the explosion containment tank during the firing. Also, the number of operations would be such that several persons would be needed. It was decided, therefore, that a motor-driven cam type sequence timer should be incorporated.

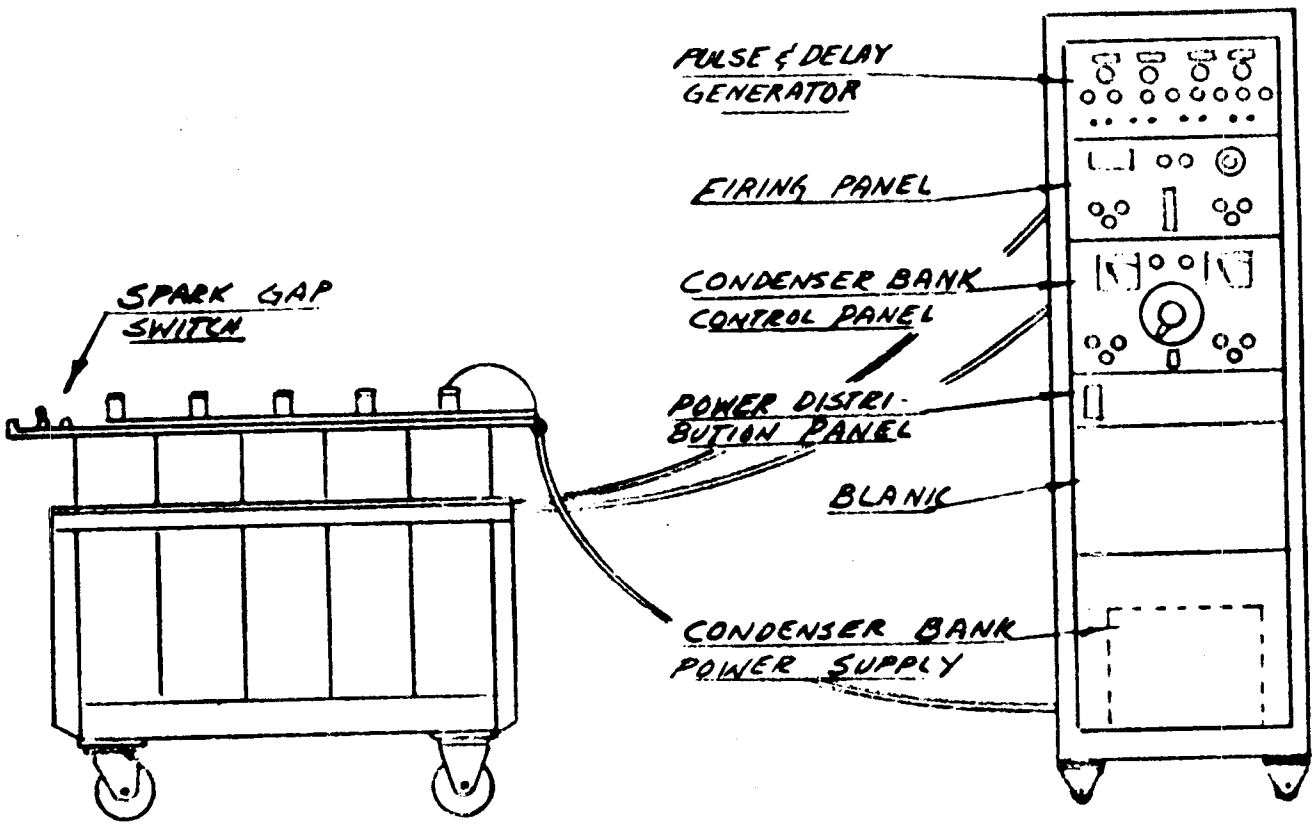

CONDENSER BANK

FIGURE C-1

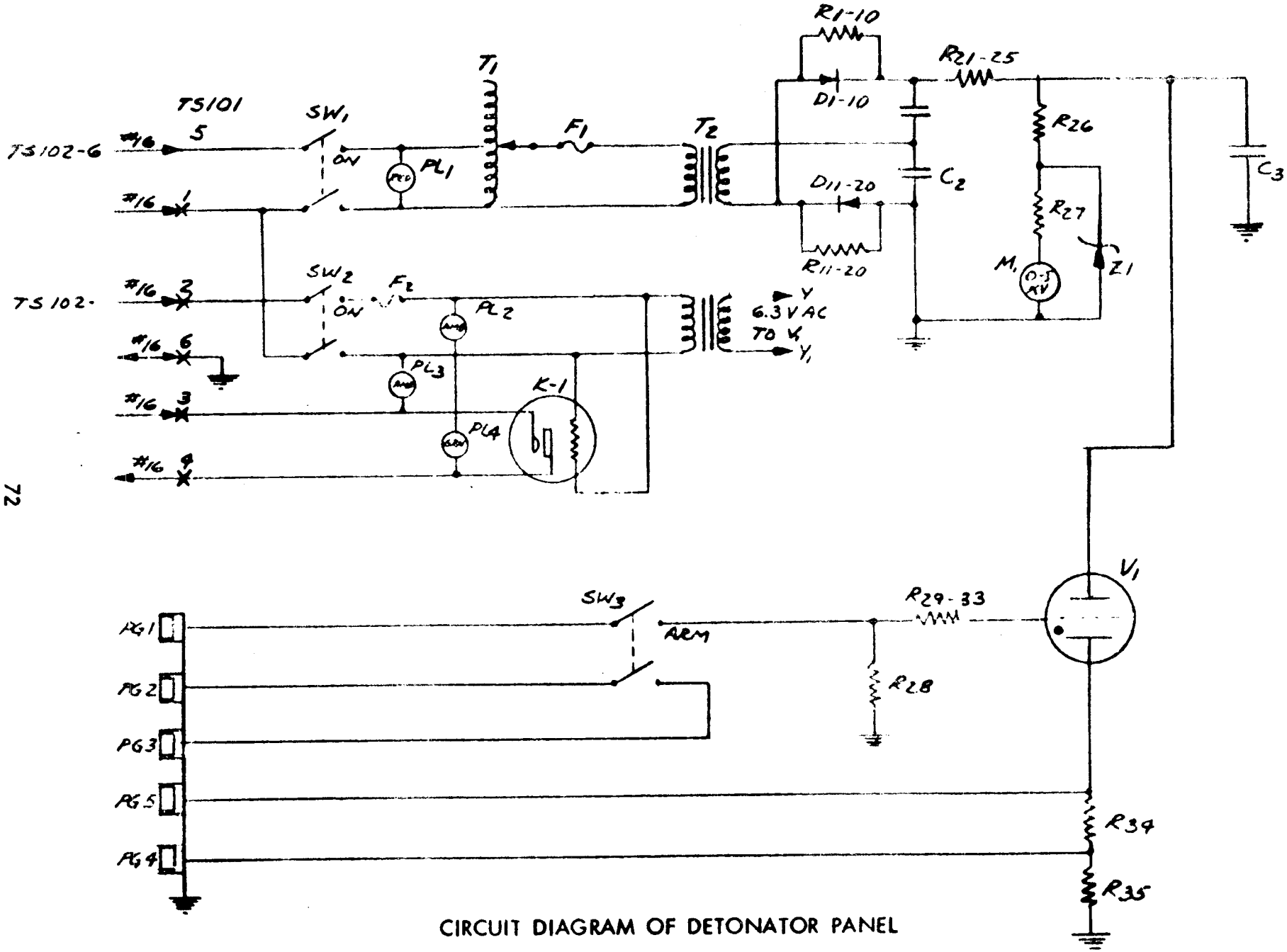

CIRCUIT DIAGRAM OF DETONATOR PANEL

FIGURE C-2

MBA 1233

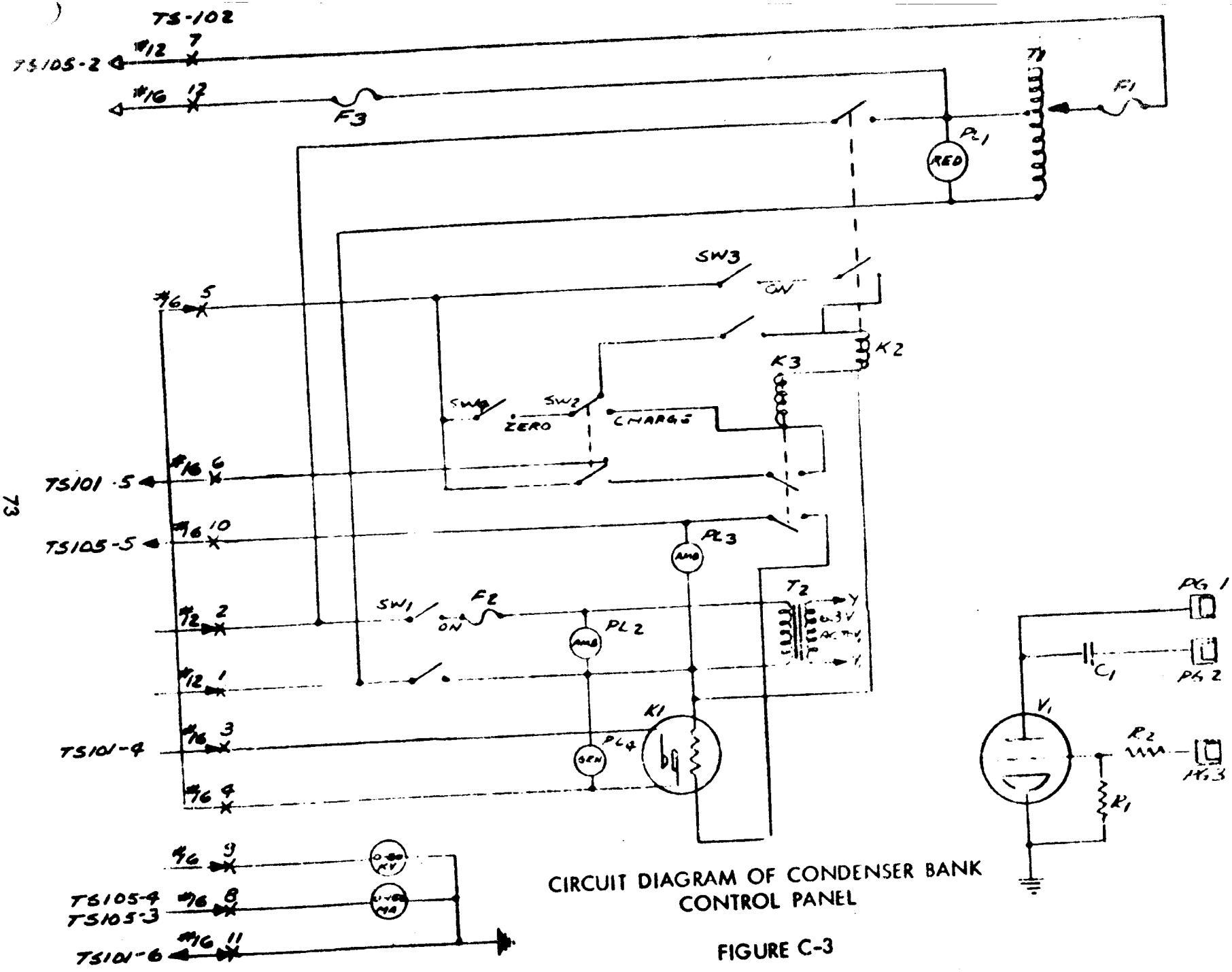

CIRCUIT DIAGRAM OF CONDENSER BANK CONTROL PANEL

FIGURE C-3

MBA 1234

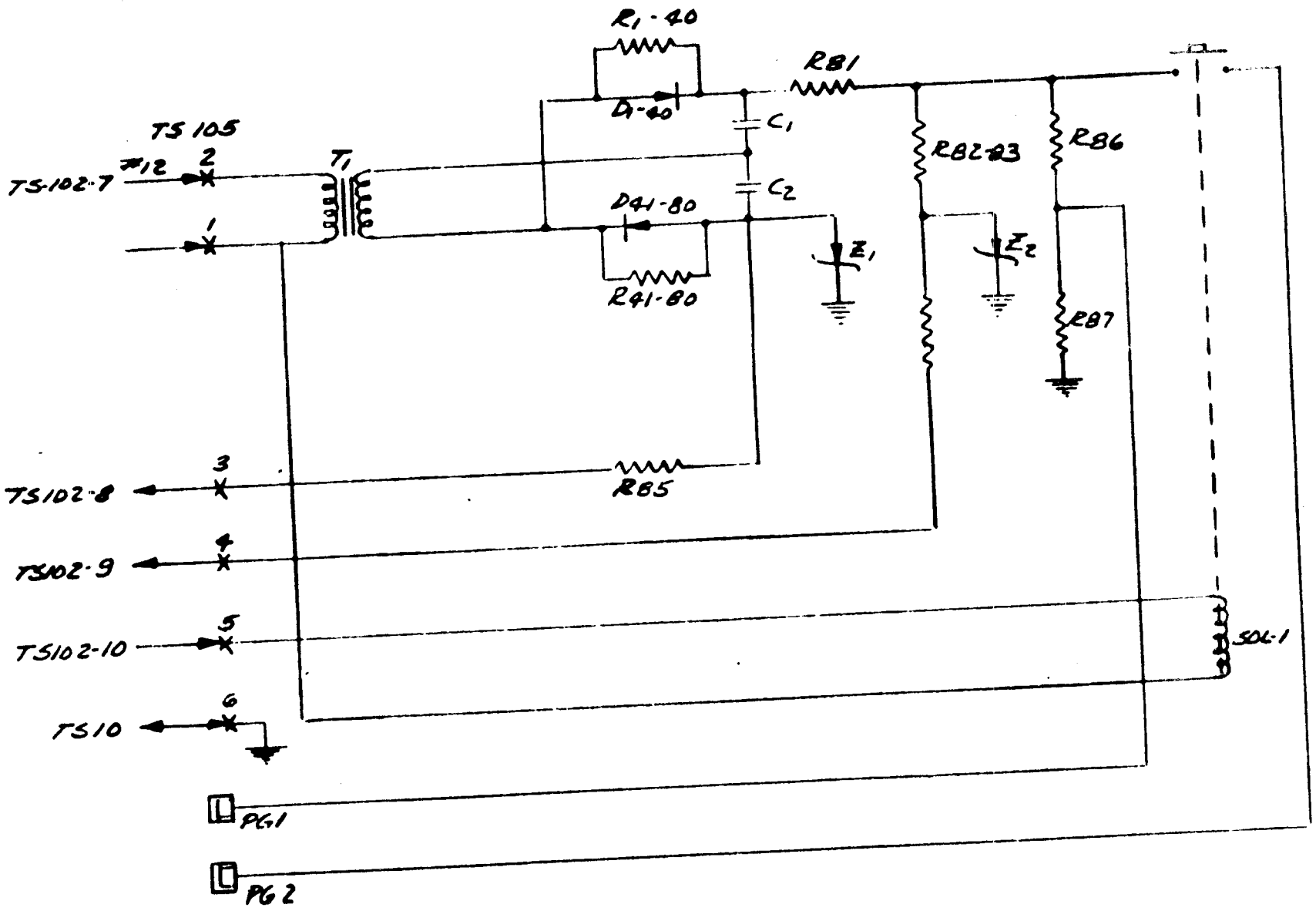

CIRCUIT DIAGRAM OF CONDENSER BANK POWER-SUPPLY

FIGURE C-4

MBA 12-

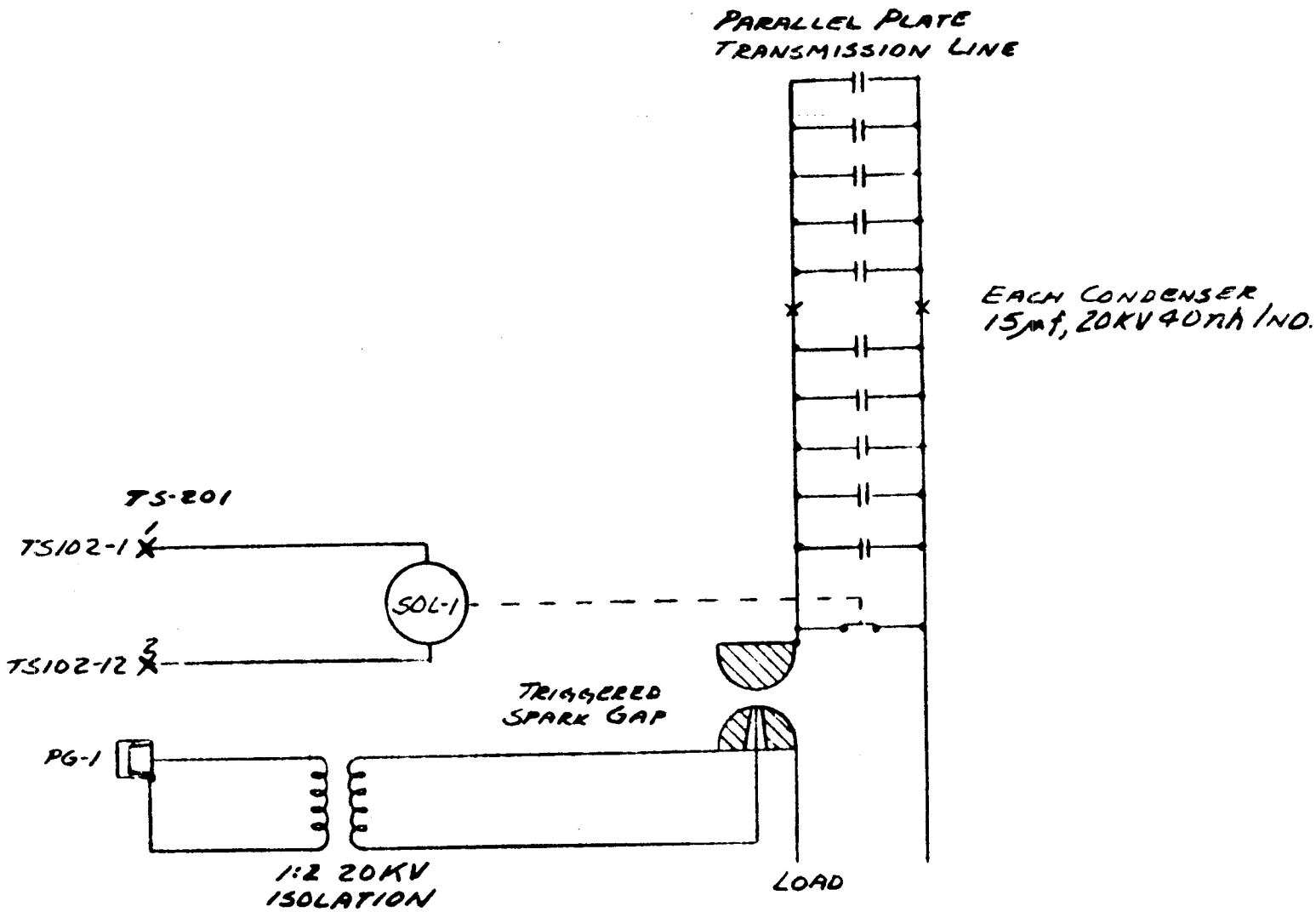

CIRCUIT DIAGRAM OF CONDENSER BANK

FIGURE C-5

The front panel of the timer contains the lights and switches necessary to its operation. It can be started locally or remotely. When started it begins at T-5 seconds and counts down to zero and then to + 2 seconds; the times being indicated by lights on the panel. Switches are provided for off, operate, and test of each of the separate functions. The sequence is as follows:

T - 5 seconds	Charging warning bell stops, interlock chain energized.
T - 4 seconds	Vacuum head gate valve closed.
T - 3 seconds	Instrumentation camera shutters open.
T - 2 seconds	Detonator and condenser bank trigger systems arm.
T - 1 second	One second to fire.
T = 0 seconds	Fire, interlock chain opens dropping crowbars.
T + 2 seconds	Purging blower head gate valve opens and blower starts. Camera shutters close, system disarms and the vacuum head gate valve stays closed.

At T = 0 the firing function is an activation of the electronic pulse generator. At this signal the electronic timing generator takes over from the electromechanical timer. The zero time pulse from the timing generator triggers the condenser bank and the first delayed pulse output triggers the detonator panel. The other three delayed channels operate oscilloscopes and other instruments as required. At the end of the operation, the interlock chain is opened which automatically drops all high voltage crowbars and disarms the entire system. When the sequence timer stops at + 2 seconds, the blower is left running and the vacuum head gate valve is still closed. These functions can then be left in that position until it is safe to change them which can be done manually from the control panel.

After the timer stops, it is necessary to manually reset it, since it does not go one full revolution. This is to allow for the functions that must remain operating after a firing sequence. Lights on the front panel indicate when it needs to be reset and when it is reset. The major indicator lights are of sufficient size to be viewed from a distance, and the system can be operated remotely and safely. All functions are automatic, thus eliminating human error during a firing.

APPENDIX D

DIAGNOSTICS

A number of diagnostic techniques were used to gain an understanding of the phenomenon occurring during the experiments. These are discussed below.

1. Piston Convergence and Velocity Measurements

Piston convergence and velocity measurements were made using "pin" techniques. A pin is a device consisting of two conductors which, when struck by the piston or the sabot and projectile assembly, completes an electrical circuit. This then discharges a small condenser and the electrical signal is recorded on an oscilloscope. If a large number of pins must be used to obtain a measurement, then a raster oscilloscope is necessary. In measuring piston convergences and velocity, typically six pins are used. They are placed in pairs at different radii and different angles within the loop assembly and are inserted through the lead epoxy loop sides. Figure D-1 shows this arrangement. The velocity at each of the radii is measured by the time of flight between the two pins comprising the pair at that radii and the convergence uniformity is determined by the uniformity of time of arrival at each of the pin pairs as related to the velocity shown by each pair.

2. Magnetic Field Measurements for the Generator

The magnetic field measurements are made by inserting a small search coil at the converging apex of the loop; that is, right behind the sabot. As the magnetic field rises in the system, the coil develops an output voltage which can be fed directly into the oscilloscope. This then is a measurement of the rate of change of magnetic field strength as given by the relation

$$V = BNA$$

where

B	=	Time rate of change of magnetic field
V	=	Voltage output of the coil
N	=	Number of turns of the coil
A	=	Area of the coil perpendicular to the magnetic lines of flux

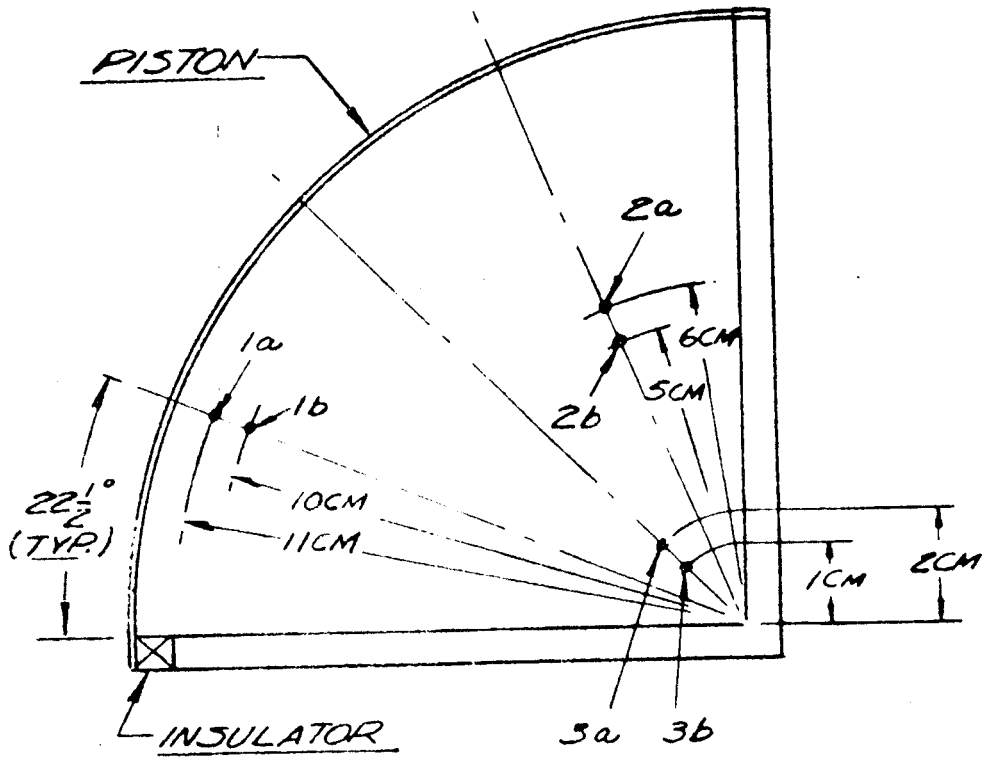

LOCATION OF PIN PROBES

Figure D-1

MBA 1193

This particular type of measurement is useful in that it is sensitive to any irregularities or sudden changes that may occur during the compression of the loop. If one integrates both sides of the equation, the magnetic field can be measured directly as a function of time. It is not necessary to do this mathematically from the B measurement, it can be done electronically by incorporating an RC integrator circuit between the coil and another oscilloscope. In this case the following expression applies.

$$V_s = \frac{BNA}{RC}$$

where

V_s = Voltage measured by oscilloscope

RC = Integration time constant

3. Ballistic Pendulum

The ballistic pendulum is a simple method of measuring velocities. However, it is subject to a number of inaccuracies. Observer errors and the influence of the moving plasma can make appreciable discrepancies in the readings. For these reasons, the ballistic pendulum was not relied upon for accurate results.

4. Photomultiplier-Velocity Screens

A velocity screen device was built to obtain accurate velocity measurements. It uses twin 0.3 mil aluminum screens on each side of a light-tight, 2 inch thick box. Two boxes are separated with a photomultiplier "looking" into each box. As the projectile penetrates the 0.3 mil aluminum foils, light enters the box. The time between light pulses on the two phototubes is displayed on a scope. Using that time, the average velocity between the boxes can be calculated. This device is shown in Figure D-2. It is estimated that it gives velocities which are accurate to $\pm$ 2%.

5. Crater Size

The above transit-time measurements are a direct way of determining the projectile velocity. However, failure of one of the many components in the measuring system occurs occasionally. As insurance against this and as an additional measure of accuracy, we measured the dimensions of the crater formed by each projectile in the lead brick target. Experimentally verified theory gives the dependence of crater depth to velocity as

$$\text{depth} \propto (\text{velocity})^{2/3}$$

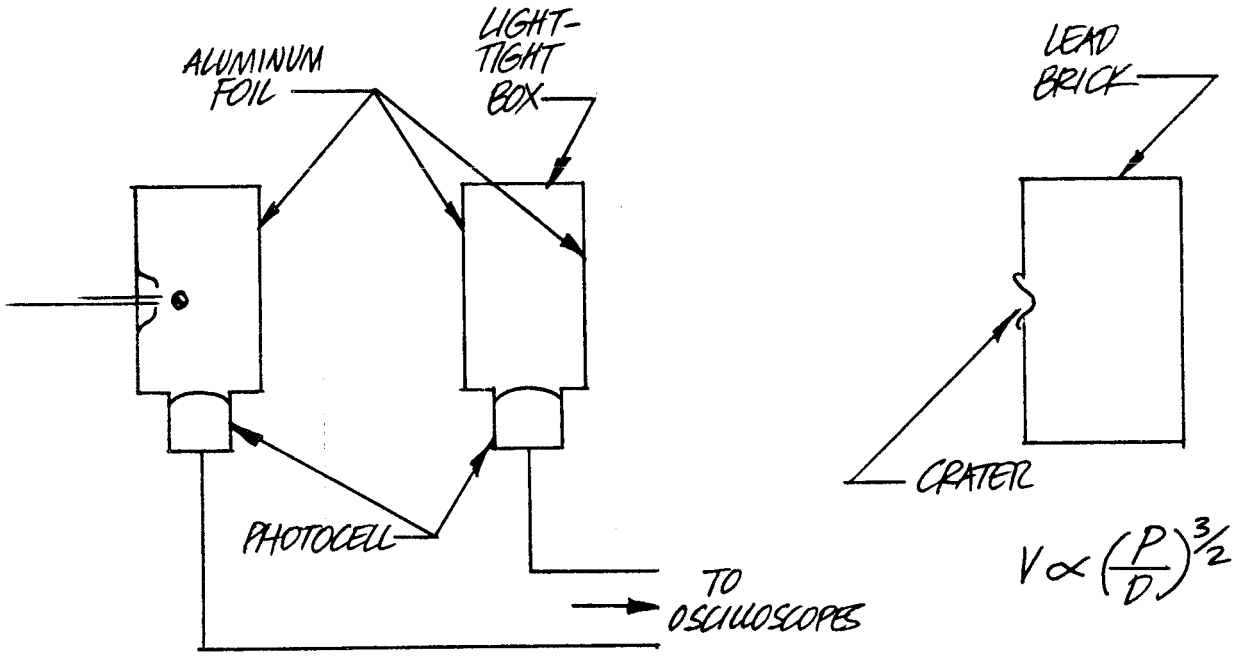

VELOCITY MEASUREMENT TECHNIQUES

FIGURE D-2

A log-log plot of our crater depth versus velocity data shows roughly a 10% scatter from a straight line of slope 2/3 between, say, 1 and 3 km/sec, but appears to increase in slope above 3 km/sec. (See Figure D-3)

6. Flux Loop Measurements

Signals from flux loops mounted as in Figure D-4 look like the lower four frames of Figure D-5 and are proportional to the rate of change of magnetic field due to the passage of the arc under the coils. Flux as a function of time is important since this indicates the structure of the arc. Ideally, therefore, one should monitor on separate oscilloscope traces the outputs of many flux loops at close intervals along the path of the arc. However, since we have only seven scope traces, and two or three of these must be used for other instrumentation, we cannot do this. But, since the arc is stable enough that the flux-versus-time profile changes continuously and only gradually over say two centimeters, it is redundant to do this. So, one or two of the remaining traces are used to record a sequence of pulses (see top of Figure D-5) from the circuit (see Figure D-6) which represents the passage under successive flux loops of one detail of the flux profile. This gives about a dozen position-versus-time data and two or three complete flux profiles. Figure D-7 is a description of the elementary circuits in the complex of Figure D-6.

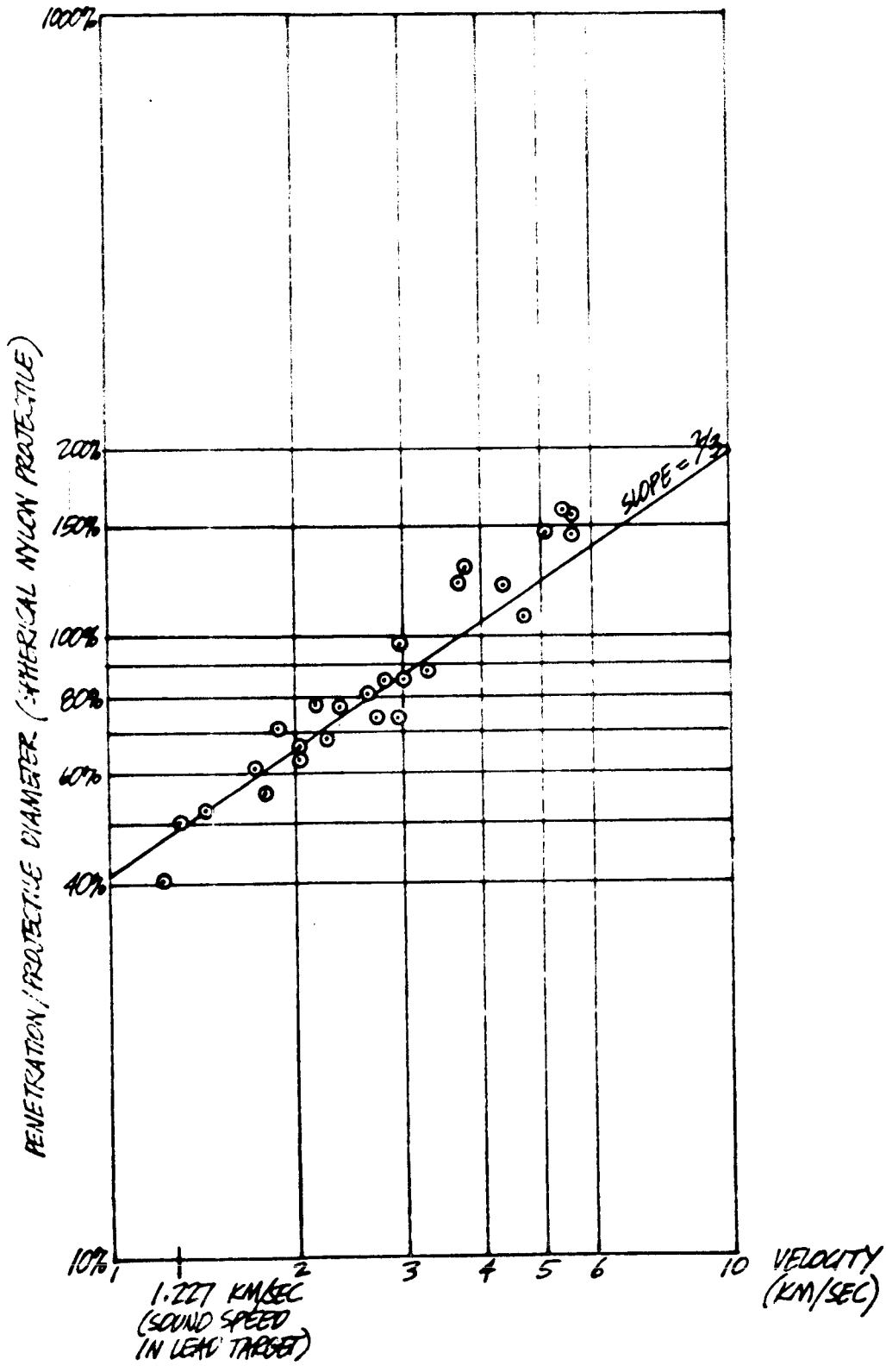

Penetration Versus Projectile Velocity at the Target

Figure D-3

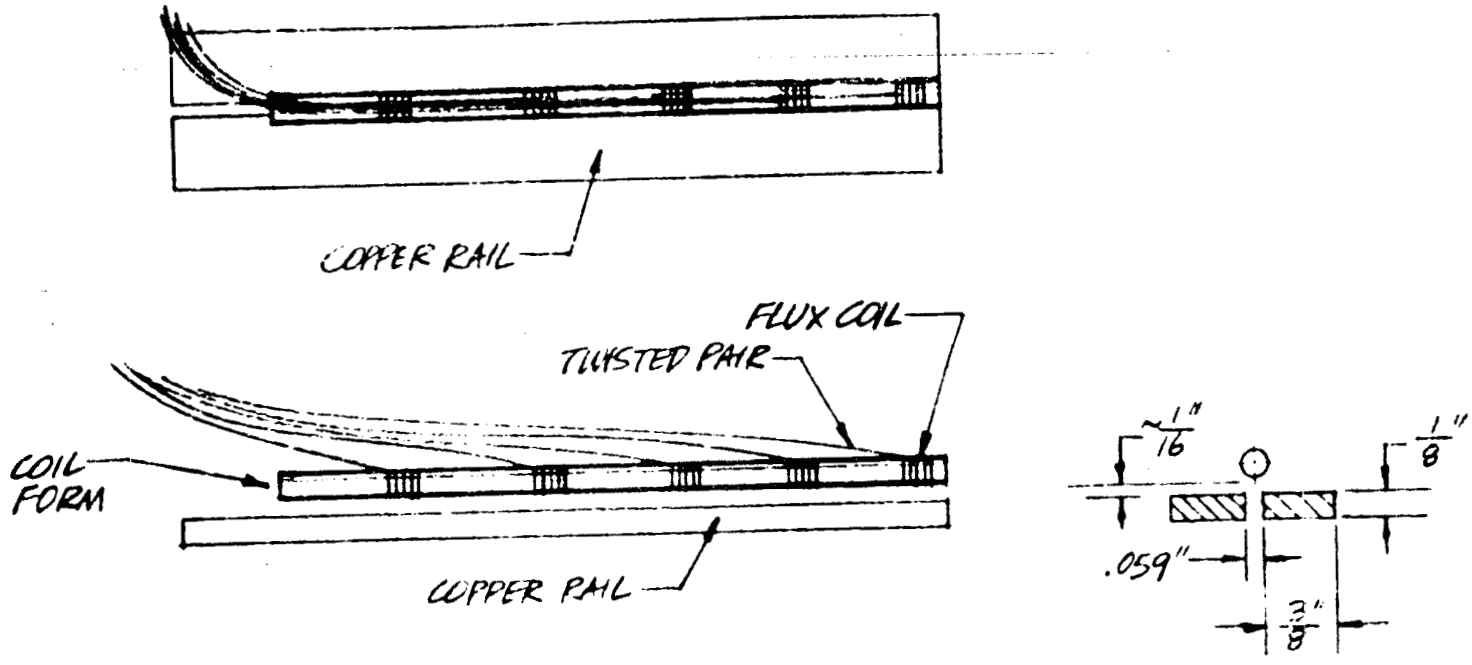

Flux Loops in Place on the Standard Rail Gun

Figure D-4

MBA 1223

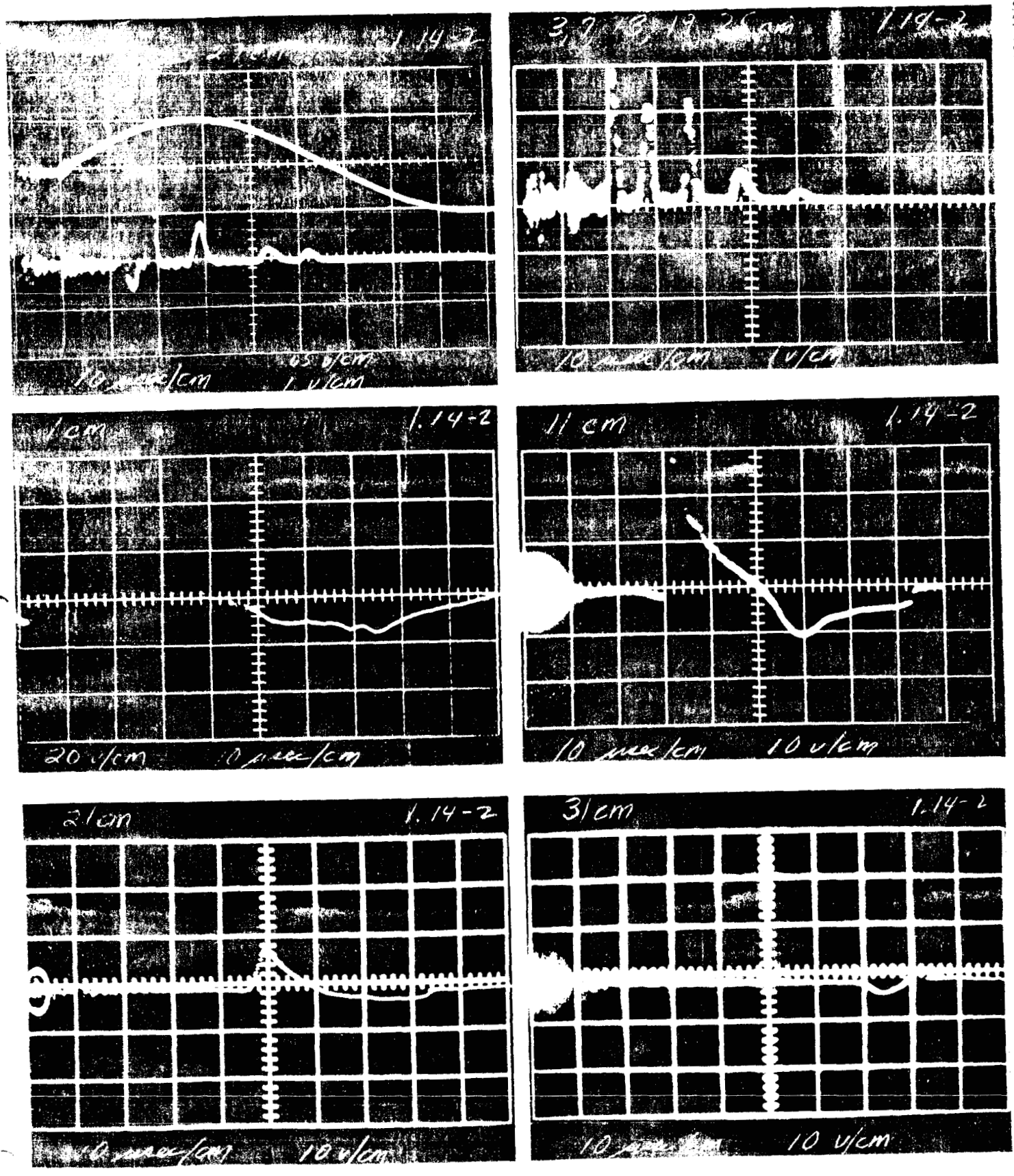

Figure [illegible]
FLUX LOOP SIGNAL TRACES

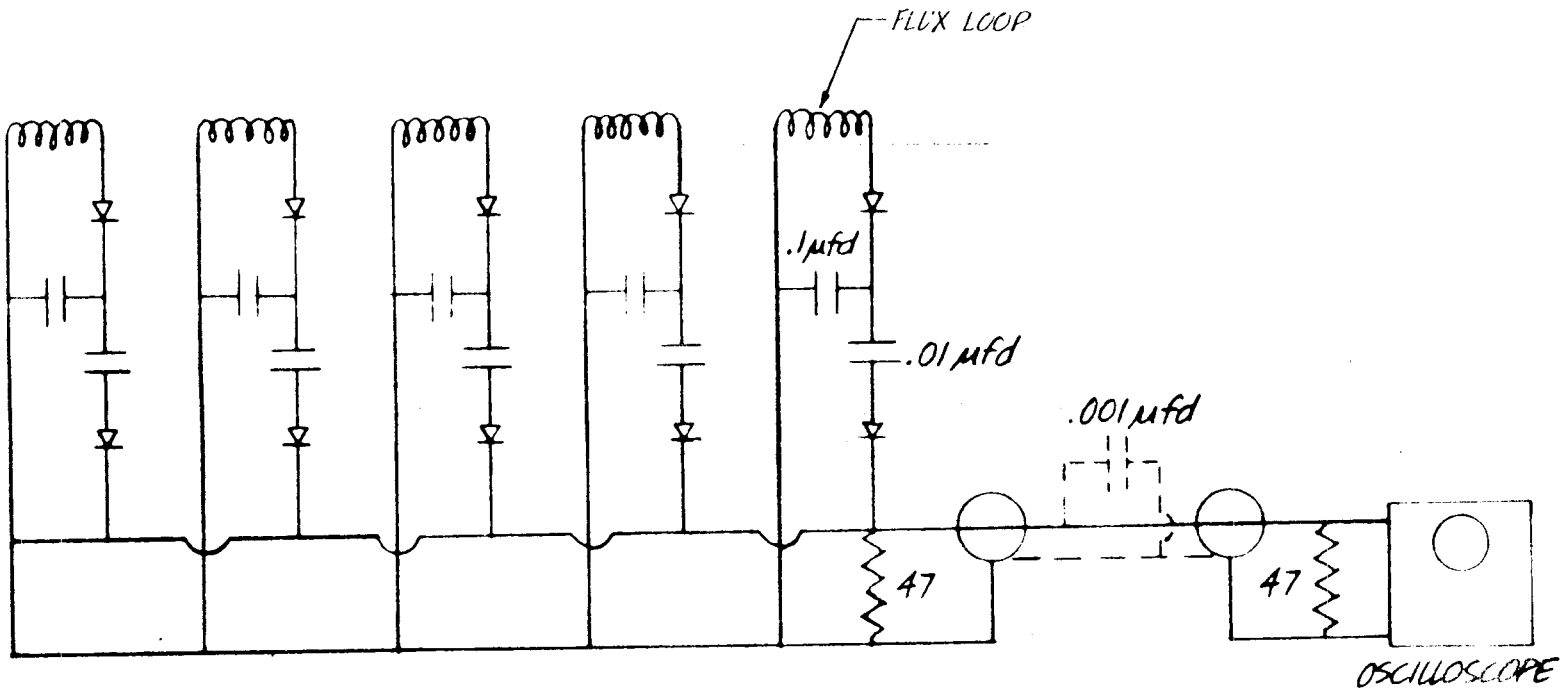

FIGURE D-2

FLUX LOOP CIRCUIT

MBA 1011

DESCRIPTION OF FLUX LOOP CIRCUIT

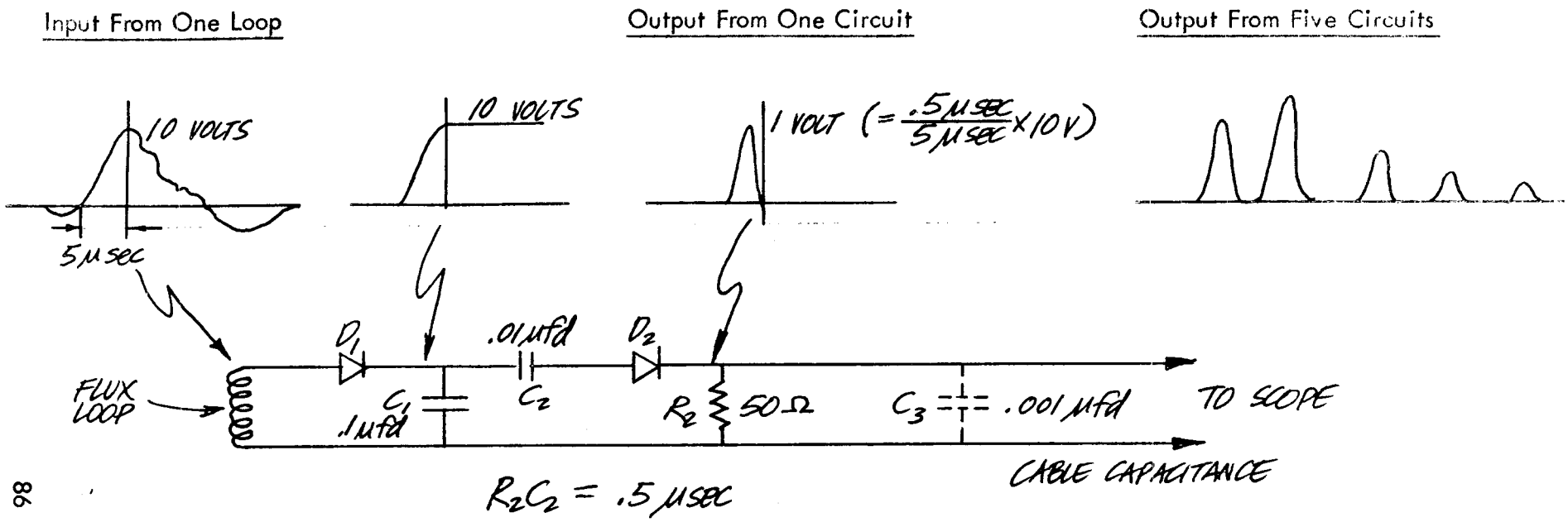

D_1	Rectifies the input.	Four other identical circuits are parallel across R_2.	$10R_2C_2 \gtrsim 5\ \mu$sec otherwise the output signal gets too small compared to noise.
C_1	Holds the 10 volts against D_1 thereby blocking any future signal less than + 10 volts.	D_2 keeps the outputs of these other circuits from being integrated by C_2 and C_1.	$C_2 \gtrsim 10\ C_3$ otherwise C_3 integrates the output.
R_2C_2	Differentiates the resulting rounded step signal to give the final 5 μsec wide output spike.	The resulting signals can be superposed without confusion to give the output above.	$C_1 \gtrsim 10\ C_2$ otherwise the potential at C_2 falls and future signals pass.
			$10R_{D_1}\ C_1 \lesssim 5\ \mu$ sec otherwise C_1 integrates the input.

FIGURE D-7

APPENDIX E

THEORY OF THE AFTER-SECTION

The device considered here is a barrel (an aftersection) attached to the muzzle of the rail gun. The projectile is loaded either into the rail gun or into the aftersection, and then the rail gun is fired in the usual way.

Limitations on the velocity that may be given to the projectile in a single aftersection arise in the following way: The force, F, on a projectile moving with velocity, v, through the arc stream of velocity, v_{arc}, and density ρ_{arc} is

$$F = 1/2\, C_D\, \rho_{arc}\, (v_{arc} - v)^2 A$$

where C_D is the drag coefficient, (approximately 0.9 for a sphere at Mach 7) and A the cross sectional area of the projectile. Therefore, for v_{arc} a constant, and v = 0 at x = 0,

$$v = v_a \left[1 - \exp\left(-\frac{x}{\ell} + \frac{1}{1 - \frac{v_{arc}}{v}}\right)\right.$$

where x is the position of the projectile and $\ell = \frac{2m_{projectile}}{C_D \rho_{arc} A}$, i.e., twice the length of the plasma column of the same cross section and mass as the projectile. So, v becomes approximately equal to v_{arc} in a distance of about ℓ.

However, v_{arc} is not constant. Rather, it decreases exponentially with distance due to skin friction with the barrel. The e-fold length is $R = \frac{D_{arc}}{2\, C_f}$, where D_{arc} is the diameter of the barrel and C_f is the coefficient of skin friction (probably about 0.001 under our experimental conditions). In order to minimize this effect, the length, L, of the aftersection should be, say, $\lesssim$ (1/2)R, but, in order to maximize the transfer of momentum, it should be $\gtrsim \ell$. Therefore, we should have $\ell \lesssim L \lesssim$ (1/2)R. In terms of the definitions of ℓ and R,

$$(\rho D)_{proj} \lesssim \frac{1}{2} \rho_{arc} L \lesssim \frac{1}{4} C_f (\rho D)_{arc} \qquad (1)$$

Thus, for a given projectile, a lower limit is set on D_{arc}. However, the total length, b, of the plasma column produced during one shot must be $\gtrsim \ell$ in order to achieve a velocity comparable to v_o. This restriction comes in as follows:

$$p = (\rho D v)_{arc}\, b$$

where p, the total momentum produced, is given by

$$p = \int F\,dt \propto \int I^2\,dt = \frac{\text{total energy}}{\text{resistance}}$$

and is, therefore, fixed for a given energy source. This puts the following upper limit on D_{arc}

$$\frac{D_{arc}}{D_{proj}} \lesssim \frac{p}{2\,m_{proj}} \tag{2}$$

Inequalities (1) and (2) together give

$$\left(\frac{p}{2\,m_{proj}}\right)^{1/2} \gtrsim \frac{D_{arc}}{D_{proj}}\; 4\,C_f\; \frac{\rho_{proj}}{\rho_{plasma}} \tag{3}$$

For a crude sample calculation we take:

$p = 2000$ mg km/sec

$m_{proj} = 2.4$ mg

$v_{arc} = 15$ km/sec

$\rho_{proj} = 1$ gm/cm^2

$\rho_{arc} = 1$ mg/cm^2

$C_f = 0.001$

Then, inequality (3) gives

$$5 \gtrsim \frac{D_{arc}}{D_{proj}} \gtrsim 4$$

This fortunate result comes from a good choice of p and v_{arc}, which are known only to an order of magnitude, and of ρ_{arc}, which is even less well known. But it does show, at least, how the experimental parameters lead to an optimal value for D_{arc}. L follows from inequality (1).

The inefficiency of this method becomes obvious in light of the fact that the fraction of arc momentum converted to projectile momentum is roughly $(D_{pr}/D_{barrel})^2$, the ratio of projectile to barrel cross sectional areas. For the case calculated, therefore, only about 4% of the momentum produced by the gun goes into the projectile.